Uncertainty in olfactory decision-making

Maria Inês A. Vicente

Dissertation presented to obtain the
Ph.D. degree in Biology | Neuroscience

Instituto de Tecnologia Química e Biológica António Xavier | Universidade Nova de Lisboa

Oeiras,
July, 2015

INSTITUTO
DE TECNOLOGIA
QUÍMICA E BIOLÓGICA
ANTÓNIO XAVIER /UNL

Knowledge Creation

Uncertainty in olfactory decision-making

Maria Inês A. Vicente

Dissertation presented to obtain the
Ph.D. degree in Biology | Neuroscience

Instituto de Tecnologia Química e Biológica António Xavier | Universidade Nova de Lisboa

Research work coordinated by:

Fundação Champalimaud

FCT
Fundação para a Ciência e a Tecnologia
MINISTÉRIO DA CIÊNCIA, TECNOLOGIA E ENSINO SUPERIOR

FUNDAÇÃO CALOUSTE GULBENKIAN
Instituto Gulbenkian de Ciência

Oeiras,
July, 2015

INSTITUTO DE TECNOLOGIA QUÍMICA E BIOLÓGICA ANTÓNIO XAVIER /UNL
Knowledge Creation

to PGCN 2007

This work was developed in the context of the International Neuroscience Doctoral Programme (INDP) of the Champalimaud Research Programme, Champalimaud Center for the Unknown, Lisbon, Portugal. The project entitled "Uncertainty in olfactory decision-making" was carried out at Instituto Gulbenkian de Ciência, Oeiras, Portugal and at the Champalimaud Research Programme, Champalimaud Center for the Unknown, Lisbon, Portugal, under the scientific supervision of Zachary Mainen, Ph.D, and under the guidance of the Thesis Committee composed by Alfonso Renart, Ph.D, and Joseph Paton, Ph.D. This work was supported by the fellowship SFRH / BD / 33274 / 2008 from Fundação para a Ciência e Tecnologia, Portugal.

Acknowledgments

Zach. The freedom to believe that everything is possible.
André. The eternal arm swirling mermaids.
Patricia. The companionship and shared growth.
Gil. The space for naturality.
Rita. The possibility of the un-limit.

The lab. The support and openness.
Masa. The first steps.
Eric. The valuable discussions.

Zach, Rui. Marta, Susana. The opportunity to grow-up with you.
Alfonso, Joe. The guidance.

PGCN 2007. Patricia, Rodrigo, Margarida, Zé, Mariana, Pedro, Patricio, Íris, Isabel. The time for dreams, magic and adventures.
Margarida, Rodrigo, Zé. The simple truths.

Catarina. The digressions that kept me on track.

Mãe, Pai, André, Avó, Família. O incondicional.
Emília, Zé. O carinho.
Zazu, Pimenta, Buga. A sensibilidade.
Zé. Pela nossa estrada.

Thank you.

Resumo

As relações entre precisão e velocidade em tomadas de decisão, ou relações velocidade-precisão (*speed-accuracy tradeoff*, SAT), têm sido estudadas extensivamente. No entanto, existe alguma variabilidade nos valores de SAT observados entre estudos, e as causas que poderão estar na origem desta variabilidade são ainda desconhecidas.

Diversas explicações têm sido sugeridas, incluindo motivação ou incentivo para velocidade vs. precisão, espécie ou modalidade sensorial. No entanto, nenhuma destas hipóteses foi ainda testada directamente. Uma explicação alternativa seria que os diferentes graus de SAT obervados estariam relacionados com a tarefa que está a ser desempenhada. Neste estudo, abordámos este problema através da comparação de SAT em duas tarefas comportamentais baseadas em odores, idênticas excepto na natureza da incerteza associada a cada tarefa: uma tarefa de categorização com misturas de odores, onde a informação relevante é manipulada variando o grau de semelhança entre os estímulos que compõem a mistura; e uma tarefa de identificação com odores puros, na qual a informação relevante é reduzida diminuindo a intensidade dos estímulos num gama de três passos logarítmicos.

Observámos que a duração de amostragem do odor (*odor sampling duration*, OSD) em relação à dificuldade do estímulo foi substancialmente maior na tarefa de identificação, em

comparação com a de categorização. Esta observação foi também verificada quando as duas tarefas foram combinadas, intercalando o conjunto de estímulos das tarefas de categorização e identificação bem como misturas intermédias. Estas duas manipulações interagiram de forma linear em relação ao OSD, sendo consistente com a ideia de que concentrações baixas de odores e contrastes reduzidos de misturas colocam fontes independentes de incerteza.

Baseado nestas observações, formulámos a hipótese de que na identificação de odores, a performance é limitada pela incerteza do estímulo, ao passo que na categorização de misturas, a performance é limitada pela variabilidade no mapeamento do estímulo a resposta, que vai sendo aprendido sequencialmente, a casa tentativa. Dada esta hipótese, investigámos se esta aprendizagem teria uma influência diferente na escolha dos animais na identificação de odores ou na categorização de misturas. Verificámos, em ambas as tarefas, uma actualização da escolha dos animais a cada tentativa. Contudo, enquanto que na tarefa de categorização o viés na escolha dos animais aumentou com a dificuldade da tentativa anterior e do respectivo resultado, na tarefa de identificação este viés dependeu apenas da identidade do odor e do resultado.

Em seguida, utilizámos uma estratégia de modelação para investigar que mecanismos computacionais poderiam explicar as mudanças comportamentais observadas na tarefa de identificação. Interessantemente, observámos que os nossos resultados poderiam

ser descritos tanto por modelos com e sem integração temporal, colocando em perspectiva o uso generalizado de modelos de integração para explicar tanto a escolha como o tempo de resposta numa gama alargada de tarefas de decisão baseadas em percepção (*perceptual decision-making*).

Finalmente, explorámos o papel da incerteza temporal em tarefas de decisão baseadas em percepção, olhando para o impacto no OSD da expectativa em relação ao início do estímulo. Observámos uma relação linear entre a média e o desvio padrão de OSD para os diferentes constrastes de misturas e concentrações de odores, consistente com a lei de Weber no domínio temporal. Para ambas as tarefas, a média de OSD foi menor quando o início do estímulo foi mais tardio (expectativa elevada). Esta diminuição foi acompanhada por um decréscimo proporcional do desvio padrão, tal como é previsto pela propriedade de escalonamento de estimativa temporal para diferentes condições de expectativa temporal. Verificámos que a magnitude desta componente sensível a expectativa está correlacionada com a dificuldade do estímulo, sendo que variações maiores no OSD correspondem a valores menores de performance. Estes resultados demonstram que o OSD é modulado por componentes não sensoriais, como a expectactiva temporal, sugerindo que os tempos de reacção são uma combinação entre processos de tomada de decisão e mecanismos relacionados com atenção que são, por sua vez, afectados por processos de estimativa temporal.

Abstract

Relationships between accuracy and speed of decision-making, or speed-accuracy tradeoffs (SAT), have been extensively studied. However, the range of SAT observed varies widely across studies for reasons that are unclear. Several explanations have been proposed, including motivation or incentive for speed vs. accuracy, species and modality but none of these hypotheses has been directly tested. An alternative explanation is that the different degrees of SAT are related to the nature of the task being performed. Here, we addressed this problem by comparing SAT in two odor-guided decision tasks that were identical except for the nature of the task uncertainty: an odor mixture categorization task, where the distinguishing information is reduced by making the stimuli more similar to each other; and an odor identification task in which the information is reduced by lowering the intensity over a range of three log steps. We found a much larger increase in odor sampling duration (OSD) with difficulty for stimulus detection compared to categorization. This was also observed when the two tasks were combined, by interleaving the full set of stimuli from the categorization and identification tasks as well as intermediate mixtures. These two manipulations interacted linearly with respect to OSD, consistent with the idea that low concentrations and low mixture contrast pose independent sources of uncertainty. We hypothesized that in odor identification,

accuracy is limited by stimulus uncertainty, whereas in mixture categorization, accuracy is limited by variability in the mapping of the stimulus to the response, which must be learnt on a trial-by trial basis. Given this hypothesis, we investigated whether ongoing learning has a different influence on the choice of animals in identification and categorization. In both tasks there was a clear trial-by-trial updating of the animal's choice function. However, whereas in categorization choice bias increased with difficulty of the previous trial and outcome, in identification this bias was dependent only on choice side and outcome.

Next, we used a modeling approach to investigate which computational mechanisms might account for the behavioral changes observed in the identification task. Interestingly, we observed that our results were well described both by models with and without temporal integration, putting into perspective the generalized use of integrator models to explain choice behavior and response times across a wide range of perceptual decision-making tasks.

Finally, we explored the role of temporal uncertainty in perceptual decision-making, by focusing on the impact of stimulus onset expectation on OSD. We observed a linear relationship between the mean and standard deviation of OSD across mixture contrasts and odor concentrations, consistent with Weber's law in the temporal domain. For both tasks, mean OSD was smaller for longer onsets (higher expectation), and this decrease was accompanied by a proportional decrease of the

standard deviation, as would be expected from the scalar property of interval timing for different temporal expectation conditions. The magnitude of this expectation-sensitive component was correlated with stimulus difficulty, with lower accuracies displaying larger changes in OSD. These results showed that OSDs are modulated by non-sensory components such as temporal expectation, suggesting that reaction times are a combination between decision-making processes and attention-related mechanisms that are affected by time estimation processes.

Abbreviations list

5-HT	Serotonin
AFC	Alternative forced-choice
BeT	Behavioral theory of timing
CV	Coefficient of variation
DDM	Drift-diffusion model
DRN	Dorsal raphe nucleus
DV	Decision variable
EEG	Electroencephalography
fMRI	Functional magnetic resonance imaging
IT	Inferotemporal cortex
LeT	Learning-to-time
LIP	Lateral intraparietal area
M	Magnocellular
MC	Mitral cells
MT	Middle temporal visual area
OB	Olfactory bulb
OC	Olfactory cortex
OFC	Orbitofrontal cortex
ORN	Olfactory receptor neuron
OSD	Odor sampling duration
OT	Olfactory tubercle
P	Parvocellular
PC	Piriform cortex
RDMD	Random-dot motion discrimination

RL	Reinforcement learning
RT	Reaction time
SA	Sequential analysis
SAT	Speed-accuracy tradeoff
SD	Standard deviation
SDT	Signal detection theory
SET	Scalar expectancy theory
ST	Scalar timing
TC	Tufted cells

Figure Index

Table Index

Author contributions

Maria Inês Vicente (MIV), André Gil Mendonça (AGM) and Zachary Frank Mainen (ZFM) designed the experiments (Chapter 2). MIV and ZFM designed the model (Chapter 4). MIV conducted the experiments with assistance from AGM. MIV analyzed the data and implemented the model (Chapters 3, 4 and 5).

Part of the work presented in Chapters 2 and 3 has been submitted to Nature Communications.

Contents

1 General Introduction

1.1 Introduction

The evolution of sophisticated brains has given us the capacity for flexible decision-making. The evidence we obtain through our senses (or from memory) need not precipitate an immediate, reflexive response. Instead our decisions can be deliberative and conditional, contingent on other sources of information, long-term goals, history and values.

A decision is a commitment to a categorical proposition and is based on a variety of factors: quality of the evidence for a particular option, prior knowledge concerning the relative merit of the options, expected costs and rewards associated with the possible decisions and their outcomes, and other costs associated with gathering evidence (e.g., the cost of elapsed time). In addition, decisions are always made in the face of uncertainty. Both natural events in the world and the consequences of our actions are fraught with unpredictability, and the neural processes generating our percepts and memories may be unreliable and introduce additional variability. Unraveling the relationship between neural and behavioral variability is fundamental to understanding how decisions are formed in the brain.

The present work has investigated the contributions of different sources of uncertainty in perceptual decision-making, by employing a combination of behavioral and modeling approaches.

In the following sections, we will: review the conceptual framework and quantitative models used to study perceptual decision-making (**1.2 Perceptual decision-making**); consider the contribution of different sources of uncertainty in perceptual decision-making, while focusing on the relation between choice behavior and response times across different perceptual decision-making tasks (**1.3 Sources of uncertainty in perceptual decision-making**); and explore the role of temporal uncertainty on perceptual decision-making and the relationship between decision-making and time estimation processes (**1.4 Temporal uncertainty in perceptual decision-making**).

1.2 Perceptual decision-making

1.2.1 Conceptual framework for studying perceptual decision-making

Perceptual decision-making is the process by which sensory information is used to guide behavior toward the external world. This involves gathering information through the senses, evaluating and integrating it according to the current goals and internal state of the subject, and using it to produce motor responses[1,2].

At any given point in time, the state of the world must be inferred based on the noisy data provided by the sensory systems, and behavior is critically dependent on the ability to quickly and accurately decide amongst the possible different states. For

instance, deciding whether or not a predator is present in a shadowy corner will dictate an animal's subsequent action and survival. Various factors must be taken into account before committing to a decision and executing the appropriate behavioral response. These include the quality of the evidence derived from the sensory observations; prior history, which determines the predicted probability of seeing a particular stimulus or receiving a particular reward in the future[3–6]; and value, the subjective costs and benefits that can be attributed to each of the potential outcomes of the decision process. These different sources of information are then accrued into a quantity – the decision variable (DV) – that is then interpreted by the decision rule to produce a particular choice[1]. A conceptually simple rule is to place a criterion value on the DV. Like this, the magnitude of the DV reflects the balance of support/opposition for a given choice, allowing the decision maker to achieve different goals, including maximizing accuracy or reward or achieving a target decision time[1]. Post-decisional processes also play a critical role in shaping future decisions, namely via learning mechanisms mediated by the evaluation, or performance monitoring, of the choice with respect to its particular goals[5,7].

1.2.2 Theoretical framework for studying perceptual decision-making

The quantitative study of perception, or psychophysics, has embraced decision theory since its inception by Fechner in

1860[8,9]. Since then, different mathematical descriptions have been proposed to better test and understand perceptual decision-making, namely signal detection theory (SDT) and sequential analysis (SA).

SDT is one of the most widely used formalisms to study perception[10,11]. It prescribes a process where performance of perceptual tasks reflects not just the inherent sensitivity of the subject to the relevant stimuli but also how the subject uses that information to generate a choice. According to SDT, the decision-maker obtains an observation of noisy evidence from the stimulus, which gives rise to the DV that is then evaluated according to the decision rule. In simple binary decisions, the DV is typically related to the likelihood ratio of the different alternatives, and then compared to a criterion. This criterion can also incorporate different priors and value, allowing SDT to provide a flexible framework to form decisions and achieve a variety of goals[1,12].

SA is a natural extension to SDT that accommodates multiple pieces of evidence observed over time. Conceptually, the idea is that in the presence of uncertainty or noise, the decision maker can benefit from sampling multiple times from the noisy distribution of values representing the stimulus. After each acquisition, a DV is calculated from the evidence obtained up to that point and compared to the decision rule, normally represented by a positive and negative criterion, which correspond to each choice alternative. Once the DV exceeds (or falls below) the

criterion bounds, the bound that is first reached determines the decision and response time of the decision maker. There are several instantiations of sequential sampling models[1,13–19]. For example, in random walk models, the DV is a cumulative sum of evidence over discrete time steps. If the evidence is the logarithm of the likelihood ratio, then this process corresponds to the statistically-optimal Sequential Probability Ratio Test[20], which anecdotally played a prominent role in World War II allowing to break the German enigma cipher[21,22]. Instead, if the evidence is sampled from a Gaussian distribution in infinitesimal time steps, the process is termed diffusion with drift or bounded diffusion.

While many models provide an account of either RT[14,23] or accuracy (SDT[10]), sequential sampling models relate shapes of RT distributions with probabilities of correct and incorrect responses, thereby explaining how RT and choice accuracy jointly vary as a function of the experimental conditions of interest.

The parameters of these sequential sampling models allow quantifying several latent psychophysical processes, namely the speed of sensory information processing, given by the rate of accumulation; response caution, from the bound height; and the amount of time spent on processes unrelated to decision formation.

In recent years, integrator models have gained prominence in the field of decision-making due to its ability to explain several features of behavioral and neural data. First, they have described accuracy as well as RTs in a variety of psychophysical tasks,

including perceptual discrimination and value-based choices[24–29]. Second, they can be tuned to fit task conditions, such as reward ratios or prior probability[30–32]. And third, these models have been used to explain neurophysiological data[1,33] and recordings of neural activity in primates have shown neural correlates resembling the DV[34].

1.3 Sources of uncertainty in decision-making

1.3.1 Speed-accuracy tradeoffs

The relationships between accuracy and speed of decision-making, or speed-accuracy tradeoffs (SATs), have been effectively modeled as integration of sensory information to a bound[13,25,34–37]. Speed and accuracy in perceptual decisions show characteristic relationships and there are at least three psychophysical experimental contexts in which the relationship between speed and accuracy has been studied: 1) sampling time manipulation: when the experimenter limits the duration of the stimulus and/or sets a deadline for response time, performance accuracy decreases with shorter sampling times; 2) speed-accuracy tradeoff: when subjects are instructed to perform rapidly, accuracy drops; conversely, when instructed to emphasize accuracy, performance slows (traditionally, this is the technical definition of 'speed-accuracy tradeoff'); 3) difficulty effects: when a participant is free to choose when to respond (a reaction time task), average reaction times increase with difficulty[38].

The random-dot motion discrimination (RDMD) task, which has been extensively studied in the field of perceptual decision-making, is a good example of a task where SAT has been observed and how this relationship can be well explained by integrator models. In this task, participants are presented with a field of flickering dots, some of which move randomly and some of which move coherently in one of two possible directions, and asked to report the net direction of motion. The difficulty of the task is changed by manipulating the fraction of coherently moving dots. SAT and the impact of temporal integration in this task have been investigated in humans and monkeys in two ways. First, by varying the viewing time and measuring the discrimination threshold for each duration, it was shown that sensitivity increases with viewing times up to ~2 s[39,40]. Then, in a reaction time (RT) version of this task, it was found that as motion coherence was decreased, RTs increased from 300 to >800 ms[25,34]. Moreover, these data could not only be fit quantitatively with a simple diffusion model[25], but neurophysiological recordings and manipulations also provided strong evidence sustaining the idea of a neural integrator that underlies the decision process[34,41–43]. Recordings from the parietal cortex (the lateral intraparietal area, LIP) showed that neuronal activity ramps up at a rate correlated with the strength of the motion signal until it reaches a level that is constant across motion strengths, as if a decision threshold was reached[34,42,44–46]. This pattern of firing matches quite closely to what is expected of the DVs posited by integrator models[45,47]. Furthermore, microstimulation experiments used to read out the

state of the DV provided added evidence supporting the integrator model as a substrate of the decision process[48,49].

In addition to the studies using the RDMD task and performed in humans and monkeys, SATs have been extensively studied across different tasks, modalities and species, including rodents and insects[1,13,25,34,36,38,50–58]. However, the range of SATs observed varies widely across studies for reasons that are unclear. For example, reported increases in RT with increased difficulty of perceptual discrimination range from over 500 ms in humans[25] and monkeys[34] performing the RDMD task, to 100 ms in mice performing a visual contrast detection task[55], to less than 30 ms in rats performing an odor mixture discrimination task[52].

In particular, studies of odor discrimination in rodents have reported SATs of different magnitudes[52–54]. Uchida and Mainen (2003)[52] used a two-alternative forced-choice (2-AFC) task in which eight different binary odor mixture stimuli were randomly interleaved and rewarded according to a categorical boundary. As mixture ratios approached the category boundary, choice accuracy dropped to near chance, yet odor sampling time increased only 30 ms[52]. On the other hand, Abraham et al. (2004)[53], using a go/no-go odor paradigm where odor mixture stimuli were presented in blocks of trials, reported that for a high level of accuracy, mice took an additional time of 70-100 ms to discriminate closely related mixtures. In addition, in mice performing a 2-AFC where the duration of odorant sampling was controlled by the experimenter in a random fashion and signaled with a ‘go’ tone,

Rinberg et al. (2006)[54] observed an improvement in performance as a function of stimulus duration across different mixture difficulties.

These apparent discrepancies were interpreted as a manifestation of SAT in olfaction[59], where speed had been favored over accuracy in the study from Uchida and Mainen (2003)[52], and the opposite in Abraham et al. (2004)[53] and Rinberg et al. (2006)[54] (accuracy had been privileged at the expense of speed).

However, in a further twist, Zariwala et al. (2013)[56], by performing a large battery of variants of the categorization task from Uchida and Mainen (2003)[52], suggested an alternative explanation for the differences amongst these tasks that was not based on differences in SAT. According to this study, the higher accuracy reported in Abraham et al. (2004)[53] and Rinberg et al. (2006)[54] could be attributed to the use of blocked rather than interleaved stimulus difficulties, which leads to a better anticipation of stimulus identity. The greater change in RTs with difficulty reported by Abraham et al. (2004)[53] could be explained by the effect of reward expectation on response speed. And finally, the increase in performance as a function of stimulus duration reported in Rinberg et al. (2006)[54] could be explained by the increase of go-signal anticipation over time (i.e. increase in hazard rate) stemming from the temporal statistics of the uniform distribution used for the go-signals in this study. In agreement with this, when Zariwala et al. (2013)[56] performed a similar manipulation, but now in a blocked fashion, i.e. by keeping

constant the time of go-signal within a block, hence not changing the anticipation, they failed to observe an increase in accuracy when the amount of time at the odor port augmented.

Together these results highlight a dissociation of accuracy from RT in the odor mixture categorization task[56], suggesting that the noise related with the stimulus is not the dominant source of uncertainty. Which other sources of uncertainty could then be limiting performance in the mixture categorization task?

1.3.2 Bridging perceptual and economic decision-making

There is a common structure to virtually all decision-making tasks employed across the literature: an agent is required to identify one or more stimuli in a given sensory modality (what is it?), and then to select a response which will maximize the probability of positive feedback or reward (what is it worth?).

Perceptual decision-making, as described above, is concerned with how observers detect, discriminate, and categorize noisy sensory information. Because uncertainty in perceptual decision-making tasks is assumed to be due to the noise associated with the stimulus, these experiments often take place in a constant stage of task performance, where the stimulus-response-reward contingencies have been learnt through extensive training, and learning is thought to be stationary. Thus, the computational models that have been used to characterize performance have focused on the choice period itself, rather than on any

reinforcement learning that occurs following feedback[60]. In the standard model of perceptual decision-making, based on the discrimination of motion direction of randomly moving dots[61], sensory neurons in the middle temporal visual area (MT) vote with their firing rates for the perceived direction of motion and their responses are then weighted, summed, and passed through a binary decision function. In this model, behavioral variability mainly arises through noise introduced in the responses of the individual neurons. Sequential sampling models, as described above, are an example of this kind of architecture, where choices depend on a serial sampling mechanism, in which evidence about the identity of the stimulus is collected and integrated until a criterion level of certainty is reached[20,37,62].

However, all perceptual decisions are ultimately motivated by reward (or the avoidance of loss). Indeed, there are examples in the literature focusing on how reward might influence sensory discrimination[30,32,63–65] and showing that rewards (or informative feedback) play a role on learning about sensorimotor acts[5,7,66,67]. This implies that, although perceptual decision-making tasks have focused on the optimization of detection or categorization judgments guided by sensory stimuli, subjects are swayed by factors mediated by reinforcement statistics. Hence, the environmental structure and the way it influences the tradeoff between information and reward acquisition should also be considered for the assessment of choice optimality[60]. In agreement with this idea, recent work has shown that, in a visual detection task, choice behavior is captured by a model involving

not only the visual responses to the current stimulus but also a bias and history term depending on the outcome of the previous trial[7].

The field of decision-making that is concerned with how subjects choose among different options on the basis of their associated reinforcement history is economic decision-making. In contrast to perceptual decision-making, economic decision-making tasks tend to employ stimuli that are perceptually unambiguous but associated with distinct reward statistics, where the uncertainty is derived from variability in internal information about the expected value of each option. One very successful class of models used in economic decision-making, that draws upon a rich literature from learning theory in experimental psychology[68] and machine learning[69], is reinforcement learning (RL), which describes the mechanisms by which the value of stimuli or actions is learned. RL proposes that these values are updated according to how surprising an outcome is – a prediction error – scaled by a further parameter that controls the rate of learning. Recently, the RL framework has been successfully applied to a perceptual decision-making task to explain improvements in perceptual performance[67]. In monkeys trained on a visual motion discrimination task, improvements in perceptual sensitivity were shown to correspond to changes in motion-driven responses of neurons in area LIP, which represents the readout to motion information to form a direction decision, but not area MT, a likely source of that motion information[70]. These changes were well described by a RL scheme in which the weights between MT-like

sensory neurons and LIP-like decision neurons were adjusted according to a prediction error signal[67]. Evidence from neurophysiological recordings, namely from parietal cortex, basal ganglia and orbitofrontal cortex (OFC), have also supported this bridge between perceptual and economic-decision making[60].

1.4 Temporal uncertainty in perceptual decision-making

Animals live in naturally complex, ever-changing environments, where identifying temporal regularities is extremely important, enabling them to predict behaviorally relevant events. Hence, to behave adaptively in these environments, animals must not only learn which actions to take in a particular context given their past experience, but also to learn the temporal information about when those actions and the respective consequences occur.

Time is a fundamental dimension of animals' experience in the world. As such, temporal information provided by stimuli that predict salient events can be shown to exert a powerful influence on the organization of behavior, suggesting that the computation of time represents a basic aspect of cognition[71,72].

1.4.1 Interval timing

Time is not sensed through a sensory epithelium, but timing is key to many aspects of behavior, especially foraging and learning. Importantly, interval timing exhibits regularities that mimic those of traditional sensory systems. The best known is a strong version of Weber's law (i.e., the just noticeable difference is proportional to the baseline for comparison[73]) known as scalar timing (ST)[74,75]. For example, in a typical duration reproduction procedure, known as 'peak-interval procedure', when participants are asked to reproduce a criterion interval that was previously learnt, the responses typically distribute around the criterion interval with a width that is proportional to the temporal criterion. Moreover, the relative trial-to-trial response variability, e.g., the coefficient of variation (CV) associated to the estimation of different intervals, appears to be constant regardless of the estimated time[74,76]. Remarkably, not only the CV, but also the entire distribution of timed responses is scale invariant, i.e., identical when plotted as a function of time relative to the mean. The ST property holds for many species and over a broad range of temporal intervals[74,75], suggesting that ST reflects something fundamental about the way organisms structure their behavior in time. In addition, it represents a very strong quantitative constraint on the neuronal mechanisms responsible for the timing of actions.

1.4.2 Models of interval timing

Traditional sensory modalities such as vision, audition or olfaction are processed by known sensory organs and brain areas. Time perception, on the other hand, still lacks a clear and direct demonstration of how it would be implemented within the nervous system. Whether the representation of temporal information is instantiated within a dedicated timing network, or distributed across different brain areas as a common property of many or all neural systems, is still a matter of debate and ongoing research[77].

Neurally-inspired models have suggested different encoding schemes for time related information, namely oscillatory or periodic activity in neural circuits[78,79], integration of noisy firing of neural populations[80] and state-dependent changes in network dynamics[81].

Additionally, several abstract models of how animals track the passage of time have been proposed, many of which fall in one of two categories: accumulator models tell time by counting pulses emitted by a pacemaker and comparing it to a remembered value (Scalar expectancy theory, SET[76]), while state based models represent time as a trajectory progressing through a sequence of states (Behavioral theory of timing, BeT[82]; Learning-to-time, LeT[83]).

SET is based on an internal clock model, in which pulses that are emitted regularly by a pacemaker are temporarily stored in an

accumulator. During training, at the time of reward or feedback, the number of pulses that have been received from the accumulator is stored in reference memory. For test trials, the response is controlled by the ratio comparison between the current subjective time/clock reading – stored in the accumulator – and a sample taken from the distribution of remembered criterion durations, which are represented as the number of pulses from previously reinforced clock readings stored in reference memory. In this framework, the scalar property derives from the assumption that the accumulation error is proportional to the criterion duration[76,79,84].

BeT (as well as LeT, a derivative of BeT) emphasizes the role of behavior in temporal discrimination[82,85]. According to this theory, certain kinds of adjunctive or superstitious behaviors, such as turning, scanning a corner, hopper inspection, occur in a consistent fashion such that they are temporally related to reinforcement delivery. These kinds of behavior may then act as conditional discriminative stimuli when an animal is required to make a temporal discrimination. Formally, these classes of adjunctive behavior correspond to hypothetical states, whose transitions are driven by pulses from a hypothetical pacemaker described by a Poisson process, with a rate proportional to the reinforcement rate. The question that is then asked is: what is the probability that an animal is in state n at time t? Varying the rate of reinforcement will generate distributions of behavior whose mean and standard deviation (SD) vary proportionately[82].

Recent work has suggested a hybrid model between SET and LeT, that preserves the overall learning structure of LeT but replaces its state-activation dynamics by a scalar-inducing dynamics equivalent to the pacemaker-accumulator structure of SET[86].

1.4.3 Temporal expectation

Our sensory systems are consistently being exposed to a rich and rapidly changing scenery. To cope with the overwhelming amount of stimulation, we constantly generate and update expectations about critical events, such as the onset of behavioral relevant stimuli, in order to optimize our interaction with unfolding sensory stimulation. Temporal anticipation has been generally studied by manipulating stimulus predictability through the hazard rate, which specifies the likelihood of a stimulus appearing, given it has not appeared so far. A long tradition of RT experiments has documented that RT decreases as the stimulus becomes more likely. These findings have been interpreted to show that observers implicitly learn to use changes in stimulus likelihood to change RTs[87–89]. And what are the underpinnings of the effects of temporal expectation on RT? Research in this field has revealed that the temporal prediction of events has pervasive effects in modulating perception and action[90].

The ability to extract temporal patterns and regularity of events has long been known to improve action preparation and

execution[90]. Early behavioral studies in humans have led to the general interpretation that stimulus predictability mainly changes the willingness of the subjects to respond[13,91]. A more recent study, using sequential sampling models to analyze the observed temporal expectation effects on task performance, showed that temporal prediction mainly affects the duration of non-decision processes[92]. In addition, electrophysiological recordings in monkeys revealed systematic changes in neural firing patterns as a function of temporal expectation in motor-related regions[89,93–97]. For instance, in primary motor cortex, neurons become more synchronized around the expected time of an imperative go-signal[93]; and in LIP, which has also been implicated in perceptual decision-making, saccade-related activity varies according to the evolving temporal conditional probability for the appearance of the task-relevant target[89,97]. Electroencephalography (EEG) and neuroimaging studies in humans have supported the interpretation that temporal expectancies modulate motor-related processes[e.g.,98–101].

However, the effects of temporal prediction are not confined to motor-related variables. The temporal certainty between events can modulate perceptual thresholds for detecting visual features[102,103] and increase perceptual processing[104–106], namely by improving the quality of sensory information, as revealed by a diffusion model-based analysis[106]. However, response criteria adjustments were also shown to be responsible for behavioral performance improvements[107]. Moreover, it has been demonstrated that perceptual judgments are enhanced by overt

rhythmic motor activity[108–112]. Electrophysiological recordings showed that temporal expectation modulates neuronal activity in the visual cortex of monkeys, namely in V1[113,114], V4[115], MT[116] and inferotemporal cortex (IT)[117], and in the primary auditory cortex of rats[118]. In humans, EEG and neuroimaging studies have also implicated sensory-related areas in temporal predictability[99,119,120].

As it is not yet clear how time perception is implemented in the brain, these studies demonstrate that there is also not a consensus about the impact of temporal expectation in modulating sensory processing and motor-related variables.

There has been the suggestion that the mechanisms that underlie temporal processing are also shared by perceptual decision-making processes[80,121,122]. Evidence has shown that time is represented in the form of a hazard function by the same type of neurons that represent a DV in area LIP[89,97]. In addition, the scalar property between the mean and SD of responses times is also predicted by diffusion models[123]. Interestingly, it was also proposed that time estimation can be explained by a bounded accumulation mechanism[80]. In future research, the use of properly designed tasks that allow manipulating independently the variables associated with the axes of perceptual decision-making (e.g., stimulus uncertainty) and time estimation (e.g., hazard rate), and evaluating how RT and accuracy are jointly modified, will give further insight about the relationship between perceptual and temporal processing.

1.5 Objectives and organization of the thesis

The present work has focused on the contributions of different sources of uncertainty in perceptual decision-making, in particular in the relationship between speed and accuracy.

In Chapters 2 and 3 we took a behavioral approach to investigate what accounts for the different degrees of SAT observed across behavioral studies. Our approach was to compare SAT in odor-guided decision tasks that would pose different sources of uncertainty for the brain. A first objective was to develop an olfactory task that would display a robust degree of SAT to be then compared to the previously described mixture categorization task[52]. Chapter 2 describes the behavioral tasks used to study this problem (odor identification and odor mixture categorization tasks) and how the data was analyzed. The behavioral results are presented in Chapter 3.

In Chapter 4 we used a modeling approach to study the computational mechanisms that underlie the behavioral changes observed in the odor identification task developed in the previous chapters.

In Chapter 5 we explored the role of temporal uncertainty in perceptual decision-making. More specifically we investigated the impact of the temporal expectation about stimulus onset on responses times and accuracy.

2 Odor identification and odor mixture categorization tasks

2.1 Introduction

Relationships between accuracy and speed of decision-making, or speed-accuracy tradeoffs (SATs), have been extensively studied in humans and other species including monkeys, rodents and insects[1,13,25,34,38,50–57]. However, the range of SAT observed varies widely across studies for reasons that are unclear. For example, reported increases in RT with increased difficulty of perceptual discrimination range from over 500 ms in humans[25] and monkeys[34] performing a RDMD task, to 100 ms in mice performing a visual contrast detection task[55], to less than 30 ms in rats performing an odor mixture discrimination task[52]. It is not known what accounts for such different degrees of SAT observed across different studies.

Motivation for speed vs. accuracy is thought to be a key parameter affecting SAT[59] and is a possible explanation for the differences observed across similar studies showing SAT of smaller[52] or larger[53,54] magnitudes. Two alternative possibilities are that longer SAT tradeoffs reflect neural mechanisms that are species-specific or sensory modality-specific. An additional possibility is that SAT differences arise from differences in the underlying computational requirements of different decision-making tasks[56]. Given that species, modality, task structure all vary across the different studies in question, these possibilities are not possible to distinguish from existing data.

Our strategy was to compare SAT in two behavioral tasks that were identical except for the nature of the stimuli that gives rise to

task difficulty. The first was an odor mixture categorization task[52] in which the difficulty was increased by making the stimuli closer to a decision or category boundary. The second was an odor identification task in which the difficulty was increased by lowering stimulus concentration. Thus, by having the same subjects performing two tasks that were different only for the set of stimuli, and by holding species, modality and motivation, we were in a condition that allowed us to test if SAT was dependent on the nature of the task.

In comparison with visual and auditory stimuli, odors are harder to control because of their intrinsic temporal dynamics[124]. Nevertheless, the use of automated olfactometers[52] has allowed a tight control of stimulus conditions, namely controlling precisely the time of odor delivery and guarantying the reproducibility of odor amplitude and time-course[125]. In addition, odor temporal profiles have been successfully used in models of the olfactory receptor neurons[124] (ORNs) and of the olfactory bulb[125] (OB) to predict physiological responses. In Chapter 4, we investigated the contribution of the odor temporal profiles on the observed behavioral data, showing that, in addition to vision and audition, odor-guided tasks are also suitable to study the relationship between time and choice in decision-making.

Below, we will depict the odor-guided behavioral tasks employed to study SAT and the analysis used to describe the data.

2.2 Animal subjects

Four Long Evans rats (200-250 g at the start of training) were trained and tested in accordance with European Union Directive 86/609/EEC and approved by Direcção-Geral de Veterinária (DGV) of Portugal. Rats were trained and tested on three different tasks: (1) a two-alternative choice odor identification task; (2) a two-alternative choice odor mixture categorization task[52]; and (3) a two-alternative choice "odor mixture identification" task. The same rats performed all three tasks and all other task variables were held constant. Each rat performed one session of 90-120 minutes per day (300–500 trials), 5 days per week for a period of ~120 weeks. Each task was tested independently in blocks of sessions numbering 10–20 for odor identification and mixture categorization tasks; 5–10 for odor mixture identification and categorization with lower contrast stimuli. Rats were pair-housed and maintained on a normal 12 hr light/dark cycle and tested during the daylight period. Rats were allowed free access to food but were water-restricted. Water was available during the behavioral session and for 20 minutes after the session at a random time as well as on non-training days. Water availability was adjusted to ensure animals maintained no less than 85% of *ad libitum* weight at any time.

2.3 Testing apparatus and odor stimuli

The behavioral apparatus for the task was designed by Z.F.M. in collaboration with M. Recchia (Island Motion Corporation, Tappan, NY). The behavioral control system (BControl) was developed by Z.F.M, C. Brody (Princeton University) in collaboration with A. Zador (Cold Spring Harbor Laboratory). The behavioral setup consisted of a box (27 x 36 cm) with a panel containing three conical ports (2.5 cm diameter, 1 cm depth)[52]. Each port was equipped with an infrared photodiode/phototransistor pair that registered a digital signal when the rat's snout was introduced into the port ("nose poke"), allowing us to determine the position of the animal during the task with high temporal precision. Odors were delivered from the center port and water from the left and right ports. Odor delivery was controlled by a custom made olfactometer[52] designed by Z.F.M.. During training and testing the rats alternated between two different boxes; the manifolds were changed every 2/3 days and the correspondence between odor valve and stimulus difficulty was not always the same.

The test odors were S-(+) and R-(-) stereoisomers of 2-octanol, chosen because they have identical vapor pressures and similar intensities. In the odor identification task, difficulty was manipulated by using different concentrations of pure odors, ranging from 10^{-4} to 10^{-1} (v/v) **(Fig. 2.1b)**. The different concentrations were produced by serial liquid dilution using propylene glycol (PG; 1,2-propanediol). Eight stimuli were

loaded in a different holder (Puradisc 13 Syringe Filter, 2.7 mm pore size, #6823-1327, GE Healthcare), joining in a symmetric manifold, about 10 cm from the odor port[52]. In the odor mixture categorization task, we used binary mixtures of these two odorants at different ratios, with the sum held constant: 0/100, 20/80, 32/68, 44/56 and their complements (100/0, etc.) **(Fig. 2.1a)**. Difficulty was determined by the distance of the mixtures to the category boundary (50/50), denoted as "mixture contrast" (e.g., 80/20 and 20/80 stimuli correspond to 60% mixture contrast). Choices were rewarded at the left choice port for odorant A (identification task) or for mixtures A/B > 50/50 (categorization task) and at the right choice port for odorant B (identification task) or for mixtures A/B < 50/50 (categorization task). In both tasks, a set of eight stimuli was randomly interleaved within the session. During testing, the probability of each stimulus being selected on a given trial was the same.

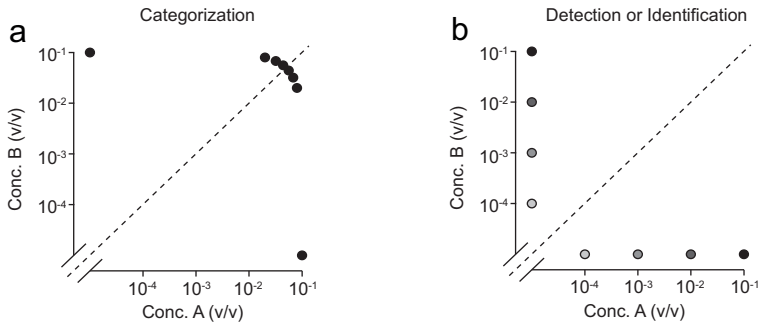

(Fig. 2.1 continues in the next page)

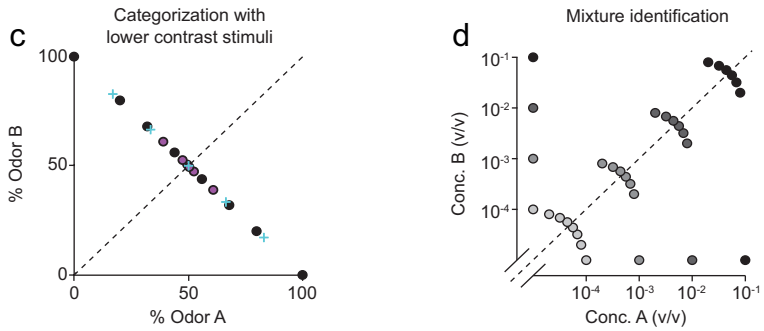

Figure 2.1 | Stimulus design for the different behavioral tasks
(a,b) Odor mixture categorization and odor identification tasks. In the mixture categorization task, two odorants, (S-(+)-2-octanol and R-(-)-2-octanol), were mixed in different ratios – 0/100, 20/80, 32/68, 44/56 and their complements – presented at a fixed total concentration of 10^{-1}, and rats were rewarded according to the majority component (a). In the odor detection or identification task, the same odorants were presented independently at concentrations ranging from 10^{-1} to 10^{-4} (v/v) and sides rewarded accordingly (b). Dot shading represents odor concentration, with highest concentration corresponding to the darkest shade. **(c)** Comparison between the different datasets used for the mixture categorization task. Black circles same as in (a). Blue crosses represent the set of stimuli with the following mixture ratios: 0/100, 17/83, 33.5/66.5, 50/50; magenta circles: 0/100, 39/61, 47.5/52.5, 49.5/50.5. **(d)** Odor mixture identification task. The same odorants were presented at different concentrations and in different ratios as indicated by dot positions. In each session, four different mixture pairs (i.e. a mixture of specific ratio and concentration and its complementary ratio) were pseudo-randomly selected from the total set of 16 mixture pairs and presented in an interleaved fashion.

Odor traces were measured using a photo ionization detector (mini-PID, Aurora Scientific, Inc). In Chapter 4 we will examine how much of the observed changes in the behavioral data can be explained by the odor temporal dynamics. For this analysis, the solvent used was mineral oil (MO) because, in contrast to MO, PG elicits a PID response, which didn't allow us to measure the actual trace corresponding to the different concentrations of odors. For each stimulus / odor valve, 50 trials were collected **(Fig. 2.2)**.

Figure 2.2 | PID signal for different odor concentrations
The PID signal was measured for the different concentrations of odorants used in the identification task. Error bars are mean ± SD (n = 400 traces). Scale bar: 500 ms. Each line corresponds to a different stimulus concentration (v/v): 10^{-1}, 10^{-2}, 10^{-3}, 10^{-4}, as indicated by color shading (highest concentration corresponding to the darkest shade). Stimulus onset (valve signal) corresponds in each case to the left-most edge of the trace.

For the experiments in **Figs. 3.1-3.4**, only mixtures with a total odor concentration of 10^{-1} were used **(Fig. 2.1a)**. For the experiment in **Fig. 3.5**, we used the same mixture contrasts with total concentrations ranging from 10^{-1} to 10^{-4} prepared using the diluted odorants used for the identification task **(Fig. 2.1d)**. In each session, four different mixture pairs were pseudo-randomly selected from the total set of 32 stimuli (8 contrasts at 4 different total concentrations). Thus, for this task, a full data set comprised 4 individual sessions. For the experiments in **Figs. 3.4a, b** we used two different sets of mixture ratios: 0/100, 17/83, 33.5/66.5, 50/50 in one experiment and 0/100, 39/61, 47.5/52.5, 49.5/50.5 in the second experiment **(Fig. 2.1c)**. In the experiment using 50/50 mixture ratios we used two filters both with the mixture 50/50, one corresponding to the left-rewarded stimulus and the other one

to the right-rewarded stimulus. Thus, for the 50/50 mixtures, rats were rewarded randomly, with equal probability for both sides.

2.4 Reaction time paradigm

The sequence and timing of task events is illustrated in **Fig. 2.3**. Rats initiated a trial by entering the central odor-sampling port, which triggered the delivery of an odor with delay (d_{odor}) drawn from a uniform distribution with a range of 300-600 ms. The odor was available for up to 1 s after odor onset. Rats could exit from the odor port at any time after odor valve opening, and make a movement to either of the two reward ports. Trials in which the rat left the odor sampling port before odor valve opening (4.2% of trials) or before a minimum odor sampling time of 100 ms had elapsed (1.1% of trials) were considered invalid. Odor delivery was terminated as soon as the rat exited the odor port. Odor sampling duration (OSD) was calculated as the difference between odor valve actuation until odor port exit (**Fig. 2.3b**).

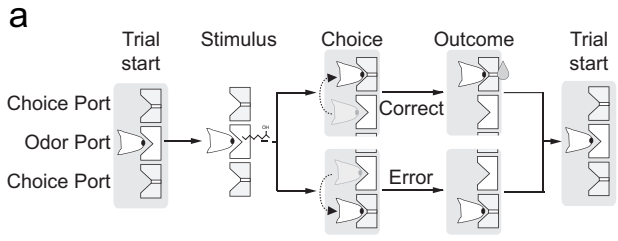

(Fig. 2.3 continues in the next page)

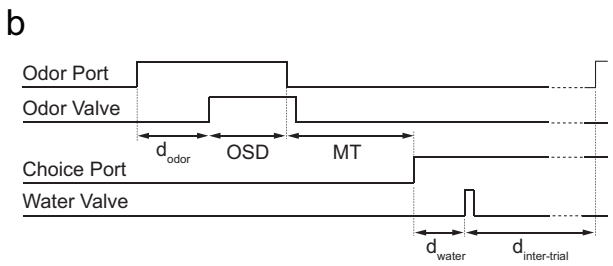

Figure 2.3 | Two-alternative odor choice task
(a) Sequence of events in a behavioral trial, illustrated using a schematic of the ports and the position of the snout of the rat. **(b)** Illustration of the timing of events in a typical trial. Nose port photodiode and valve command signals are shown (thick lines). Measurements of odor sampling duration (OSD) and movement time (MT), as well as imposed delays (d_{odor}, d_{water} and $d_{inter\text{-}trial}$) are indicated by arrows. Dashed lines indicate omitted time.

The stimulus onset delay (d_{odor}) was drawn from a uniform distribution between 300 and 600 ms, which creates a rising hazard rate (i.e., the probability that an event is likely to occur, given that it hasn't occurred already), hence increasing stimulus onset expectation during this period[56,107]. For comparison of low and high stimulus-expectation, two groups of trials were selected, an early onset, low stimulus-expectation condition, d_{odor} = 300-400 ms, and a late onset, high stimulus-expectation condition, d_{odor} = 500-600 ms. Analysis of OSD and accuracy for these two stimulus-expectation conditions were performed by conditioning OSD and accuracy on these two different time periods of d_{odor}. The CV was calculated as the ratio of the SD to the mean of OSD.

Movement time (MT) was defined as the difference between odor port exit and choice port entry time. For correct trials, water was delivered from gravity-fed reservoirs regulated by solenoid valves after the rat entered the choice port, with a delay (d_{water}) drawn

from a uniform distribution with a range of [0.1, 0.3] s. Reward was available for correct choices for up to 4 s after the rat left the odor sampling port. Trials in which the rat failed to respond to one of the two choice ports within the reward availability period (0.5% of trials) were also considered invalid. Reward amount (w_{rew}), determined by valve opening duration, was set to 0.024 ml and calibrated regularly. A new trial was initiated when the rat entered odor port, as long as a minimum interval ($d_{inter\text{-}trial}$), of 4 s from water delivery, had elapsed. Error choices resulted in water omission and a "time-out" penalty of 4 s added to $d_{inter\text{-}trial}$. Behavioral accuracy was defined as the number of correct choices over the total number of correct and incorrect choices.

The influence of previous rewards on the choice function of the rats was estimated by calculating the psychometric curve conditional on the presence of a reward in the preceding trial for each odor stimulus (odor A or odor B).

Choice bias was calculated as the difference between left ("A-side") and right ("B-side") choices divided by the total number of choices, averaged across all trials. This measures the overall tendency of the rats to go left (*Choice bias* > 0) or right (*Choice bias* < 0). The influence of reward and difficulty of previous stimuli on choice bias was estimated by calculating the choice bias for each current stimulus difficulty conditional on the previous reward and stimulus difficulty.

The three types of invalid trials (in total 5.8 ± 0.8% of trials, mean ± SEM, n = 4 rats) were not included in the calculation of

performance accuracy or reaction times (odor sampling duration or movement time).

2.5 Training

The training sequence consisted of: (I) handling (2 sessions); (II) water port training (1 session); (III) odor port training, in which a nose poke at the odor sampling port was required before water was available at the choice port. The required center poke duration was increased from 0 to 300 ms (4 – 8 sessions); (IV) introduction of test odors at a concentration of 10^{-1}, rewarded at left and right choice ports according to the identity of the odor presented (1 – 5 sessions); (V) introduction of increasingly lower concentrations (more difficult stimuli) (5 – 10 sessions); (VI) training on odor identification task (10 – 20 sessions); (VII) training on mixture categorization task (10 – 20 sessions). Testing was done afterwards.

During training, in phases V-VII, we used adaptive algorithms to adjust the difficulty and to minimize bias of the animals. We computed an online estimate of bias:

$$x_t = (1 - \lambda) r_t + \lambda x_{t-1} \qquad \textbf{(1.1)}$$

where x_t is the estimated bias in the current trial, x_{t-1} is the estimated bias in the previous trial, r_t is the choice of the current trial (0 if right, 1 if left) and λ is the decay rate (λ = 0.05 in our experiments). The probability of being presented with a right-side

rewarded odor $\alpha = p(s_t = right)$ was adjusted to counteract the measured bias using:

$$\alpha_{t+1} = 1 - \frac{1}{1 + e^{(x_t - x_0)/\beta}} \quad \textbf{(1.2)}$$

where x_0 is the target bias (set to 0.5), and β (set to 0.25) describes the degree of non-linearity.

Analogously, the probability of a given stimulus difficulty was dependent on the performance of the animal, i.e., the relative probability of difficult stimuli was set to increase with performance. Performance was calculated using **Equation 1.1** where x_t estimates the performance at the current trial and r_t is the outcome of the current trial (0 if error, 1 if correct). A difficulty parameter, δ, was adjusted as a function of the performance,

$$\delta_{t+1} = -1 + \frac{2}{1 + e^{(x_t - x_0)/\beta}} \quad \textbf{(1.3)}$$

where x_0 is the target performance (set to 0.95), and β (set to 0.25) describes the degree of non-linearity. The probability of each stimulus difficulty, $\gamma = p(s = s_i)$, was drawn from a geometric cumulative distribution function (GEOCDF, Matlab)

$$\gamma_{t+1} = \frac{1 - GEOCDF(i, |\delta_{t+1}|)}{\sum_{j=1}^{N} 1 - GEOCDF(j, |\delta_{t+1}|)} \quad \textbf{(1.4)}$$

where N is the number of stimulus difficulties in the session, and takes a value from 2 to 4 (when N = 1, i.e. only one stimulus

difficulty, this algorithm is not needed); i corresponds to the stimulus difficulty and is an integer from 1 to 4 (when $\delta > 0$, the value 1 corresponds to the easiest stimuli and 4 to the most difficult one, and vice-versa when $\delta < 0$). In this way, when $|\delta|$ is close to 0, corresponding to an average performance close to 0.95, the distribution of stimuli was close to uniform (i.e. all difficulties are equally likely to be presented). When performance is greater, then the relative probability of difficult trials increased; conversely, when the performance is lower, the relative probability of difficult trials decreased.

2.6 Statistical analysis

All the analysis was performed in Matlab® 2010a (7.10.0, The MathWorks, Inc). Psychometric and accuracy curves were fitted with a cumulative Weibull function using a maximum-likelihood procedure (FMINSEARCH, Matlab). OSD curves were fitted to a quadratic regression, for individual odors, and to a linear regression, for collapsed odors, using a least squares approach (NLINFIT, Matlab).

For **Fig. 2.2**, error bars are mean ± SD (n across number of PID traces). For **Fig. 3.1,** error bars are 95% confidence intervals (n across trials for **Figs. 3.1 a-d**; n across sessions for **Figs. 3.1 e-h**) calculated using a bootstrap procedure (BOOTCI, Matlab). For the remainder figures, error bars are mean ± SEM (n across rats, except for **Fig. 5.3**, n across trials).

To evaluate the dependence of OSD on stimulus difficulty, we used a one-way ANOVA (ANOVA1, Matlab) for the identification and categorization tasks and a two-way ANOVA (ANOVA2, Matlab) for the mixture identification task. The dependence of the CV on stimulus difficulty was evaluated using a one-way ANOVA. To assess the dependence of accuracy, OSD and CV for the different odor delay conditions, we used a two-way ANOVA. ANCOVA (AOCTOOL, Matlab) and post-hoc Tukey-Kramer (MULTCOMPARE, Matlab) tests were used to evaluate the linear relationship between OSD mean and OSD SD across the different odor delay conditions. The change in slopes of the linear regression between OSD and mixture contrast or odor concentration for the different odor delay conditions were assessed using a paired sample t-test (TTEST, Matlab). Differences were considered significant if $P < 0.05$.

3 Speed-accuracy tradeoffs in olfaction

3.1 Introduction

In this chapter, we summarize the behavior of the rats trained on the odor identification and mixture categorization tasks described in Chapter 2.

First, we characterized the behavior in terms of response accuracy and average reaction times (odor sampling duration, OSD) as a function of the stimulus parameters. In the last section, we investigated the impact of trial history on the animal's choice function.

3.2 Odor identification and odor mixture categorization tasks

We trained and tested Long Evans rats on two different two-alternative choice olfactory reaction time tasks that were similar except for the stimulus concentrations (**Figs. 2.1a, b and 2.3**). The first task was a previously studied odor mixture categorization task[52] in which two odors were presented at a fixed total concentration but in different ratios. The task difficulty was determined by the distance of the stimulus to the category boundary (50/50), denoted as "mixture contrast" (e.g., 56/44 and 44/56 stimuli correspond to 12% mixture contrast) (**Fig. 2.1a**). The second task was an odor identification task in which only one of the two odors was presented on a given trial, but difficulty was increased by diluting odors over a range of three log steps (1000-fold) (**Fig. 2.1b**). To quantify reaction time, we used the odor

sampling duration (OSD) (**Fig. 2.3b**) – throughout the thesis, OSD and RT will be used interchangeably. In a given session, eight randomly interleaved stimuli from one of the two tasks were presented. Critically, to ensure that any differences in performance were due to the manipulated stimulus parameters, all comparisons were done using the same rats performing the two tasks on different days with all other task variables being held constant.

We observed a strong dependence of performance accuracy on both mixture contrast and stimulus concentration (representative session, **Fig. 3.1a, c**; representative rat, **Fig. 3.1e, g**; all rats, **Fig. 3.2a, c**). As described previously[52], for the mixture categorization task, RTs showed a small and not significant increase from the easiest to the most difficult stimuli (31 ± 18 ms; mean ± SEM, n = 4 rats; $F(3,12) = 1.14$, $P > 0.2$, ANOVA; representative session, **Fig. 3.1b, d left**; representative rat, **Fig. 3.1f, h left**; all rats, **Fig. 3.2b, d left**). In contrast, for the same animals performing the identification task, RTs increased much more substantially (108 ± 29 ms; $F(3,12) = 7.77$, $P < 0.005$; representative session, **Fig. 3.1b, d right**; representative rat, **Fig. 3.1f, h right**; all rats, **Fig. 3.2b, d right**).

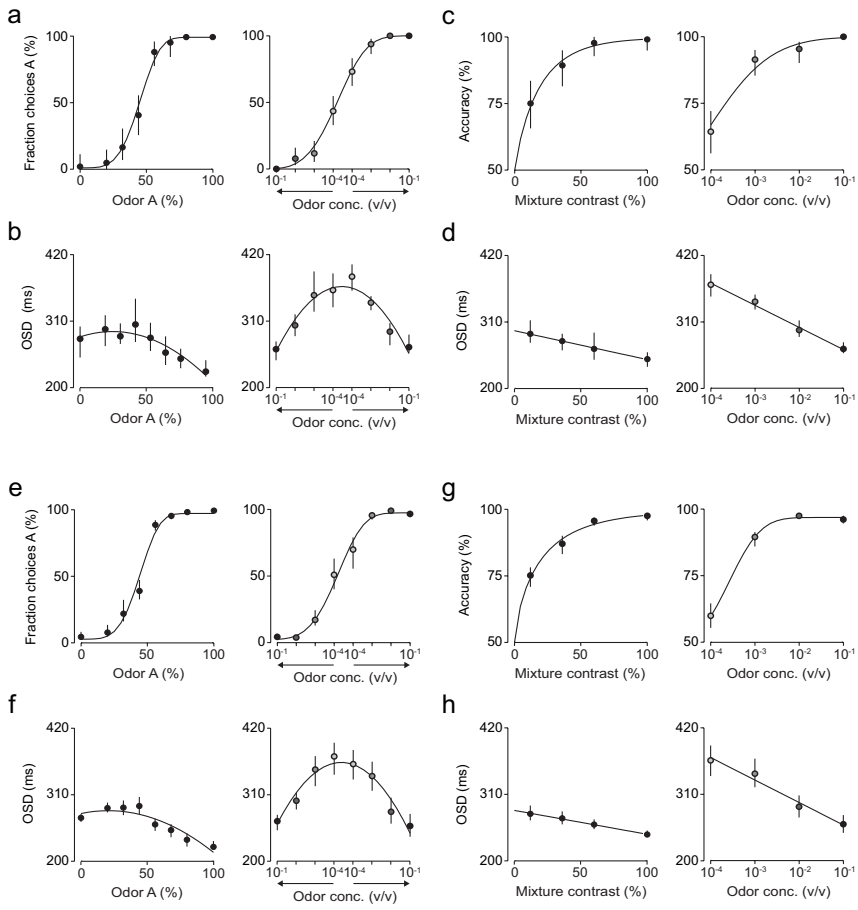

Figure 3.1 | Comparison between odor mixture categorization and odor identification tasks – session and rat data

(a-d) Data from a representative session. **(a)** Psychometric curve in discriminating S-(+)-2-octanol from R-(-)-2-octanol as a function of odor percentage in the mixture (a, left) or odor concentration (a, right). Dot shading represents odor concentration, with highest concentration corresponding to the darkest shade. **(b)** Median odor sampling duration (OSD) plotted as a function of odor percentage in the mixture (b, left) or odor concentration (b, right). **(c)** Accuracy as a function of mixture contrast (c, right) or odor concentration (c, left). Mixture contrast is defined as the absolute percent difference between the two odors (i.e. the pair 100/0 and 0/100 yield 100% contrast, 80/20 and 20/80 yield 60% contrast and so on). **(d)** Median OSD plotted as a function of mixture contrast (d, right) or odor concentration (d, left). Error bars are 95% bootstrap confidence intervals (n across trials, 367 and 562 trials for categorization and identification, respectively). **(e-h)** Data from a representative rat. **(e)** Mean psychometric curve as a function of odor percentage in the mixture (e, left) or odor concentration (e right). **(f)** Mean of median OSD plotted as a function of odor percentage in the mixture (f, left) or

odor concentration (f, right). **(g)** Mean accuracy as a function of mixture contrast (g, right) or odor concentration (g, left). **(h)** Mean of median OSD plotted as a function of mixture contrast (h, right) or odor concentration (h, left). Error bars 95% bootstrap confidence intervals (n across sessions, 14 and 13 sessions for categorization and identification, respectively).

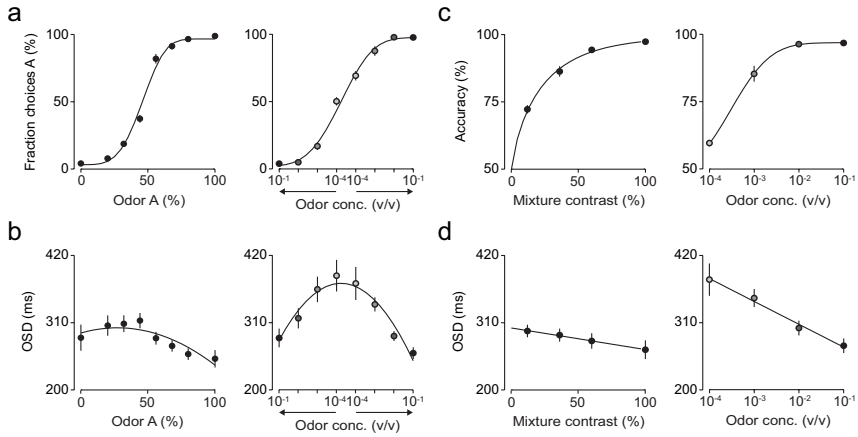

Figure 3.2 | Comparison between odor mixture categorization and odor identification tasks – population data
(a) Mean psychometric curve in discriminating S-(+)-2-octanol from R-(-)-2-octanol as a function of odor percentage in the mixture (a, left) or odor concentration (a, right). Dot shading represents odor concentration, with highest concentration corresponding to the darkest shade. **(b)** Mean of median OSD plotted as a function of odor percentage in the mixture (b, left) or odor concentration (b, right). **(c)** Mean accuracy as a function of mixture contrast (c, right) or odor concentration (c, left). **(d)** Mean of median OSD plotted as a function of mixture contrast (d, right) or odor concentration (d, left). Error bars are mean ± SEM (n = 4 rats).

Movement times did not vary significantly with difficulty in either task (categorization, $F(3,12) = 0.05$, $P > 0.8$; identification, $F(3,12) = 0.23$, $P > 0.8$, ANOVA; **Fig. 3.3**).

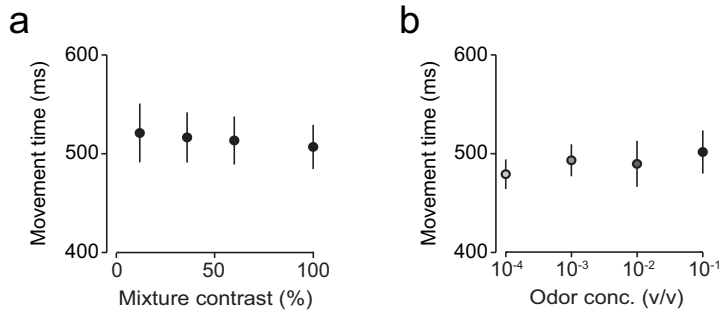

Figure 3.3 | Movement time for odor mixture categorization and odor identification tasks
(a,b) Mean of the median movement time plotted as a function of mixture contrast (a) or odor concentration (b). Dot shading represents odor concentration, with highest concentration corresponding to the darkest shade. Error bars are mean ± SEM (n = 4 rats).

In order to control for the possibility that a slightly smaller range of performance accuracy for the categorization task accounted for differences in SAT, we re-ran this task with two sets of stimuli with wider ranges of mixture contrasts including harder, lower contrast stimuli (**Fig. 2.1c**). This yielded a range of accuracies as broad as those in the identification task (**Fig. 3.4a)**. The change in OSD across all difficulties was 39 ± 25 ms and 48 ± 19 ms for the two datasets tested (**Fig. 3.4b)**, slightly higher than the one observed for the original categorization dataset, yet still much smaller than the OSD change for identification (**Figs. 3.4c, d**). Therefore, the difference observed in SAT for odor identification vs. mixture categorization was not due to differences in the range of task difficulties.

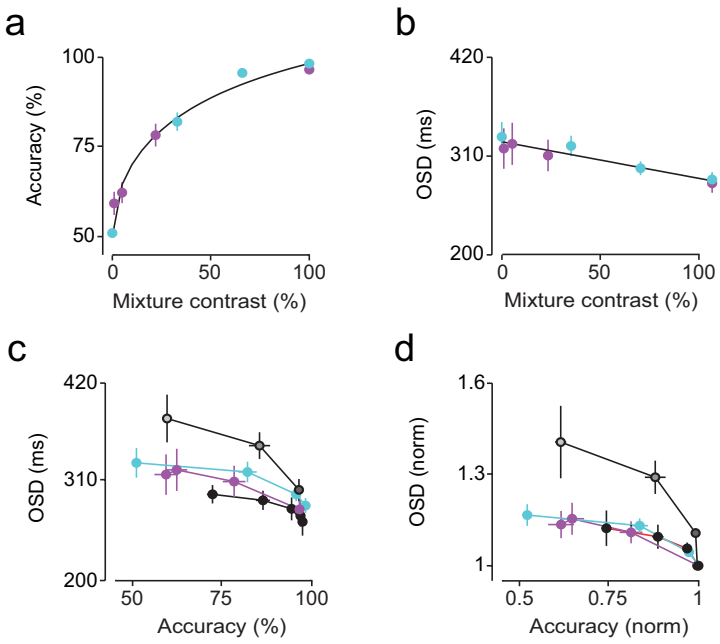

Figure 3.4 | Odor mixture categorization with lower contrast stimuli
(a) Mean accuracy **(b)** and mean of median odor sampling duration (OSD) plotted as a function of mixture contrast. Blue circles represent the set of stimuli: 0, 33, 66, 100% contrast; magenta circles: 1, 5, 22, 100% contrast. These sets of stimuli were run in different sessions. For the first dataset (blue circles), OSD showed an increase of 48 ± 19 ms, from 283 ± 8 to 331 ± 17 ms, from the easiest to the most difficult stimuli ($F(3,12) = 3.61$, $P = 0.046$, one-way ANOVA); for the second dataset (green circles), OSD increased by 39 ± 25 ms, from 279 ± 11 to 318 ± 23 ms ($F(3,12) = 1.17$, $P > 0.3$, one-way ANOVA). **(c)** Mean of median OSD as a function of mean accuracy. Dot shading represents odor concentration, with highest concentration corresponding to the darkest shade; black circles represent the set of stimuli: 12, 36, 60, 100% contrast; blue and magenta circles are the same as in (a,b). **(d)** Normalized mean of median OSD as a function of normalized mean accuracy. Error bars are mean ± SEM (n = 4 rats).

3.3 Odor mixture identification task

Because identification and categorization tasks were run in separate sessions, we also considered the possibility that rats might shift their decision criteria between tasks. To address this,

and to cover the stimulus space more thoroughly, we devised a "mixture identification" task in which we interleaved the full set of stimuli from the categorization and identification tasks as well as intermediate mixtures (**Fig. 2.1d**). Thus, on each trial the stimulus was chosen randomly from one of four mixture ratios at one of four concentrations. Consistent with the previous observations, reaction times in this joint task were strongly affected by concentration but not by mixture contrast (**Figs. 3.5b-d**). A two-way ANOVA showed that OSD changed significantly across the different odorant concentrations ($F(3,48) = 17.68$, $P < 10^{-7}$); but for a given total concentration of the odorants, this change was not significant across the different mixture contrasts ($F(3,48) = 1.47$, $P = 0.2$). There was no significant interaction of odorant concentration and mixture contrast ($F(9,48) = 0.18$, $P > 0.9$).

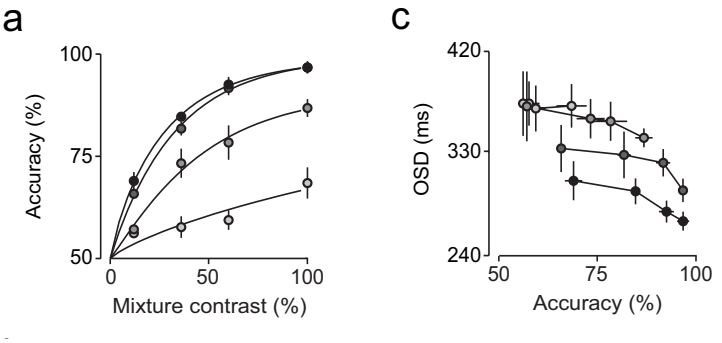

(Fig. 3.5 continues in the next page)

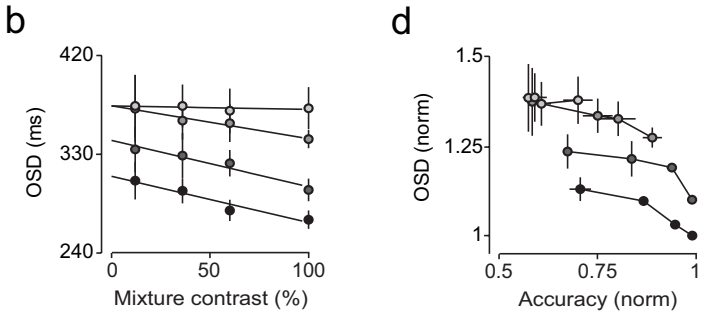

Figure 3.5 | Odor mixture identification task
(a,b) Mean accuracy (a) and mean of median odor sampling duration (OSD) (b) plotted as a function of mixture contrast. **(c)** Mean of median OSD plotted as a function of mean accuracy. **(d)** Normalized mean of median OSD plotted as a function of normalized mean accuracy. Each point represents a single mixture ratio. Dot shading represents odor concentration, with highest concentration corresponding to the darkest shade. Error bars are mean ± SEM (n = 4 rats).

3.4 Trial-by-trial learning

The results from the previous sections are consistent with the idea that low concentration and low mixture contrast create independent sources of uncertainty. We hypothesized than in odor identification, accuracy is limited by stimulus uncertainty whereas in mixture categorization, accuracy is limited by variability arising from the constant updating of the category boundary based on the outcome of previous trials. Given this hypothesis, we investigated whether ongoing learning has a different influence on the choice of animals in identification and categorization.

In both tasks there was a clear trial-by-trial updating of the animal's choice function, i.e., after a correct trial, the choice was biased towards the side that had been rewarded in the previous trial (**Fig. 3.6a**).

We next asked whether this trial-by-trial learning also depended on the difficulty of the previous trial. We observed that, after a correct trial, in the categorization task choice bias increased with the difficulty of the previous trial (**Fig. 3.6c, left**), whereas in identification this bias was dependent only on choice side (**Fig. 3.6c, right**).

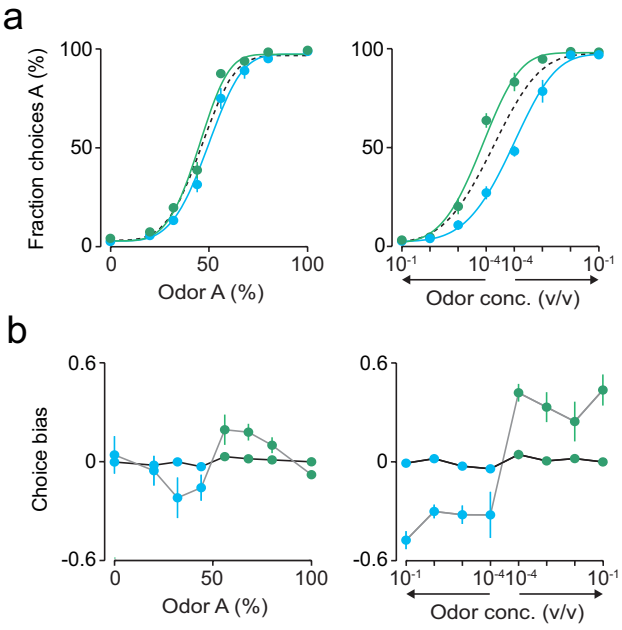

Figure 3.6 | Trial-by-trial learning
(a) Mean psychometric curve as a function of odor percentage in the mixture (left) or odor concentration (right) after a correct trial. Green and blue correspond to odor A and odor B-rewarded stimuli, respectively. Dashed line corresponds to the mean psychometric function. **(b)** Choice bias as a function of previous odor percentage in the mixture (left) or odor concentration (right) after a correct response for easy (100% contrast or 10^{-1} concentration; black curve) and hard (12% contrast or 10^{-4} concentration; gray curve) current stimuli. Corrected for average bias. Error bars are mean ± S.E.M (n = 4 rats).

3.5 Discussion

These results demonstrate the existence of robust SAT in rats when task difficulty was increased by lowering concentration. This change was much larger compared to that observed when difficulty was increased by decreasing the distance of stimuli from the response category boundary. Thus, holding other parameters (species, modality, motivation, etc.), SAT was dependent on the nature of the task, as defined here by the set of stimuli. When the two tasks were combined, the two manipulations interacted linearly with respect to RT, consistent with the idea that low concentrations and low mixture contrast pose independent sources of uncertainty.

In both tasks, choice behavior depended partly on reward history, as shown recently for mice performing a visual contrast detection task[7]. However, whereas in odor identification choice bias was only dependent on previous side and outcome, for mixture categorization this bias was also modulated by the difficulty of the previous stimulus. These biases might generate fluctuations in the internal decision criterion, useful in initial learning but suboptimal in a task with fixed categories[7,126,127]. How are these priors incorporated into the developing decisions? We hypothesize that for categorization, this trial-by-trial learning leads to a continual updating of the category boundary, i.e., the mapping of the stimulus to the appropriate response, which we believe is the dominant source of uncertainty in this task. Because this mapping can only be improved when reinforcement is given after a trial, prolonged stimulus sampling on a single trial is

ineffective at improving performance[56]. On the other hand, for odor identification, although ongoing learning leads to a choice bias towards the rewarded side, we believe accuracy is limited by rapid (millisecond-by-millisecond) fluctuations in the firing of sensory neurons that can be mitigated by integration[25,34,37], and that the increase in RTs is due to the reduced amount of odor information at lower concentrations. Our results are therefore consistent with our initial hypothesis that SAT is dependent on the nature of the task, suggesting that the problem of identifying an odor at low concentrations and the problem of distinguishing closely related odors make very different demands for the brain.

In the last two chapters, we described the behavioural approach taken to investigate why the range of SAT varies widely across studies. By comparing two behavioural tasks that were identical except for the stimuli that gave rise to task difficulty, we proposed that SAT is dependent on the nature of task.

In the next chapter, we will focus on the task that showed the higher degree of SAT – the identification task – and by taking a modelling approach, we will investigate the underlying computational mechanisms that might explain the changes observed in response time and choice behavior.

4 A modeling approach for the study of the identification task

4.1 Introduction

In Chapter 3 we showed that for a similar level of difficulty, identifying odors at low concentrations requires a much larger increase in stimulus sampling time than does discriminating similar mixtures, even when species, modality and motivation are controlled for.

In Chapter 4, by taking a modeling approach, we want to investigate the computational mechanisms that might account for the changes in RT and response accuracy observed in the task with the higher degree of SAT – the identification task.

Integrator or accumulator models, such as the drift-diffusion model (DDM), have been used to explain a wide range of response time and choice behavior data in species from primates[25,128] to insects[36]. The DDM posits that decisions are made when a decision variable (DV), whose drift rate reflects the accumulating evidence and that has some internal noise, reaches a response bound[18,37,62,129,130]. The drift rate is proportional to the strength of the evidence but noise gives rise to variability in the response even upon repeated presentation of the identical stimulus.

Despite the general use of integrator models to describe RT and choice behavior, it was shown that integration is not the only operation that can be used in decision-making processes, and different operations have also been applied and suggested[131–134].

Namely, an exhaustive modeling study focused on the RDMD task, which has been widely modeled as accumulation of sensory information to a bound[25,47], revealed that this task can be explained by a variety of models, including ones without temporal integration[131]. This indicates that identifying a computational mechanism that can account for a particular dataset does not automatically mean that it is the only one that could explain the data. In addition, this study also showed that a standard DDM was incompatible with the observed RT distributions, calling for additional components and parameters in the DDM in order to be able to explain the distributions[131].

To investigate the computational mechanisms underlying the behavior in the identification task, we used a modeling strategy where we took the DDM framework as a starting point and implemented a flexible model structure that allowed us to explore different mechanisms. These different mechanisms were implemented by changing the combination of components active in the model: temporal integration, 'noise', and variability in non-decision time. This allowed us to explore which combinations of model features were able to describe the data from the identification task and which components of the model were well constrained by the data.

Another important objective of this approach was also to evaluate the contribution of the odor's temporal dynamics on the observed behavioral changes. For that, a time-varying input described by

the measured odor waveforms was also considered as a component of the model.

Finally, we wanted to investigate how sniffing dynamics, namely inhalation variability, influences the model predictions. Although sniffing hasn't been measured in the identification task, a previous study reported that sniff frequency does not change as task difficulty is increased by lowering odorant concentration[135]. Moreover, it was shown that the rate of respiration in an olfactory discrimination task, similar to the categorization task used here, increases before rats enter the odor sampling port, going from a low frequency (2-4 Hz) mode before entry, to a high-frequency (6-9 Hz) mode during odor sampling[135]. This change in sniff frequency was mainly attributed to a truncation of exhalation periods[135]. Here, we looked at the impact of inhalation variability by adding variance to the starting time of stimulus sampling, and by testing different durations of exhalation periods.

In this chapter, we start by describing the modeling approach used to investigate the computational mechanisms underlying the behavior in the identification task (**4.1 Modeling framework approach**), and after that, we present the model fitting results and predictions (**4.2 Model fitting results**).

4.2 Modeling framework approach

4.2.1 The diffusion model framework

The basis structure of the model implemented here was grounded on the bounded DDM[25], which has been applied to several datasets to explain choice behavior and response time[25,36,128].

In the diffusion model, evidence in favor of stimuli S_A and S_B is accumulated over continuous time until an upper or lower bound is reached (A or $-B$), which triggers a response, R_A or R_B. The expected rate at which evidence accumulates is determined by the drift rate μ and the expected rate of growth of the variance of the evidence by the squared diffusion coefficient σ^2. Bias toward one or the other response can be represented by the relative values of the bounds A and B.

In a discrete time version of this process, the momentary evidence, e, gathered in each time step Δt, is drawn from a Gaussian distribution with mean and variance of $\mu\Delta t$ and $\sigma^2\Delta t$, respectively. Thus, the accumulated evidence, termed the decision variable, DV, at time $t = n\Delta t$, is given by:

$$DV(n\Delta t) = \sum_{i=1}^{n} e_i \qquad \textbf{(4.1)}$$

The process terminates when the DV reaches the upper or lower decision bound. The bound reached first by the accumulated evidence determines the choice, and the decision time, t_D, is

determined by how long it takes to reach that bound. Response time is a combination of this decision time and an additional non-decision time, t_{ND}, which accounts for any non-decision-related delays (sensory delays, motor preparation, etc.).

In this model, three assumptions were made. First, the drift rate was assumed to be the only parameter affected by stimulus strength, x, and was determined by:

$$\mu = sign(x)|kx|^{\beta} \quad \textbf{(4.2)}$$

where k is a measure of sensitivity and β a scaling exponent[25]. The sign function is defined as -1 if $x < 0$ and 1 if $x > 0$. Second, no response bias was assumed, thus $A = B$. And third, the noise defined by the diffusion coefficient σ was assumed to be constant for all conditions and set to 0.1. In summary, the model parameters were the following: bound A, sensitivity k, scaling exponent β and mean non-decision time t_{ND}.

The structure described above constitutes the basis of the model used in this study and upon which the different model variants were implemented by changing the combination of components active in the model (temporal integration, 'noise' and variability in non-decision time) and the type of input (constant or time-varying). In the next section, we describe the different variants of the model.

4.2.2 Variants of the model

The different model variants were characterized by different combinations of the following features:

1) Stimulus strength, x. For a given concentration, the stimulus strength could be: 1) constant, as in the DDM described above; 2) time-varying, being described by an exponential function which corresponds to the best-fit curve of the mean of the odor time-courses (**Fig. 4.1**; exponential function, $C(1-e^{-t/\tau})$, least-squares procedure, FMINSEARCH, Matlab); or 3) time-varying, being described, on each trial, by a single-trial odor time-course.

2) 'Noise', diffusion coefficient, σ. The diffusion coefficient was a constant that and could be: 1) different from zero, as in the DDM; or 2) equal to zero.

3) Temporal integration. There could be: 1) temporal integration, by accumulating evidence, as in the DDM; or 2) no temporal integration, by comparing directly the evidence to the bound.

4) Non-decision time, t_{ND}. The non-decision time could be: 1) constant; or 2) variable, following a Gaussian distribution[131,136]. In the latter case, the SD of the non-decision time distribution was also a free parameter of the model.

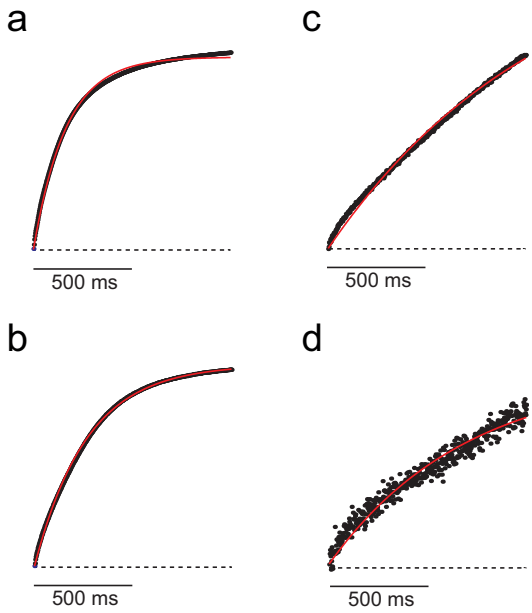

Figure 4.1 | Exponential fit of the odor temporal profiles for different concentrations
(a-d) Mean PID signal for the different concentrations of odorants (v/v) used in the identification task: 10^{-1} (a), 10^{-2} (b), 10^{-3} (c) and 10^{-4} (d). Red line corresponds to the fit to an exponential function, $y = C(1 - e^{-t/\tau})$.

Figure 4.1 illustrates the general structure of the model and **Table 4.1** summarizes the different model variants.

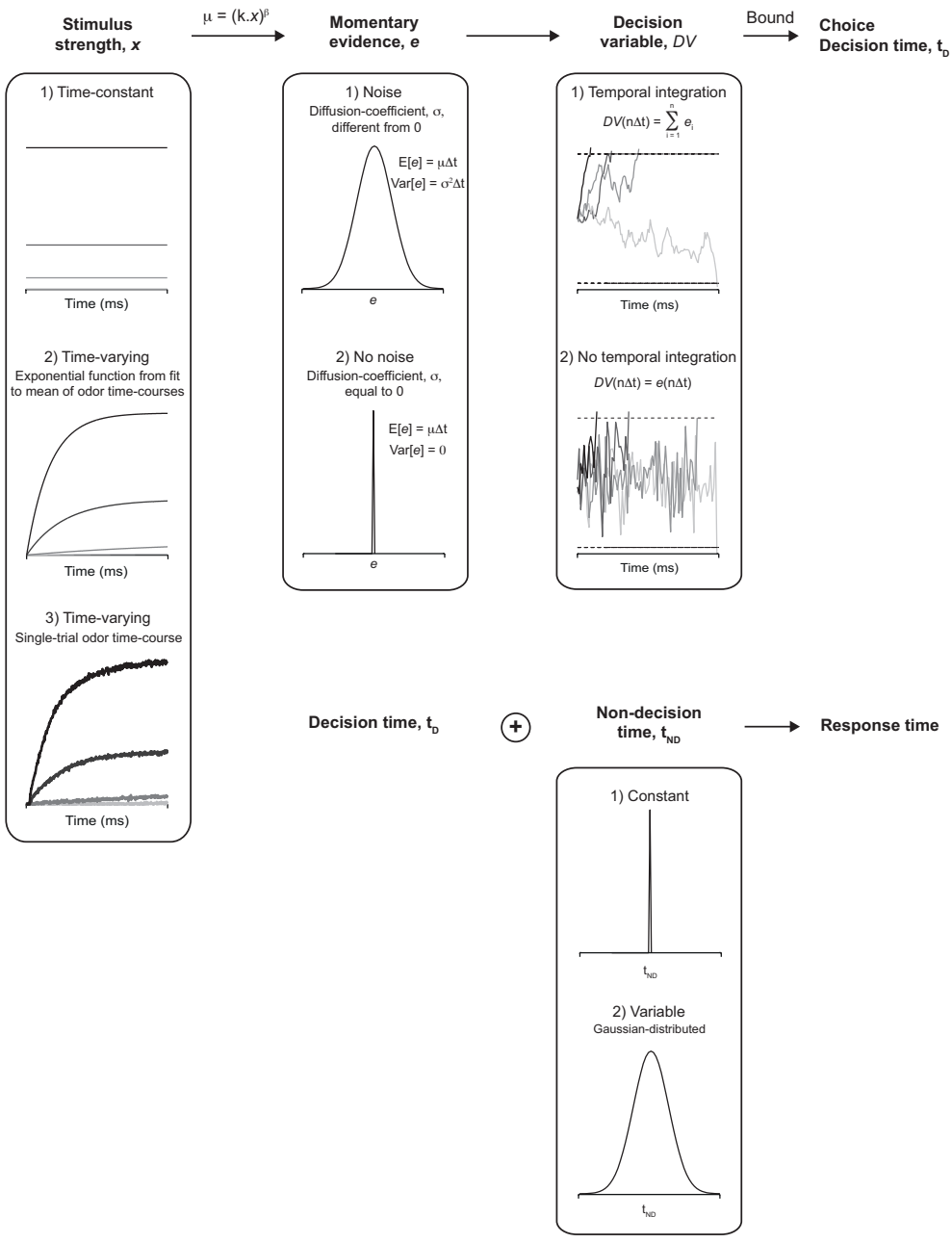

Figure 4.2 | Model structure
Structure of the model used to fit the behavioral data from the identification task. The details of the model were described in **4.2.1 The diffusion model framework** and **4.2.2 Variants of the model**.

Table 4.1 | Model variants used to fit the behavioral data from the identification task

Model #	Stimulus strength	Diffusion coefficient	Temporal integration	Non-decision time
1	Constant	0.1	Yes	Fixed
2	Time-varying PID-fit	0.1	Yes	Fixed
3	Constant	0.1	No	Fixed
4	Time-varying PID-fit	0.1	No	Fixed
5	Constant	0	Yes	Fixed
6	Time-varying PID-fit	0	Yes	Fixed
7	Time-varying PID-fit	0	No	Fixed
8	Time-varying Single trial PID trace	0	No	Fixed
9	Constant	0.1	Yes	Gaussian
10	Time-varying PID-fit	0.1	Yes	Gaussian
11	Constant	0.1	No	Gaussian
12	Time-varying PID-fit	0.1	No	Gaussian

Accuracy and RTs were generated by running numerical simulations of the models described above.

Model 1 also has analytical solutions for response accuracy P_C, mean RT t_T and variance of RTs VAR[25], which are respectively:

$$P_c(\mu) = \delta \frac{1}{1 + e^{-2A'\mu'}} \tag{4.3}$$

$$t_T(\mu) = \frac{A'}{\mu'} \tanh(A'\mu') + t_{ND} \tag{4.4}$$

$$VAR[T_t(\mu)] = \frac{A'[\tanh(A'\mu') - A'\mu' \sec h(A'\mu')^2]}{\mu'^3} \tag{4.5}$$

where A' and μ' are the bound and drift rate normalized by the diffusion coefficient, and δ is the empirically determined fraction of correct choices for the easiest concentration, 10^{-1} (0.97, mean across 4 rats).

For Model 7, the analytical solution for the decision time t_D was derived as follows. The mean of the odor time-courses was fit to a single-exponential, $C(1 - e^{-t/\tau})$. For a stimulus strength x described by a single-exponential, according to **Eq. 4.2** the drift rate μ is given by

$$\mu = \left[kC(1 - e^{-t/\tau}) \right]^{\beta} \tag{4.6}$$

Since in Model 7 the diffusion coefficient was set to 0 and there is no temporal integration, the evidence is equal to the values of the drift rate for the different time steps, and the decision time is then

determined by the time t at the which the values of the drift rate cross the bound A. Therefore, by setting $\mu = A$, and replacing t by t_D, we get the following expression:

$$A = \left[kC(1 - e^{-t_D/\tau})\right]^{\beta} \tag{4.7}$$

By solving this equation for t_D, the analytical solution for the decision time as a function of odor stimulus, here defined by C and τ, is the following:

$$t_D(C,\tau) = -\tau \ln\left(1 - \frac{A^{1/\beta}}{kC}\right) \tag{4.8}$$

4.2.3 Model fitting

Accuracy and mean RT, calculated from the pooled data of all sessions from all rats ('super-rat'), were simultaneously fit to the accuracy and mean RT functions given by **Eqs. 4.3 and 4.4** using a maximum likelihood procedure[25]. For mean response time, the relevant distribution is the sampling distribution of the sample mean, rather than the sample distribution across individual trials. According to the Central Limit Theorem, the sampling distribution of the sample mean has a Gaussian distribution for asymptotically large samples. It can be described by the predicted mean RT $t_T(\mu)$ and predicted standard error of the mean, $\sigma_{\bar{t}} = \sqrt{VAR[T_T(\mu)/n]}$, where VAR is the predicted variance and n is the number of trials. Given this Gaussian approximation, the

likelihood L_T of the observed mean RT $\bar{t}_T(\mu)$, given the predicted mean response times $t_T(\mu)$, is

$$L_T = \frac{1}{\sigma\sqrt{2\pi}} e^{-[t_T(\mu)-\bar{t}_T(\mu)]^2 / (2\sigma_{\bar{t}}^2)} \tag{4.9}$$

For accuracy, we assume the probability of observing r correct choices out of n trials obeys the binomial distribution. Thus, the likelihood L_P of the observed proportions of correct responses r/n given the predicted proportion correct P_C is

$$L_P(x) = \frac{n!}{r!(n-r)!} P_C(x)^r (1 - P_C(x))^{n-r} \tag{4.10}$$

The log likelihoods were summed over stimulus strength conditions to produce a combined log likelihood of

$$\ln(L) = \sum_x \ln[L_T(x)] + \ln[L_P(x)] \tag{4.11}$$

which was maximized by iteratively adjusting the model parameters (FMINSEARCH, Matlab).

RT distributions and SD predictions were generated by running a numerical simulation of the DDM, which corresponds to Model 1 from **Table 4.1**, using the resulting best-fit parameter values.

For the fit of RT mean and variance, **Eqs. 4.4 and 4.5** were used, and a maximum likelihood procedure was also applied. For the

variance of RTs, the relevant distribution is the sampling distribution of the sample variance. Under the assumption that the samples are drawn from a normal distribution, $VAR[T_T(\mu)] \times (n-1) \Big/ VAR[T_T(\mu)]$ follows a Chi-square distribution with *(n-1)* degrees of freedom. Given this approximation, the likelihood L_{VAR} of $z = VAR[\bar{T}_T(\mu) \times (n-1)] \Big/ VAR[T_T(\mu)]$ is given by:

$$L_{VAR} = \frac{z^{n-3/2} \exp(-z/2)}{2^{(n-1)/2} \Gamma[(n-1)/2]} \qquad \textbf{(4.12)}$$

where $\Gamma(.)$ is the Gamma function.

The log likelihoods were summed over stimulus strength conditions to produce a combined log likelihood of

$$\ln(L) = \sum_x \ln[L_T(x)] + \ln[L_{VAR}(x)] \qquad \textbf{(4.13)}$$

which was maximized by iteratively adjusting the model parameters.

RT distribution predictions were generated by running a numerical simulation of the DDM (Model 1), using the resulting best-fit parameter values.

Accuracy and mean RTs were fitted to the Models 2-7 described in **Table 4.1** using a least-squares approach (FMINSEARCH, Matlab).

The goal of Model 8 was to examine if the changes observed in the identification task, particularly for the RTs, could be solely explained by the trial-by-trial odor dynamics. Therefore, to allow the model to try to explain as best as possible the RT data, only mean RT was fit to this model; accuracy was predicted using the resulting best-fit parameter values.

The objective of Models 9-12 was to investigate the contribution of variability in non-decision times to explaining the RT distributions. For that, we fitted the SD of RTs to Models 9-12, where the parameters A (bound), k (sensitivity), β (scaling exponent) and t_{ND} (mean non-decision time) were fixed and set to the best-fit parameter values from Models 1-4, respectively, and the only free parameter was the SD of the Gaussian distribution for non-decision times. A least-squares approach (FMINSEARCH, Matlab) was used. Accuracy, RT distributions, and mean RT predictions were generated using the resulting best-fit parameter values.

4.2.4 Inhalation variability

We tested the influence of inhalation (sniffing) variability by running a simulation with Model 8, using the resulting best-fit parameter values from this model, but where the time for the

beginning of stimulus sampling was given by a uniform distribution ranging from 0 to v. We ran this simulation for the following values of v: 50, 150 and 250 ms; these values were chosen based on the duration of exhalations during an olfactory task (Fig. 5c, d from reference [135]). Stimulus values below the sampled time for inhalation were set to zero.

4.3 Model fitting results

This section is divided into three sub-sections. In the first sub-section (**4.3.1 Fitting mean reaction time and accuracy**), we used Models 1-8 (see **4.2.2 Variants of the model**) to fit response accuracy and mean RT and to predict RT distributions. We observed that even the models that matched the data for accuracy and mean RT were incompatible with the RT distributions. In the second sub-section (**4.3.2 An attempt to capture the reaction time distributions**), we focused on this issue and we explored two different approaches to try to capture the RT distributions. Finally, given that odor stimuli are only sampled during the inhalation phase of sniffing, we investigated the impact of incorporating inhalation variability into the model (**4.3.3 Inhalation variability**).

4.3.1 Fitting mean reaction time and accuracy

Our first approach was to confirm that the DDM could capture the choice behavior and response times from the identification task, as shown for many other datasets[e.g.,25,36,128]. For that, first we fitted the accuracy and mean RT to the analytical expressions for the psychometric and chronometric functions (**Eqs. 4.3 and 4.4,** respectively[25]), and we observed that the DDM provided a good match to the behavioral data (**Fig. 4.3d, e**). Next, we ran the corresponding numerical simulation of this model (Model 1, **Fig. 4.3a-c**) with the resulting best-fit parameter values (**Table 4.2**). This confirmed the fits from the analytical solutions for accuracy and mean RT (**Fig. 4.3d, e**) and allowed us to predict the RT distributions (**Fig. 4.3g**) and respective SD (**Fig. 4.3f**).

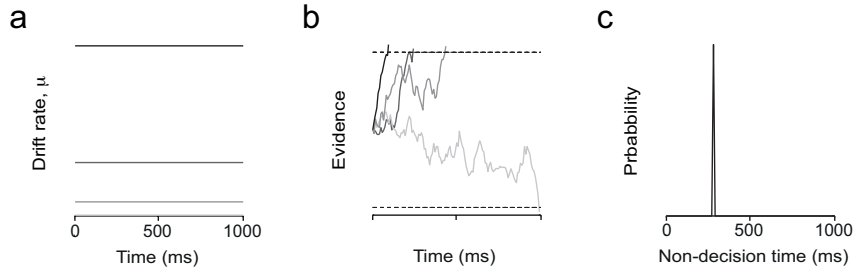

(Fig. 4.3 continues in the next page)

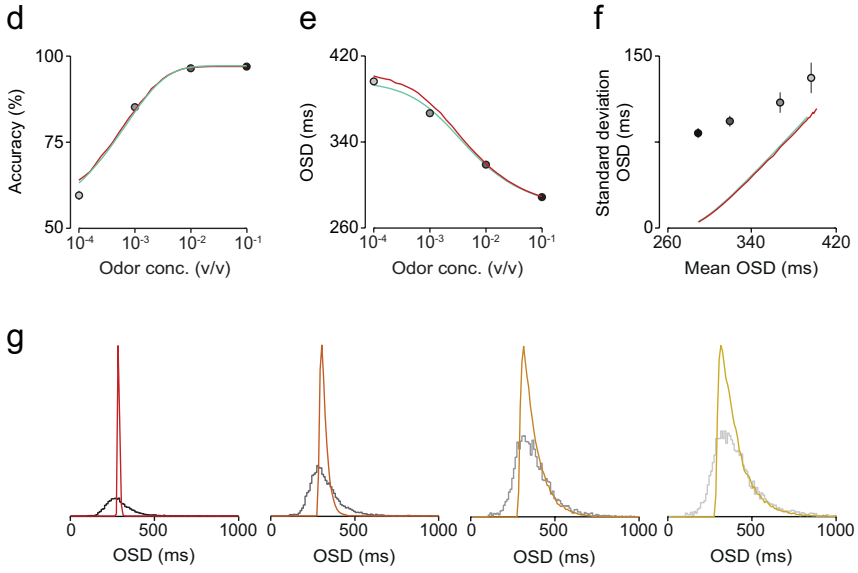

Figure 4.3 | Drift-diffusion model with constant input (Model 1)
(a-c) Model components: Drift rate (a) and evidence (b) as a function of time and distribution of non-decision times (c). **(d,e)** Accuracy (b) and mean odor sampling duration (OSD) (c) plotted as a function of odor concentration. Black lines correspond to the behavioral data from a 'super-rat'; green and red lines correspond to the best-fit curves from the analytical and numerical solutions of the model, respectively. **(f)** Standard deviation of OSD as a function of mean OSD. **(g)** Histograms of OSD (10 ms bin) for the different odor concentration stimuli. Line shading represents stimulus difficulty, with easier stimuli corresponding to the darkest shade. Colored lines correspond to the best-fit curves from the numerical solution of the model.

Table 4.2 | Best-fit parameter values from the different models (k, sensitivity; β, scaling exponent; A, bound; t_{ND}, mean non-decision time; $\sigma_{t_{ND}}$, standard deviation of non-decision time; Acc, accuracy; mRT, mean reaction times; vRT, variance of reaction times; sdRT, standard deviation of reaction times)

Model #	k	β	A	t_{ND}	$\sigma_{t_{ND}}$	Fitted variables
1	58.08	4.73×10^{-1}	3.50×10^{-2}	2.73×10^{-1}	_	Acc, mRT
1	1.66×10^{-3}	4.67×10^{-2}	1.93×10^{-1}	9.0×10^{-15}	_	mRT, vRT
2	67.53	4.75×10^{-1}	4.05×10^{-2}	2.35×10^{-1}	_	Acc, mRT
3	1.0×10^{3}	4.73×10^{-1}	8.30×10^{-3}	2.90×10^{-1}	_	Acc, mRT
4	2.24×10^{3}	5.95×10^{-1}	8.35×10^{-3}	2.87×10^{-1}	_	Acc, mRT
5	1.27×10^{4}	1.93×10^{-1}	1.54×10^{-1}	2.57×10^{-1}	_	Acc, mRT
6	1.33×10^{4}	2.02×10^{-1}	1.53×10^{-1}	2.40×10^{-1}	_	Acc, mRT
7	1.27×10^{4}	2.04×10^{-1}	9.78×10^{-4}	3.20×10^{-1}	_	Acc, mRT
8	6.43×10^{3}	5.16×10^{-1}	5.52×10^{-3}	2.95×10^{-1}	_	Acc, mRT
9	_	_	_	_	8.33×10^{-2}	sdRT
10	_	_	_	_	7.17×10^{-2}	sdRT
11	_	_	_	_	8.15×10^{-2}	sdRT
12	_	_	_	_	8.57×10^{-2}	sdRT

The model structure of the numerical simulation of the DDM was used as the basic structure upon which all the different model variants were implemented.

The sequence of models tested and the respective similarities and differences are depicted in **Table 4.3** (for all these models non-decision time was defined as a constant value).

Table 4.3 | Sequence of model variants tested with constant non-decision time

Model #	Stimulus strength	Diffusion coefficient	Temporal integration
1			
2	*		
3			
4	*		
5			
6	*		
7	*		
8	**		

Green: Constant
Blue: Time-varying
* PID fit
** Single trial trace

Orange: 0.1
Purple: 0

Red: Yes
Brown: No

Figures 4.3 and 4.4 show that both Model 1 (constant input, **Fig. 4.3 a-c**) and Model 2 (time-varying input, **Fig. 4.4 a-c**) – with temporal integration and 'noise' – were able to explain accuracy and mean RT as a function of concentration reasonably well (**Figs. 4.3d, e and 4.4d, e**). However, these models did not capture the shape of the RT distributions (**Figs. 4.3g and 4.4g)** and consequently the relationship between the mean and SD of RT (**Figs. 4.3f and 4.4f**). This was consistent with a previous study showing that while a standard DDM model could account for the choice behavior and mean RT of the RDMD task, it turned out to be incompatible with the observed RT distributions[131]. Nevertheless, it was interesting to note that both Models 1 and 2

predicted a linear relationship between the mean and SD of RT, as had been described for the DDM[123], however the slope was much steeper when compared to the data. We explored this issue later, in **4.3.2 An attempt to capture the reaction time distributions.**

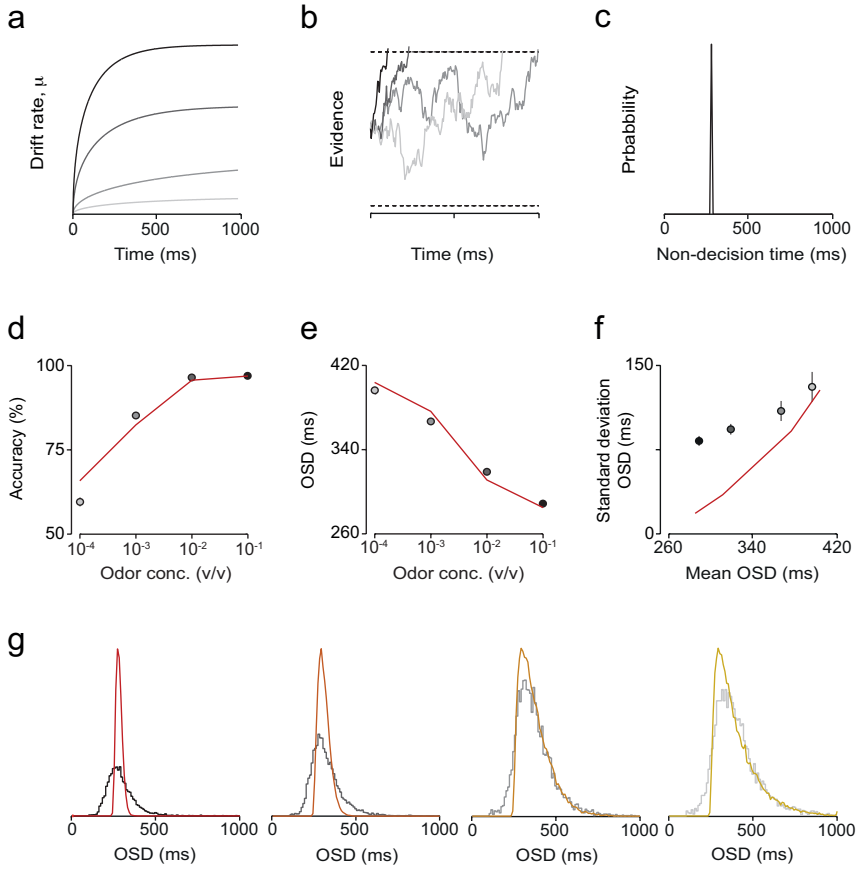

Figure 4.4 | Drift-diffusion model with time-varying input from exponential fit of mean odor time-courses (Model 2)
(a-c) Model components: Drift rate (a) and evidence (b) as a function of time and distribution of non-decision times (c). **(d,e)** Accuracy (d) and mean odor sampling duration (OSD) (e) plotted as a function of odor concentration. Black lines correspond to the behavioral data from a 'super-rat'; red lines correspond to the best-fit curves. **(f)** Standard deviation of OSD as a function of mean OSD. **(g)** Histograms of OSD (10 ms bin) for the different odor concentration stimuli. Line shading represents stimulus difficulty, with easier stimuli corresponding to the darkest shade. Colored lines correspond to the best-fit curves.

Next, we asked if a model without temporal integration, where the evidence is compared directly to the bound (**Figs. 4.5a-c** and **4.6a-c)**, could capture the data, as had been shown before for the RDMD task[131]. Indeed, a model like this was also able to explain accuracy and mean RT, both with constant (Model 3; **Figs. 4.5a-e**) and time-varying stimulus (Model 4; **Figs. 4.6a-e**). Again, these models failed to capture the shape of the RT distributions (**Figs. 4.5f-g and 4.6f-g**).

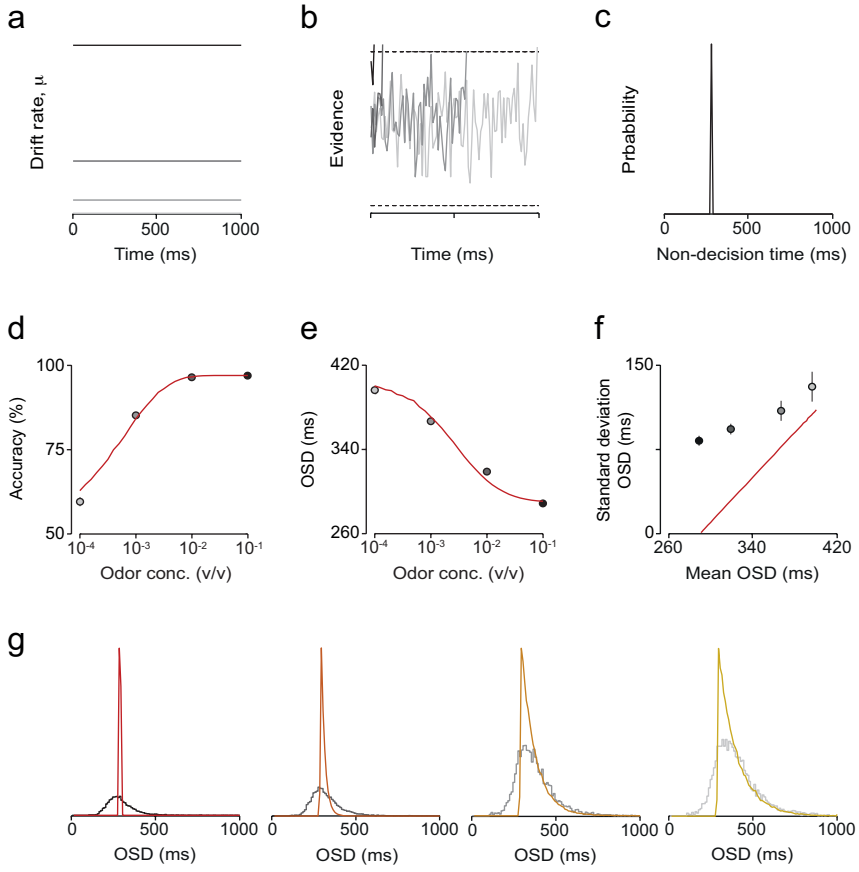

(Legend of Fig. 4.5 in the next page)

Figure 4.5 | Model with no temporal integration and constant input (Model 3)

(a-c) Model components: Drift rate (a) and evidence (b) as a function of time and distribution of non-decision times (c). **(d,e)** Accuracy (d) and mean odor sampling duration (OSD) (e) plotted as a function of odor concentration. Black lines correspond to the behavioral data from a 'super-rat'; red lines correspond to the best-fit curves. **(f)** Standard deviation of OSD as a function of mean OSD. **(g)** Histograms of OSD (10 ms bin) for the different odor concentration stimuli. Line shading represents stimulus difficulty, with easier stimuli corresponding to the darkest shade. Colored lines correspond to the best-fit curves.

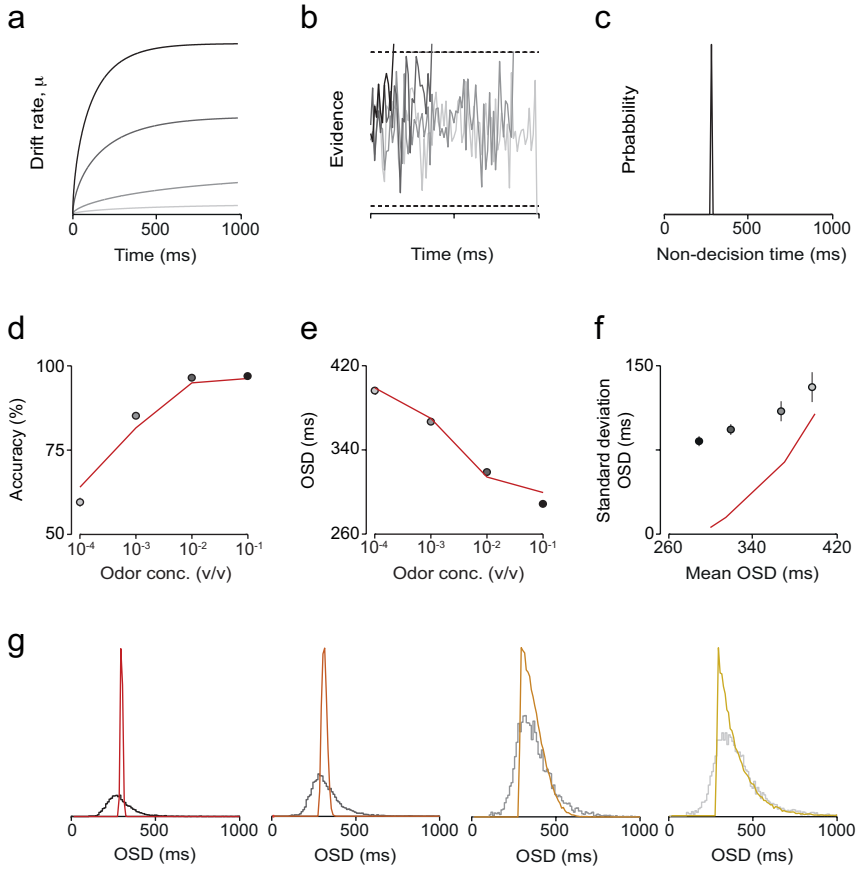

(Legend of Fig. 4.6 in the next page)

Figure 4.6 | Model with no temporal integration and time-varying input from exponential fit of mean odor time-courses (Model 4)
(a-c) Model components: Drift rate (a) and evidence (b) as a function of time and distribution of non-decision times (c). **(d,e)** Accuracy (d) and mean odor sampling duration (OSD) (e) plotted as a function of odor concentration. Black lines correspond to the behavioral data from a 'super-rat'; red lines correspond to the best-fit curves. **(f)** Standard deviation of OSD as a function of mean OSD. **(g)** Histograms of OSD (10 ms bin) for the different odor concentration stimuli. Line shading represents stimulus difficulty, with easier stimuli corresponding to the darkest shade. Colored lines correspond to the best-fit curves.

We next asked what happens when the model includes temporal integration but no 'noise' (diffusion coefficient equal to zero; **Figs. 4.7a-c and 4.8a-c**). In this case, the models captured the RT changes (**Figs. 4.7e and 4.8e**) but not the accuracy (**Figs. 4.7d and 4.8d**), showing that the within-trial variability is essential for explaining the accuracy. Similar results were obtained for the constant (Model 5; **Fig. 4.7a-c**) and time-varying stimulus (Model 6; **Fig. 4.8a-c**). As expected in a situation when there is no noise in the decision process, the SD of the RT distributions was equal to zero (**Figs. 4.7f-g and 4.8f-g**).

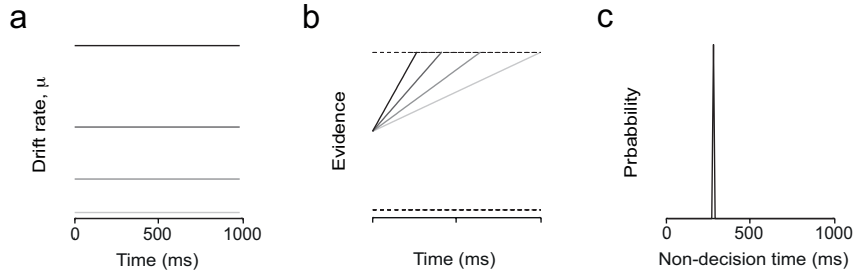

(Fig. 4.7 continues in the next page)

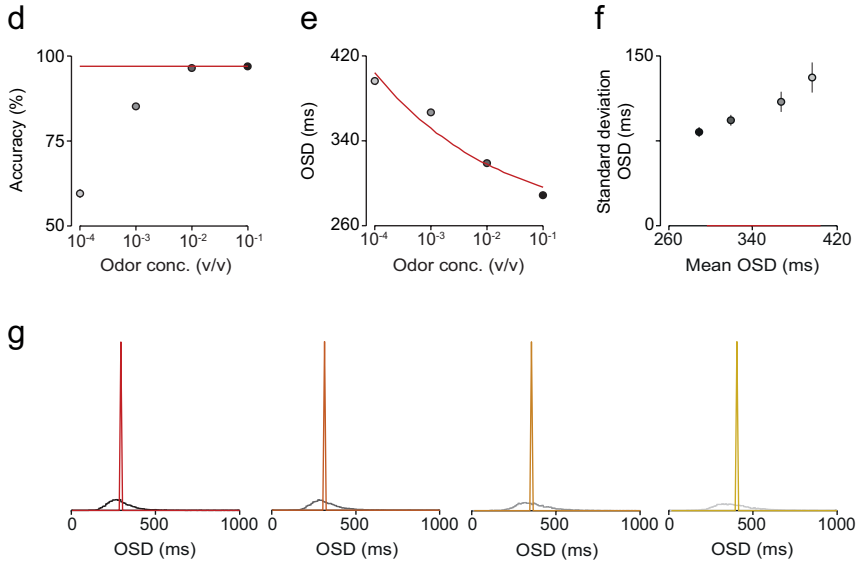

Figure 4.7 | Evidence-accumulation model with diffusion coefficient set to zero and constant input (Model 5)
(a-c) Model components: Drift rate (a) and evidence (b) as a function of time and distribution of non-decision times (c). **(d,e)** Accuracy (d) and mean odor sampling duration (OSD) (e) plotted as a function of odor concentration. Black lines correspond to the behavioral data from a 'super-rat'; red lines correspond to the best-fit curves. **(f)** Standard deviation of OSD as a function of mean OSD. **(g)** Histograms of OSD (10 ms bin) for the different odor concentration stimuli. Line shading represents stimulus difficulty, with easier stimuli corresponding to the darkest shade. Colored lines correspond to the best-fit curves.

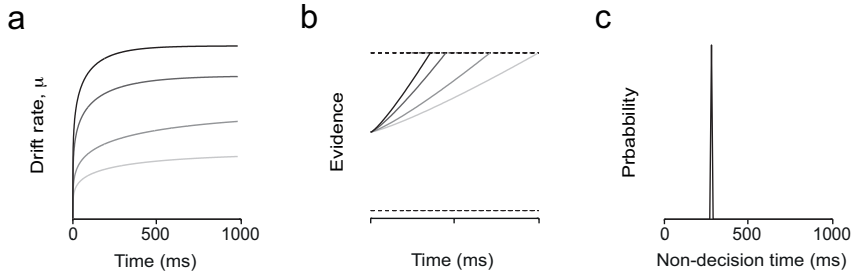

(Fig. 4.8 continues in the next page)

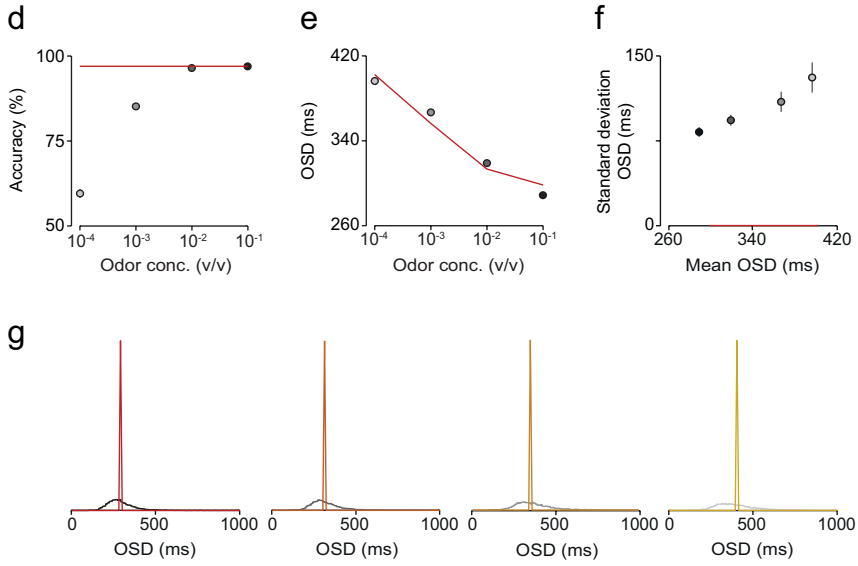

Figure 4.8 | Evidence-accumulation model with diffusion coefficient set to zero and time-varying input from exponential fit of mean odor time-courses (Model 6)
(a-c) Model components: Drift rate (a) and evidence (b) as a function of time and distribution of non-decision times (c). **(d,e)** Accuracy (d) and mean odor sampling duration (OSD) (e) plotted as a function of odor concentration. Black lines correspond to the behavioral data from a 'super-rat'; red lines correspond to the best-fit curves. **(f)** Standard deviation of OSD as a function of mean OSD. **(g)** Histograms of OSD (10 ms bin) for the different odor concentration stimuli. Line shading represents stimulus difficulty, with easier stimuli corresponding to the darkest shade. Colored lines correspond to the best-fit curves.

The goal of Models 7 (**Fig. 4.9a-c**) and 8 (**Fig. 4.10a-c**) was to address the question whether odor temporal dynamics were sufficient to explain the behavioral changes observed across different odor concentrations in the identification task, particularly for RTs. In Model 7, the input was described by an exponential function, which corresponded to the best-fit curves of the mean of the odor time-courses for the individual concentrations (**Fig. 4.1**). This problem could also be solved

analytically, as demonstrated in Chapter 4 (**4.2.2 Variants of the model**), showing that for Model 7 the decision time t_D as a function of odor stimulus was described by a logarithmic function – **Eq. 4.8**.

Both the analytical and the numerical solution (**Fig. 4.9**) led to the same type of result: for a model where the input is time-varying and described by an exponential function **(Fig. 4.1)** and there is no temporal integration, the shape of the curve for mean RT as a function of stimulus intensity follows a logarithmic shape (**Fig. 4.9e**), which is in contrast with the linear relationship describing the behavioral RT as a function of odor concentration (**Figs. 3.1 and 3.2**).

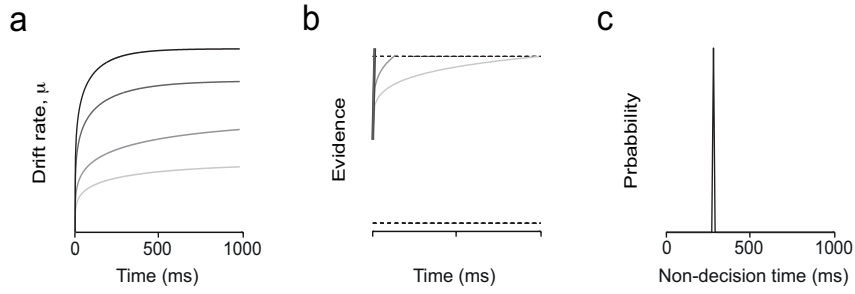

(Fig. 4.9 continues in the next page)

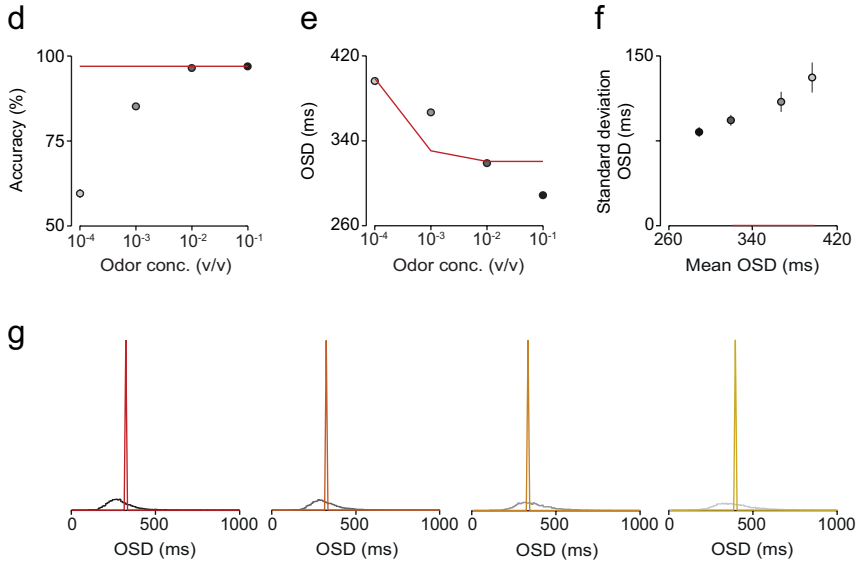

Figure 4.9 | Model with no temporal integration, diffusion coefficient set to zero and time-varying input from exponential fit of mean odor time-courses (Model 7)
(a-c) Model components: Drift rate (a) and evidence (b) as a function of time and distribution of non-decision times (c). **(d,e)** Accuracy (d) and mean odor sampling duration (OSD) (e) plotted as a function of odor concentration. Black lines correspond to the behavioral data from a 'super-rat'; red lines correspond to the best-fit curves. **(f)** Standard deviation of OSD as a function of mean OSD. **(g)** Histograms of OSD (10 ms bin) for the different odor concentration stimuli. Line shading represents stimulus difficulty, with easier stimuli corresponding to the darkest shade. Colored lines correspond to the best-fit curves.

In Model 8, the input on any given trial and for any given concentration was described by a single-trial odor time-course (**Fig. 4.10a**). Compared to Model 7, this model incorporates an additional source of variability, which reflects the trial-by-trial variation of the odor time-course. Despite this variability, with no additional model variability, the result of this fitting led to the same observations as Model 7: for a time-varying input with an exponential-like shape, even in the presence of trial-by-trial

variability in the odor time-course, the shape of the RT curve was qualitatively different from the one observed in the data (**Fig. 4.10e**). This model also did not capture the shape of the RT distributions (**Fig. 4.10f-g**).

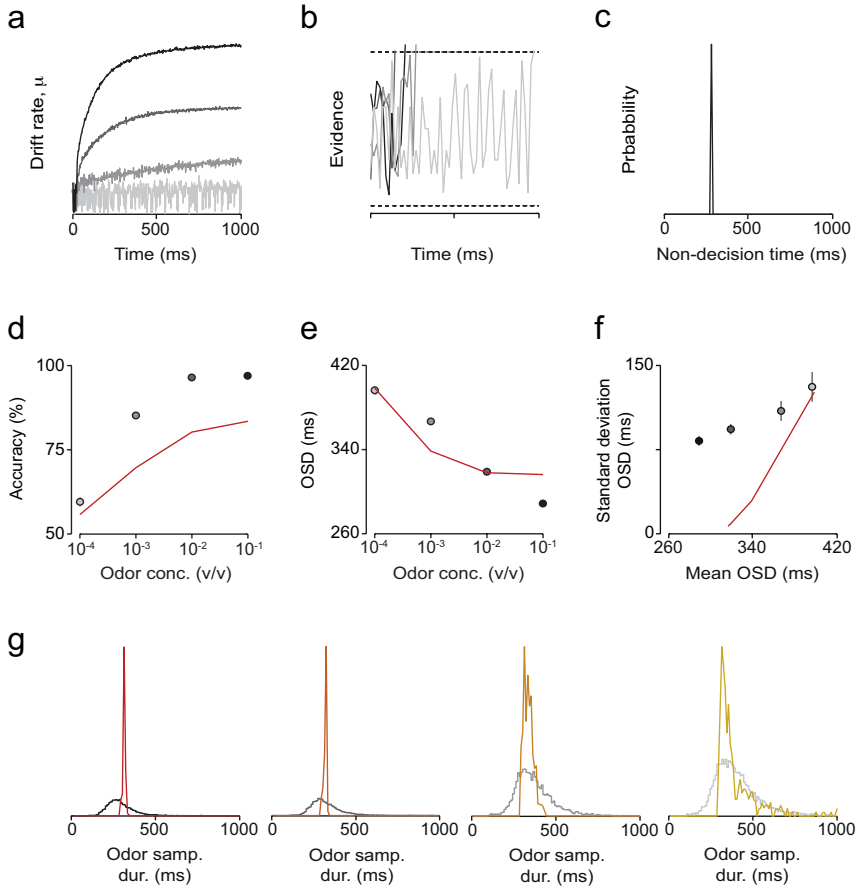

Figure 4.10 | Model with no temporal integration, diffusion coefficient set to zero and time-varying input from single-trial odor time-courses (Model 8)

(a-c) Model components: Drift rate (a) and evidence (b) as a function of time and distribution of non-decision times (c). **(d,e)** Accuracy (d) and mean odor sampling duration (OSD) (e) plotted as a function of odor concentration. Black lines correspond to the behavioral data from a 'super-rat'; red lines correspond

to the best-fit curves. **(f)** Standard deviation of OSD as a function of mean OSD. **(g)** Histograms of OSD (10 ms bin) for the different odor concentration stimuli. Line shading represents stimulus difficulty, with easier stimuli corresponding to the darkest shade. Colored lines correspond to the best-fit curves.

In summary, with the model structure described in Chapter 4 (**Fig. 4.2**), we observed that both models with or without temporal integration, and with constant or time-varying input were compatible with the behavioral data in terms of accuracy and mean RT as long as the diffusion (noise) coefficient was different from zero (Models 1-4). However, none of these models was able to capture the RT distributions.

Additionally, Models 7 and 8 showed that the odor temporal dynamics led to qualitatively different predictions for the mean RT when compared to the data: whereas these models predict a logarithmic-like shape for the RT curve, the behavioral data is better described by a linear relationship. This suggests that the odor dynamics cannot readily explain the changes in RTs observed for the identification task.

4.3.2 An attempt to capture the reaction time distributions

None of the models tested in the previous section was able to capture the shape of RT distributions. We attempted to address this by introducing trial-by-trial variability in the non-decision time[131,136] to the diffusion models that were able to match accuracy and RT data in the previous section (Models 1-4). Given

that the distributions of non-decision times could not be directly derived from the data, we made the simplifying assumption that non-decision times were normally distributed[131,136]. Since we wanted to examine the impact of this variability on the RT distributions as well as on the mean RT and accuracy, we took the following approach: 1) the parameters A (bound), k (sensitivity), β (scaling exponent) and t_{ND} (mean non-decision time) were fixed and set to the values of the best-fit parameters from Models 1-4; 2) the only parameter allowed to vary was the SD of the Gaussian distribution of non-decision times; and 3) only the SD of RTs was fit to these models. In this way we were able to test if variability in non-decision times alone could rescue the shape of RT distributions, and then ask, by looking at the predictions for mean RT and accuracy, what was the impact of this extra variability in these features of the data.

For all the models tested (Models 9-12), we observed that the variability in non-decision times helped indeed capturing the RT distributions (**Figs. 4.11g – 4.14g**), as well as the relationship between mean and SD of RTs (**Figs. 4.11f – 4.14f**). The addition of this parameter did not have any apparent impact on accuracy and mean RT (**Figs. 4.11d, e – 4.14d, e**).

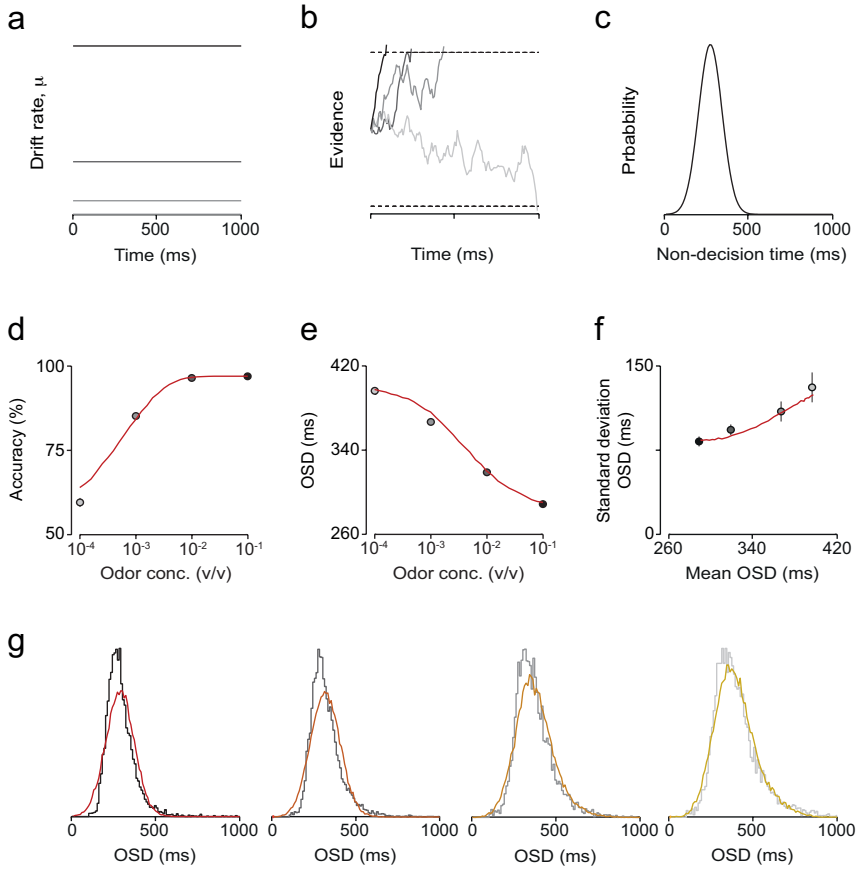

Figure 4.11 | Model 1 with Gaussian variability in non-decision time (Model 9)

(a-c) Model components: Drift rate (a) and evidence (b) as a function of time and distribution of non-decision times (c). **(d,e)** Accuracy (d) and mean odor sampling duration (OSD) (e) plotted as a function of odor concentration. Black lines correspond to the behavioral data from a 'super-rat'; red lines correspond to the best-fit curves. **(f)** Standard deviation of OSD as a function of mean OSD. **(g)** Histograms of OSD (10 ms bin) for the different odor concentration stimuli. Line shading represents stimulus difficulty, with easier stimuli corresponding to the darkest shade. Colored lines correspond to the best-fit curves.

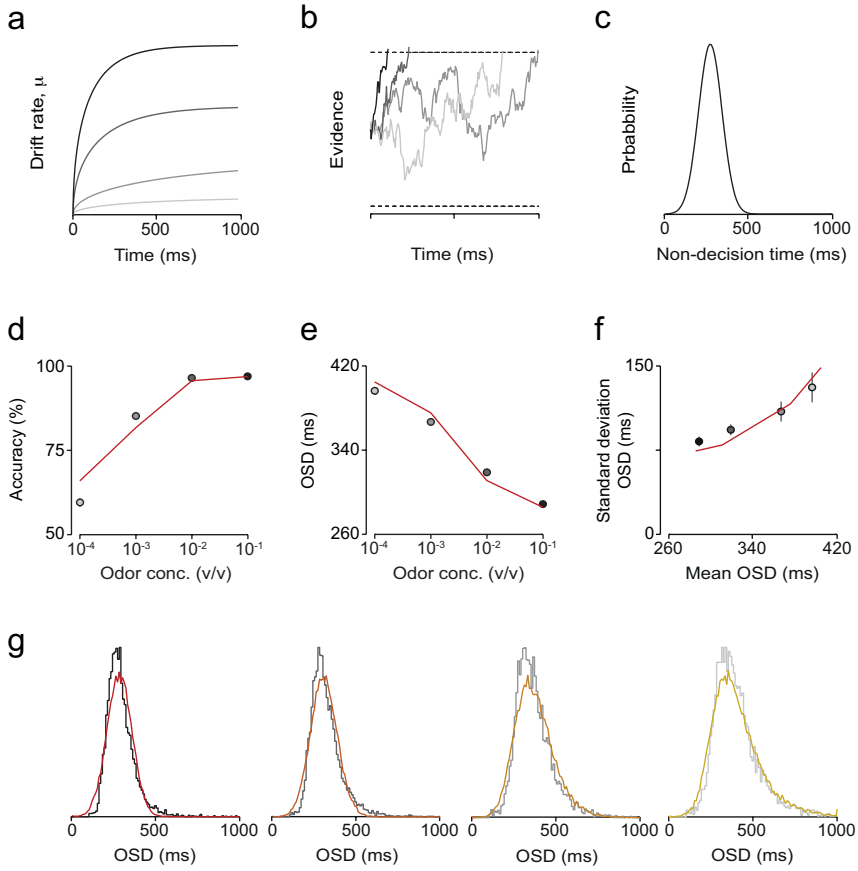

Figure 4.12 | Model 2 with Gaussian variability in non-decision time (Model 10)

(a-c) Model components: Drift rate (a) and evidence (b) as a function of time and distribution of non-decision times (c). **(d,e)** Accuracy (d) and mean odor sampling duration (OSD) (e) plotted as a function of odor concentration. Black lines correspond to the behavioral data from a 'super-rat'; red lines correspond to the best-fit curves. **(f)** Standard deviation of OSD as a function of mean OSD. **(g)** Histograms of OSD (10 ms bin) for the different odor concentration stimuli. Line shading represents stimulus difficulty, with easier stimuli corresponding to the darkest shade. Colored lines correspond to the best-fit curves.

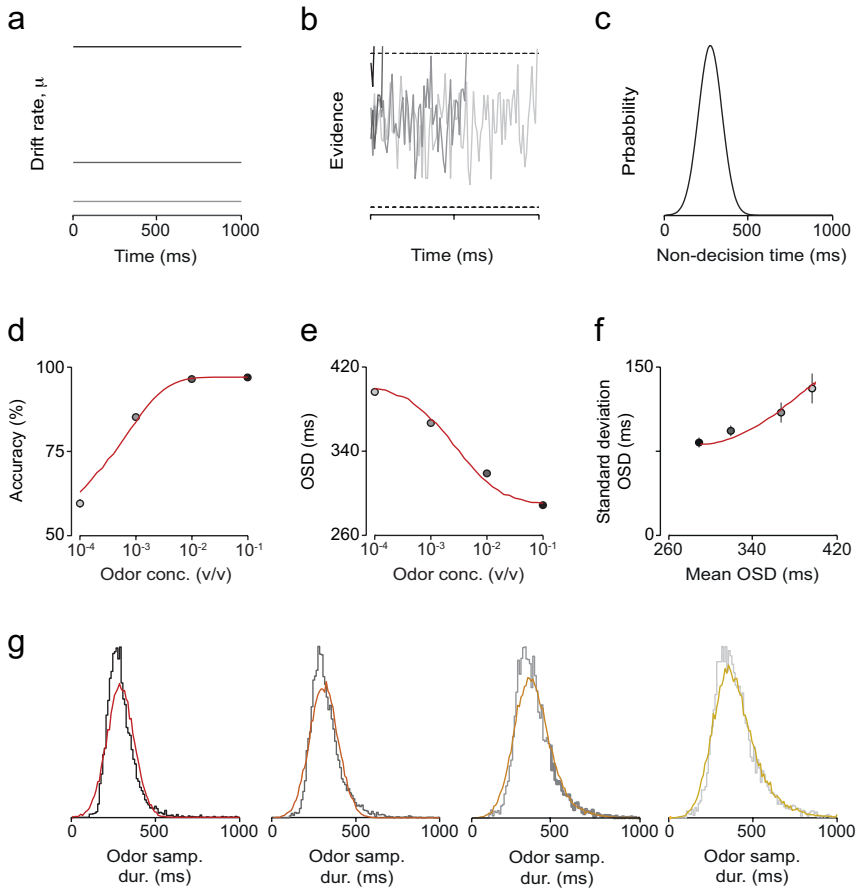

Figure 4.13 | Model 3 with Gaussian variability in non-decision time (Model 11)

(a-c) Model components: Drift rate (a) and evidence (b) as a function of time and distribution of non-decision times (c). **(d,e)** Accuracy (d) and mean odor sampling duration (OSD) (e) plotted as a function of odor concentration. Black lines correspond to the behavioral data from a 'super-rat'; red lines correspond to the best-fit curves. **(f)** Standard deviation of OSD as a function of mean OSD. **(g)** Histograms of OSD (10 ms bin) for the different odor concentration stimuli. Line shading represents stimulus difficulty, with easier stimuli corresponding to the darkest shade. Colored lines correspond to the best-fit curves.

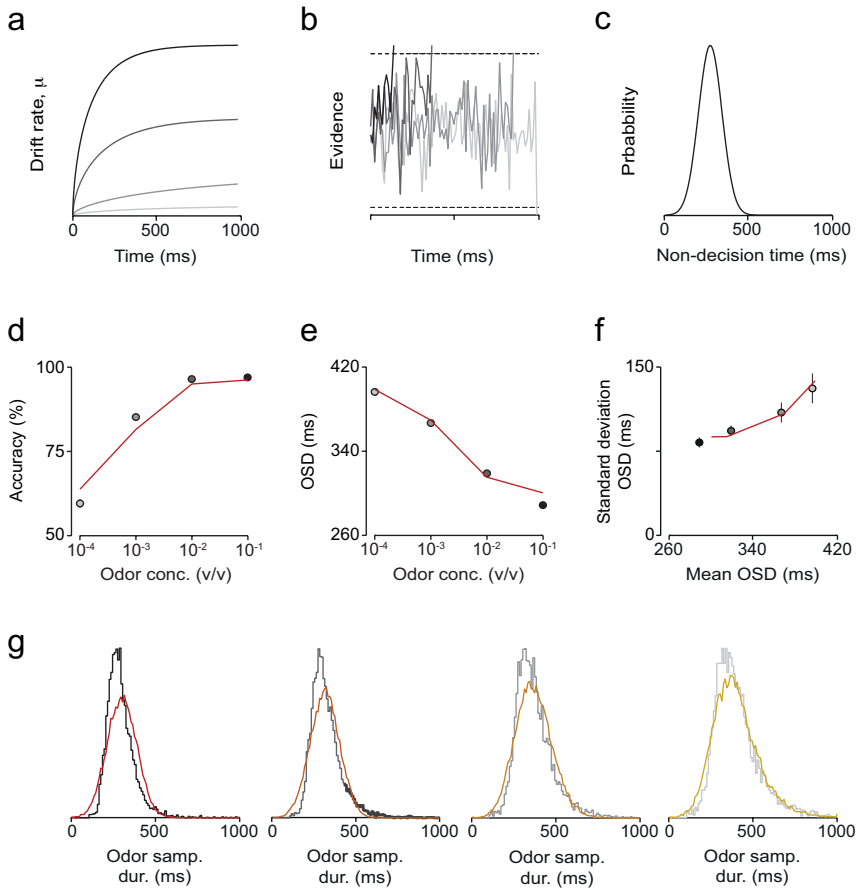

Figure 4.14 | Model 4 with Gaussian variability in non-decision time (Model 12)
(a-c) Model components: Drift rate (a) and evidence (b) as a function of time and distribution of non-decision times (c). **(d,e)** Accuracy (d) and mean odor sampling duration (OSD) (e) plotted as a function of odor concentration. Black lines correspond to the behavioral data from a 'super-rat'; red lines correspond to the best-fit curves. **(f)** Standard deviation of OSD as a function of mean OSD. **(g)** Histograms of OSD (10 ms bin) for the different odor concentration stimuli. Line shading represents stimulus difficulty, with easier stimuli corresponding to the darkest shade. Colored lines correspond to the best-fit curves.

Next, we explored an alternative approach, where instead of fitting accuracy and mean RT as before, we decided to fit mean and variance of RTs. It has been described before that standard

DDM and random walk models predict an approximately linear relation between RT mean and SD for changing drift rates[123,137]. However, in these studies accuracy was not considered, so we wondered if by fitting mean and variance of RTs, instead of accuracy and mean RT, we could find a combination of parameter values that could actually capture the RT distributions without having to add any extra variability to the parameters. Indeed, that was the case. We observed that the RT distributions and the relation between mean and SD, as well as the actual shape of the RT distributions, were very nicely captured by this procedure (**Fig. 4.15b-d**); however the predicted accuracy was very high (**Fig. 4.15a**). This shows that there is a combination of the parameter values that allows capturing the RT distributions without the need of having variability in non-decision times or any other additional parameter. However, it also suggests the need for an additional source of uncertainty that would affect accuracy but not RTs. This is actually in agreement with our main hypothesis, which proposes that the differences in SAT in the identification and categorization tasks arise from differences in the sources of noise that are limiting performance.

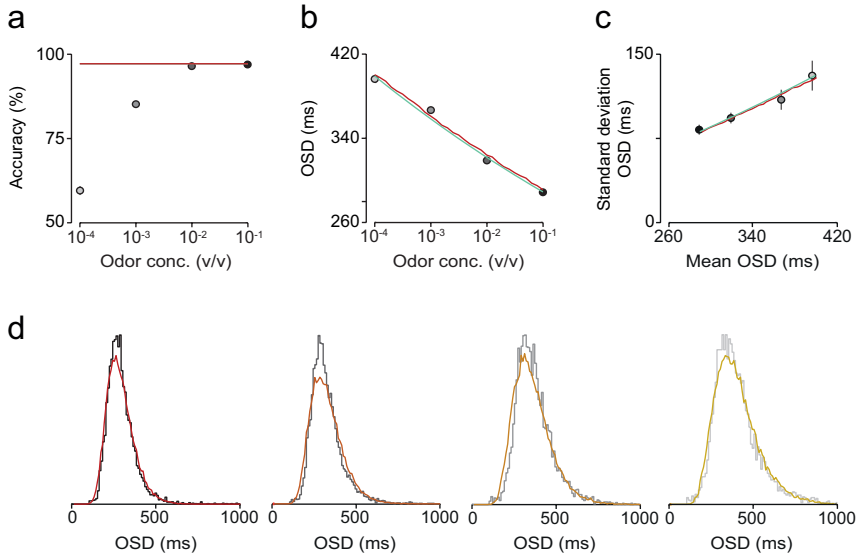

Figure 4.15 | Drift-diffusion model fit to mean and standard deviation of reaction times
(a,b) Accuracy (a) and mean odor sampling duration (OSD) (b) plotted as a function of odor concentration. Black lines correspond to the behavioral data from a 'super-rat'. **(c)** Standard deviation of OSD as a function of mean OSD. Green and red lines correspond to the best-fit curves from the analytical and numerical solutions of the model, respectively; for accuracy, these lines are model predictions and not fits. **(d)** Histograms of OSD (10 ms bin) for the different odor concentration stimuli. Line shading represents stimulus difficulty, with easier stimuli corresponding to the darkest shade. Colored lines correspond to the best-fit curves from the numerical solution of the model.

4.3.3 Inhalation variability

As a consequence of sniffing, odors are sampled in discrete olfactory 'snapshots', which have significant implications for olfactory processing[127,135,138–140]. Although sniffing hasn't been measured in the identification task, it was shown that sniff frequency does not change as task difficulty is increased by lowering odorant concentration[141]. In addition, sniffing measurements during an olfactory discrimination task similar to

the categorization task used here, showed that the rate of respiration increases before rats enter the odor sampling port, going from a low frequency (2-4 Hz) mode before entry, to a high-frequency (6-9 Hz) mode during odor sampling[135]. This change in sniff frequency was mainly due to a reduction in the exhalation duration or equivalently an increase in the rate at which inhalations occurred, i.e. while the exhalation periods decreased from approximately 250 ms to 50 ms, the change in inhalation was relatively small (~10-30 ms)[135].

We wanted to investigate the impact of adding inhalation variability to Model 8 on accuracy and RTs. For that, we ran a simulation with this model with three different inhalation variability conditions, where the time for the beginning of stimulus sampling was given by a uniform distribution ranging from 0 to 50, 150 or 250 ms; these values were chosen based on the duration of exhalations reported previously during the categorization task (Fig. 5c, d from reference [135]). In other words, the odor stimulus would be turned on in the beginning of each simulated trial, but the sampling of the stimulus would only start at the sampled inhalation time for that specific trial (described by a uniform distribution ranging from 0 to 50, 150 or 250 ms, depending on the condition).

We predicted that the accuracy and RTs resulting from this manipulation would be a combination of, at least, two different scenarios: 1) if the stimulus evidence at the sampled inhalation time is smaller than the bound, the decision happens when the

evidence crosses the bound – this type of trials leads to the same accuracy and RTs independently of the manipulation; 2) if the stimulus evidence at the sampled inhalation time is higher than the bound, the decision time is given by the inhalation time – for distributions of inhalation times with higher upper limits, this type of trials leads to larger values of mean and SD of RT and higher values of accuracy (since it's a rising stimulus, the probability of making a correct response increases with time). This type of trials will be more frequent for higher concentrations and for inhalation time distributions with higher upper limits.

As predicted, when compared to the no-exhalation condition (blue trace; this condition is the same as Model 8), we observed an overall increase in accuracy (**Fig. 4.16a**), RT mean (**Fig. 4.16b**) and SD, particularly for higher concentrations (**Fig. 4.16c**), for the three different conditions, which was larger for inhalation time distributions with higher upper limits (**Fig 4.16**, from blue to purple: no exhalation, 50 ms, 150 ms, 250 ms). Moreover, the obtained shape of the curve for mean RT as a function of stimulus concentration was qualitatively similar to the one without inhalation variability (**Fig 4.16b**), resembling a logarithmic-like shape, whereas the behavioral RTs were better described by a linear relationship (**Figs. 3.1** and **3.2**). This suggests that even in the presence of inhalation variability, the odor dynamics cannot readily explain the changes in RTs observed for the identification task.

We are aware that this is a quite simplistic approach for simulating inhalation variability – although we varied the starting time of stimulus sampling, we did not impose any time constraints on the inhalation period and we did not take into account any putative dynamics that could be happening in the beginning of inhalation. However, these features would be more relevant if there was evidence that sniff frequency was changing across concentrations or if neuronal response latencies depended on sniff frequency, which doesn't seem to be the case based on previous studies[125,138,141]. Nevertheless, measurements of the temporal odor profiles and respiration while the animal is performing the identification task would clearly provide important information and help to constrain future versions of the model[35,124,125].

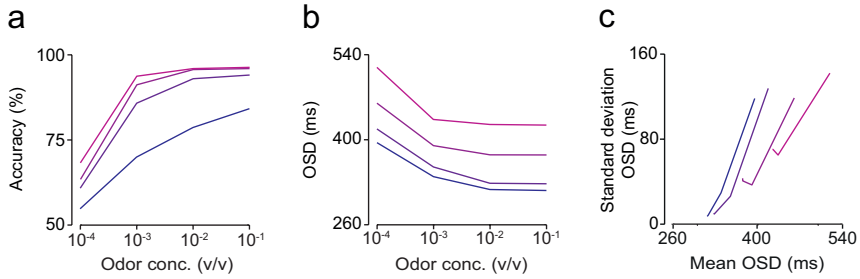

Figure 4.16 | Inhalation variability simulation
Inhalation variability was tested by performing a simulation with Model 8, using the resulting best-fit parameter values from this model, where the time for the beginning of stimulus sampling was given by a uniform distribution ranging from 0 to 50, 150 and 250 ms. **(a,b)** Accuracy (a) and mean odor sampling duration (OSD) (b) plotted as a function of odor concentration. **(c)** Standard deviation of OSD as a function of mean OSD. Colors from blue to purple indicate increasing values of exhalation duration (no exhalation, 50 ms, 150 ms, 250 ms).

4.4 Discussion

We showed that different variants of the model, which included temporal integration or not, either with constant or time-varying input, were able to reproduce the behavioral data for response accuracy and mean RTs, but they required that the diffusion coefficient was different from zero. Our results are consistent with a modeling study showing that the behavioral data from the RDMD task could be captured by a variety of models based on a 'race-to-threshold model', including models with or without temporal integration[131]. In addition, it has been shown that models based on independent sampling, often known as probability summation[134,142,143], can also produce dependence of reaction times and performance on stimulus difficulty[131–133]. For example, for a visual detection task, an independent sampling model was able to predict the Weibull psychometric function and similarly shaped chronometric function[132,133]. Although with our current dataset we were not able to tease apart between the models with and without temporal integration, our results support the contention[131] that presumably many behavioral datasets that have been modeled as integration of sensory information to a bound could also be captured without invoking integration.

It was previously shown that standard DDMs predict a linear relationship between the mean and SD of RTs for changing drift rates[123] and that random walk models are able to explain the RT distributions from a RT cognitive task[137]; it is important to mention that in both studies, accuracy was not considered in the

models. Conversely, there is also evidence that a standard DDM does not capture the RT distributions from the RDMD task[131] and that more parameters are needed to explain the data[131,136]. Our results are consistent with this apparent conundrum: fitting mean RT and accuracy does not capture the RT distributions, while fitting mean and variance of RTs explains the distributions but predicts a very high accuracy. This demonstrates that depending on the combination of parameter values, the DDM can lead to one solution or to the other. However, in order to be able to fit simultaneously accuracy, mean and variance of RTs, extra parameters would be needed, either: 1) variability in non-decision times if we are fitting mean RT and accuracy; or 2) a source of uncertainty that would affect accuracy but not RTs if mean and variance of RT are being fit. Work in progress from our laboratory has shown that adding variance to the drift rate leads to a decrease in accuracy, particularly for more difficult stimuli, and has a small impact on mean RT[144], making this source of variability a likely candidate. Importantly, it was also shown that the source of this trial-to-trial variability in the drift rate is related with an on-going learning based on the previous history of rewards and stimuli, which is fundamental to explain the choice behavior of the animals, particularly for the categorization task[145,146].

An important outcome of our modeling approach was the demonstration that the odor temporal dynamics, even in the presence of inhalation variability, led to qualitatively different

predictions from the data that could not explain the changes in RTs observed for the identification task.

Overall, even though we were not able to distinguish between some of the proposed computational mechanisms, this modeling approach showed that: in order for the accuracy to be captured, the model has to include noise in the drift rate (diffusion coefficient); the increase in RTs observed in the identification task was mainly explained by the decrease in the amount of odor information at lower concentrations, and not much by the odor temporal dynamics.

5 Temporal uncertainty in odor identification and mixture categorization

5.1 Introduction

The ability to prepare for future events, or to make decisions guided by their expected outcome, relies on our ability to predict such events, their timing and outcome. Prior information about the timing of future events induces temporal expectation and allows for temporal preparation[90]. However, if such information is partial or absent, this preparation will be limited by temporal uncertainty[147,148]. Temporal uncertainty affects temporal expectation, which in turn has been shown to have effects both at the level of sensory processing[104–107] and action[90,91].

Perceptual decision-making and time estimation processes have been proposed to share the same underlying mechanisms[80,121,122]. The scalar property of interval timing, which posits a linear relationship between the mean and SD of response times[75], can also be predicted by diffusion models, which have been extensively applied to perceptual decision-making[123]. Interestingly, it was also shown that time estimation can be accounted by a bounded accumulation mechanism that integrates the noisy firing of neural populations[80]. Furthermore, the same type of neurons from the area LIP that have been identified as representing the DV during perceptual decision-making tasks[34] were also shown to represent elapsed time in the form of a hazard function, i.e., the probability that the stimulus is about to occur[89,97].

In this chapter we want to investigate what is the impact of temporal uncertainty in perceptual decision-making. More

specifically, we ask how the uncertainty about the time of stimulus onset affects simultaneously RTs and accuracy In Chapters 2 and 3 we showed that odor identification and mixture categorization display different SAT relationships, suggesting that identifying an odor at low concentrations and distinguishing related odors pose different sources of uncertainty for the brain. In this chapter, we want to compare the effect of the same temporal expectation manipulation on these two different tasks, in order to disambiguate which components of the decision-making process are affected by this type of temporal uncertainty.

5.2 Properties of reaction time distributions

Our first approach was to examine the RT distributions, which have been shown before to display relevant properties that can provide important insights about the underlying mechanisms that generate them[13,79,121,137,149]. The OSD distributions, for both categorization and identification tasks and across the different stimuli, displayed an asymmetrical shape with a skew to the right, where the spread of the distributions increased with the mean (**Fig. 5.1a**). These distributions were scale invariant, as shown by the overlap of the distributions when plotted as a function of RT relative to the mean (**Fig. 5.1b**), and the CV did not show a significant change across the different mixture contrasts or odor concentrations (categorization, $F(3,12) = 2.01$, $P = 0.17$; identification, $F(3,12) = 0.18$, $P = 0.91$, ANOVA; **Fig. 5.1c**). Moreover, the relationship between the mean and SD of OSDs

was well described by a linear function (**Fig. 5.1d**). Interestingly, this scalar property between the mean and SD of response times, which resembles Weber's Law[73] in the temporal domain, has been described frequently in the literature of interval timing[79,121]. This shared property between perceptual decision-making and time estimation processes suggests that temporal contingencies might play a role in the observed RT distributions. We explored this question by looking at the impact of temporal expectation on both the identification and categorization tasks.

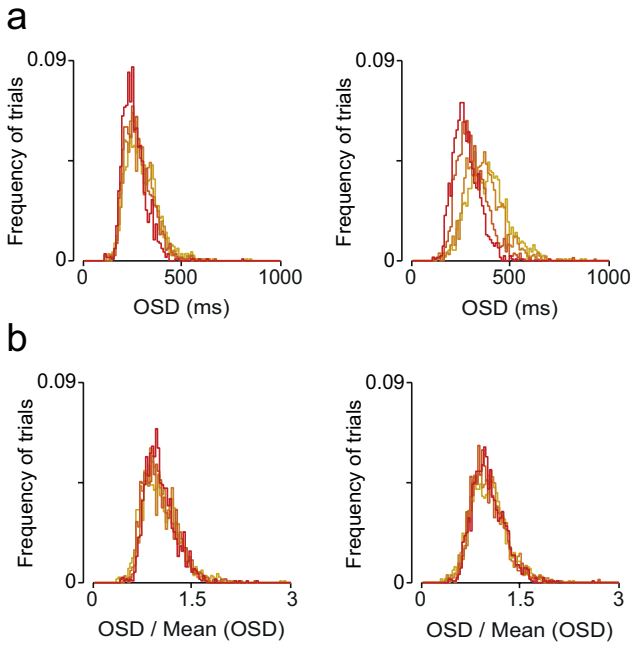

(Fig. 5.1 continues in the next page)

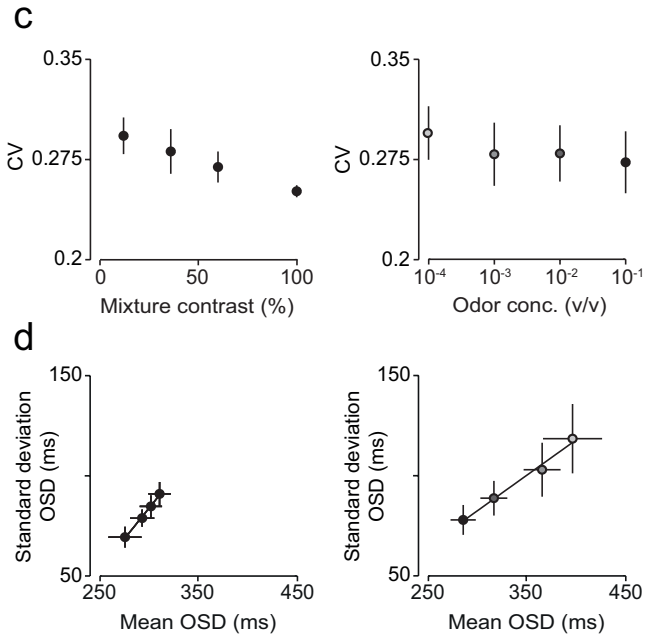

Figure 5.1 | Properties of reaction time distributions
(a) Histograms of odor sampling duration (OSD; 10 ms bin) for the different mixture contrast (left) and odor concentration (right) stimuli for a representative rat (same rat as in Fig. 3.1). Line color represents stimulus difficulty, with the easiest stimuli corresponding to the red color. **(b)** Histograms of OSD normalized by the mean for the different mixture contrast (left) and odor concentration (right) stimuli. **(c)** Coefficient of variation (CV; OSD standard deviation / OSD mean) as a function of mixture contrast (left) or odor concentration (right). **(d)** Mean of the standard deviation of OSD as a function of the mean of mean OSD for the different mixture contrast (left) and odor concentration (right) stimuli. Error bars are mean ± SEM (n = 4 rats).

5.3 Temporal expectation

In our experiments, odor valve opening was randomly delayed using a uniform distribution from 300 to 600 ms (**Fig. 5.2a**; see Chapter 2, 2.4 Reaction time paradigm). This creates a rising hazard rate, hence increasing expectation of stimulus onset, from 300 to 600 ms[56,107]. For comparison of low and high stimulus-expectation, two groups of trials were selected, an early onset,

low stimulus-expectation condition, d_{odor} = 300-400 ms, and a late onset, high stimulus-expectation condition, d_{odor} = 500-600 ms. Analysis of OSD and accuracy for these two stimulus-expectation conditions were performed by conditioning OSD and accuracy on these two different time periods of d_{odor}.

Insofar as RTs depend on temporal expectation, we expected to see a decrease in OSD with increasing anticipation[88,90]. The odor valve delay made no difference in accuracy (**Fig. 5.2b;** for categorization, F(1,24) = 1.78, P = 0.19; for identification, F(1,24) = 0.22, P = 0.64, 2-way ANOVA), but OSDs were significantly larger for shorter odor delays in both tasks (**Fig. 5.2c**; categorization, F(1,24) = 15.65, P = 0.006; identification, F(1,24) = 9.97, P = 0.0043, 2-way ANOVA).

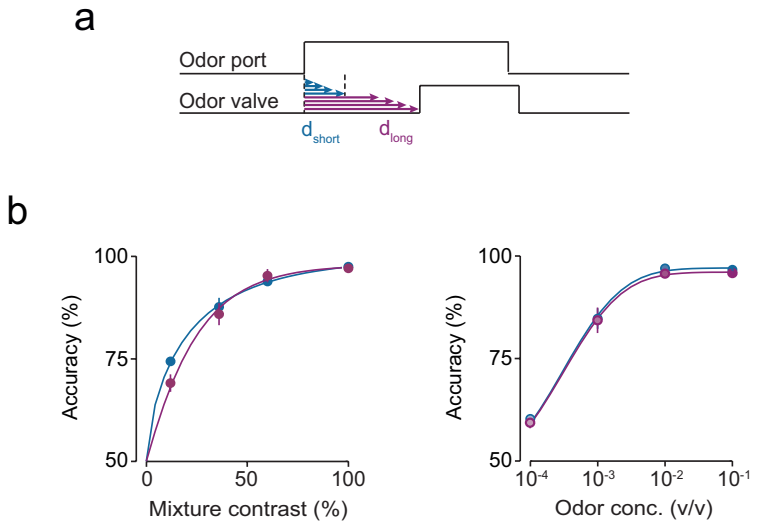

(Fig. 5.2 continues in the next page)

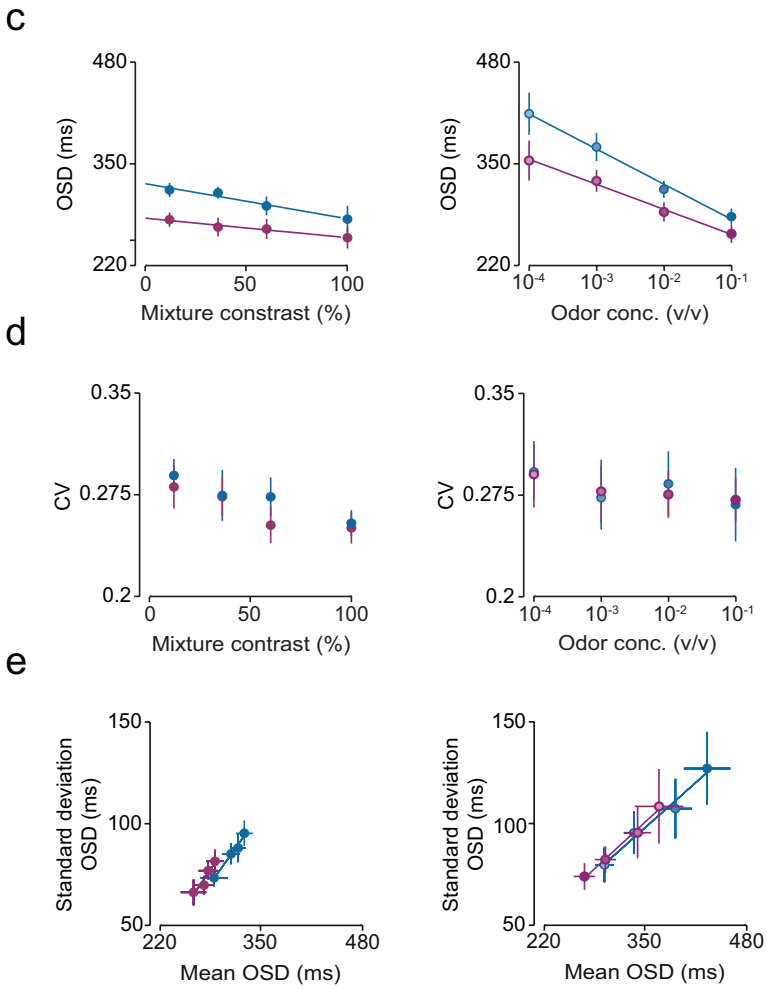

Figure 5.2 | Effect of stimulus expectation on reaction times
(a) Stimulus onset delay distribution (d_{odor}). The stimulus onset delay, that is the time between identification of the subject at the odor sampling port and the time of the trigger sent to the odor valve, was drawn from a uniform distribution between 300 and 600 ms. The hazard rate for stimulus onset and therefore stimulus expectation is therefore rising during this period (see Chapter 2). For comparison of low (blue) and high (purple) stimulus expectation, two groups of trials are illustrated, an early onset, low stimulus expectation condition, d_{odor} = 300–400 ms (blue), and a late onset, high stimulus expectation condition, d_{odor} = 500–600 ms (purple). **(b)** Mean accuracy plotted as a function of mixture contrast (left) or odor concentration (right). Dot shading represents odor concentration, with the highest concentration corresponding to the darkest color. **(c)** Mean of median odor sampling duration (OSD) plotted as a function of mixture contrast (left) or odor concentration (right). **(d)** Mean of the coefficient of variation (CV) plotted as a

function of mixture contrast (left) or odor concentration (right). **(e)** Mean of the standard deviation of OSD as a function of mean of the mean OSD for the different mixture contrast (left) and odor concentration (right) stimuli. Error bars are mean ± SEM, n = 4 rats.

If the animals were estimating the time for stimulus onset and considering that this estimation changes with temporal expectation, then we would expect to see a proportional change of the mean and SD of RTs for different temporal expectation conditions, as predicted from the scalar property of interval timing. This was the case for both tasks. For the high temporal expectation condition (higher odor delays), the mean and SD of OSD decreased proportionally when compared to the low temporal expectation condition (shorter odor delays) (**Fig. 5.2e**; for categorization, $F(7,16) = 1.68$, $P = 0.19$; for identification, $F(7,16) = 1.3$, $P = 0.32$, ANOCOVA; $P > 0.05$, post-hoc Tukey-Kramer test for slope and intercept, identification and categorization). This was also demonstrated by the lack of change in the CVs across the odor delay conditions (**Fig. 5.2d**; categorization, $F(1,24) = 2.03$, $P = 0.4$; identification, $F(1,24) < 10^{-3}$, $P = 0.98$, 2-way ANOVA).

Next we asked whether this expectation-sensitive component depended on the task parameters, like task difficulty or stimulus properties (e.g., odor concentration). First, we compared the slopes of the linear regression for OSD as a function of mixture contrast, or odor concentration, between the two temporal expectation conditions. We observed that the variation in OSD was significantly larger for the low temporal expectation

condition (categorization, $t(3) = 5.97$, $P = 0.005$; identification, $t(3) = 7.11$, $P = 0.003$, paired t-test), showing that the expectation-sensitive component of RTs depends on the task parameters. We hypothesized that this effect could be either due to task difficulty or odor concentration. These two conditions could be easily disambiguated with our current behavioural setup, given that, in the categorization task, difficulty was manipulated by varying the relative concentration of the individual odors in the mixtures while keeping constant the total odor concentration, whereas in the identification task, the total odor concentration was the variable being changed.

To investigate this question, we looked at the data from the mixture identification task, in order to eliminate any extra variability that could be introduced by running the identification and categorization tasks separately. Given that for the mixture identification task, the number of trials available per rat is smaller, we decided to pool the data from all the rats. For each stimulus and odor delay condition, we calculated the median OSD and then we quantified the expectation-sensitive component (eOSD) by calculating the difference between the respective median OSDs across the two odor delay conditions.

To test the dependence on task difficulty we decided to look at eOSD as a function of accuracy. And to test the dependence on odor concentration, we looked at eOSD as a function of the concentration of the individual odors in the mixtures.

In order to disambiguate between the two different hypotheses that eOSD would be dependent either on task difficulty or concentration, we assumed a linear relationship between eOSD and accuracy (**Fig. 5.3a, left**) or concentration (**Fig. 5.3b, right**) that allowed us to predict the values of eOSD for the difficulty- and concentration-dependent conditions, respectively. Then, for the difficulty-dependent condition, we plotted the predicted eOSD as a function of the concentration of the individual odors in the mixtures (**Fig. 5.3b, right**); and for the concentration-dependent condition, we plotted the predicted eOSD as a function of the respective data values of accuracy (**Fig. 5.3c, right**). By comparing these predictions with the behavioural data (**Fig. 5.3c**), we observed that the condition that best described the data was the difficulty-dependent one (**Fig. 5.3a**).

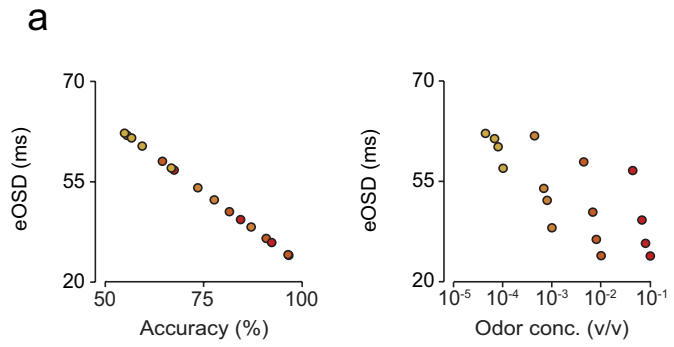

(Fig. 5.3 continues in the next page)

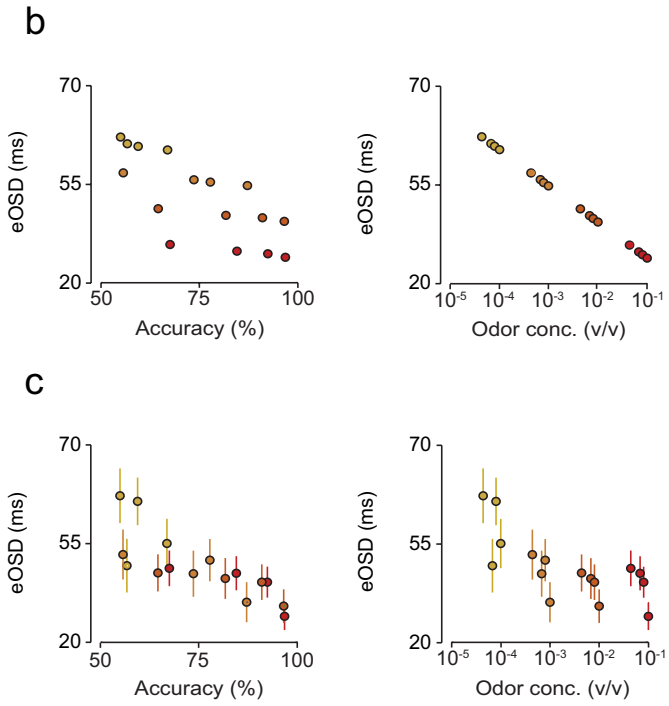

Figure 5.3 | Temporal expectation-sensitive component
(a) Difficulty-dependent condition: the temporal expectation-sensitive component of odor sampling duration (eOSD) was calculated by assuming a linear relationship with accuracy. eOSD as a function of accuracy (left) or concentration of odor A (or B) in the mixture stimuli (right) from the mixture identification task. Each point represents a single mixture ratio. Dot color represents total odor concentration, with the highest concentration corresponding to the red color. **(b)** Concentration-dependent condition: eOSD was calculated by assuming a linear relationship with the concentration of the individual odors in the mixtures. Left and right figures are the same as in (a). **(c)** Behavioral data. eOSD corresponds to the difference between the median low expectation-OSD (d_{odor} = 300–400 ms) and the median high expectation-OSD (d_{odor} = 500–600 ms). Left and right figures are the same as in (a). Error bars are ± SEM (n across trials for the data pooled across all sessions and all rats).

5.4 Discussion

We showed, for both identification and categorization tasks, that the RT distributions mimic several properties observed in the literature of interval timing. The trial-to-trial response variability associated with the different mixtures contrasts or odor concentrations (quantified by the CV) was constant across the different odor stimuli, and interestingly the values of the CV were similar for both tasks. This is equivalent to the linear relationship observed between the mean and SD of RTs. Furthermore, the distributions of RTs were scale invariant, i.e., identical when plotted as a function of RT relative to the mean. These features of the RT distributions associated with the different odor stimuli resemble the scalar property of interval timing described for estimated times[74,75] and not for stimulus-driven response times, suggesting that the observed RTs might be a combination of decision-making and time estimation processes[80,121,122]. Indeed, we observed that a component of the RTs was sensitive to temporal expectation, here manipulated by the time of stimulus onset, displaying smaller RTs when the temporal expectation was higher. Interestingly, we did not observe a change in accuracy for the different temporal expectation conditions suggesting that this manipulation is most likely affecting action preparation[90] rather than stimulus processing. The decrease in mean RTs for higher expectation was accompanied by a proportional decrease of the SD, as would be expected from the scalar timing property for different temporal expectation conditions. This reinforces the

interpretation that animals are estimating time and this is being reflected in the properties of the distributions.

Finally, we observed that the expectation-sensitive component of RTs seems to depend on task difficulty. Does this imply an interaction between temporal estimation processes and the mechanisms that account for choice accuracy in a decision-making process? This seems unlikely given that such interaction would likely produce a change in accuracy for the different temporal expectation conditions, which we did not observe. An alternative explanation would be that it is not task difficulty that is mediating this modulation but a variable correlated with it, such as reward expectation for example, which has been shown before to influence RTs[56,150,151]. The design of behavioural experiments that allow disambiguating between all these different variables will be important to understand the mechanisms underlying RT distributions.

6 General discussion

6.1 Overview of empirical findings

In this thesis we focused on the contributions of different sources of uncertainty in perceptual decision-making. More specifically, we explored why the range of SAT varies so widely across studies. We hypothesized that the different degrees of SAT are related to the nature of the task being performed. In order to address this issue, we studied odor identification and categorization in parallel in the same animals, using tasks that were identical except for the relevant stimulus parameters. We found that OSDs increased substantially when odor concentrations approached detection threshold but they remained almost constant as odor mixtures became closer to the category boundary. This was true even for categorization at threshold concentrations. We hypothesized that in odor identification, accuracy is limited by stimulus uncertainty, whereas in mixture categorization, accuracy is limited by variability in the mapping of the stimulus to the response, which must be learnt on a trial-by trial basis. Given this hypothesis, we investigated whether ongoing learning had a different influence on the choices of animals in identification and categorization. In both tasks there was a clear trial-by-trial updating of the animal's choice function. However, whereas in categorization choice bias increased with difficulty of the previous trial and outcome, in identification this bias was dependent only on choice side and outcome.

Next, we used a modeling approach to investigate which computational mechanisms might account for the behavioral

changes observed in the identification task. Interestingly, we observed that our results were well described both by models with and without temporal integration, as had been observed before for the RDMD task[131], questioning the generalized use of integrator models to explain choice behavior and response times across a wide range of perceptual decision-making tasks.

Finally, we explored the role of temporal uncertainty in perceptual decision-making, by focusing on the impact of stimulus onset expectation on OSD. We observed a linear relationship between the mean and SD of OSD across mixture contrasts and odor concentrations, consistent with Weber's law in the temporal domain. For both tasks, mean OSD was smaller for longer onsets (higher expectation), and this decrease was accompanied by a proportional decrease of the SD, as would be expected from the scalar property of interval timing for different temporal expectation conditions. The magnitude of this expectation-sensitive component was correlated with stimulus difficulty, with lower accuracies displaying larger changes in OSD. These results show that RTs are modulated by non-sensory components such as temporal expectations, suggesting that RTs are a combination of decision-making processes and attention-related mechanisms, which are in turn affected by time estimation processes.

6.2 Sources of uncertainty in decision-making

6.2.1 Speed-accuracy tradeoff and the origin of decision noise

In most perceptual decision-making tasks, variability in choice for difficult stimuli is assumed to be due to the uncertainty about the stimulus, or noise in the respective sensory system. In conformity with this assumption, performance typically increases with stimulus sampling duration[35,152]. However, there are situations, such as the odor mixture categorization task presented in this thesis and described before[52,56] where SAT is not observed, suggesting that the rapid performance observed in this task is not simply a tradeoff of accuracy for speed. The rapid responses in odor categorization, even for low contrast mixtures, reflect the large amount of evidence available, relative to what is accessible for comparable accuracy in the identification task, but the accuracy is still low. As a specific hypothesis, we propose that the trial-by-trial variability in odor mixture categorization may arise from a constant updating of the category boundary between left and right odor classes that is set by the experimenter and must be learnt by the subjects through trial-by-trial reinforcement[56]. Indeed, by looking at the influence of trial history on the choice of the animals, we observed a clear trial-by-trial updating of the animal's choice function, which depended both on the difficulty of previous trial and outcome[153].

Temporal integration benefits decision-making by averaging out noise over time, thereby increasing the signal-to-noise ratio.

However, this reduction of noise through averaging only works efficiently as long as the noise is not temporally correlated along the relevant dimension. For instance, correlated noise in the activity across a neuronal population can dramatically limit the usefulness of pooling spikes across more neurons in order to increase the signal-to-noise ratio[154]. Similarly, correlations of noise across time can defeat an integrator by limiting the ability of averaging to reduce noise, thereby diminishing the benefits of repeated sampling[155]. Therefore, the effectiveness of temporal integration depends on the nature of the limiting noise. Considering that the behavioral variability in the mixture categorization task arises from the constant updating of the category boundary based on the outcome of previous trials, then this source of noise would be completely correlated within individual trials. Therefore, if uncertainty about the precise category boundary dominates over stimulus uncertainty, the benefits of integration within a single trial would be curtailed. In this regard, tasks that are dominated by uncorrelated sensory noise may indeed show the expected benefits of extended stimulus sampling (RDMD task, e.g. [34]; Poisson clicks task, [35]). Based on our behavioral and modeling results, we believe that the identification task falls on this category.

Work in progress[145,146] has been taking a modeling approach to investigate the contribution of these different sources of uncertainty (fluctuations in sensory uncertainty vs. fluctuations in the weights of the stimulus-to-choice mapping) to explain the relationship between RT and performance in the identification

and categorization tasks[146]. Preliminary results have shown that a standard integration-to-bound model fails to capture the performance in both tasks simultaneously, leading to the hypothesis that the performance in the categorization task might be limited by trial-to-trial fluctuations introduced by RL. This hypothesis was tested by expanding the standard sensory integration model to include a learning rule that changes the mapping from sensory evidence to decision category after a decision has been made. After fitting the performance data, this model predicted a specific magnitude and pattern of history-dependent choice biases, which were in quantitative agreement with the data. Altogether, this suggested that on-going RL is a critical non-stochastic source of decision variability that can limit the benefit of evidence accumulation favoring faster RTs in some decisions[146].

An optimal agent that runs through the same perceptual decision-making task day after day would eventually learn that task contingencies do not change, and then switch to a deterministic strategy, as one could imagine for the animals performing the identification and categorization tasks. However, despite stable performance over sessions, we observed that learning of stimulus-to-choice mapping is still occurring, implying that animals assume a non-stationary environment and might rely on simple and less computationally costly behavioral strategies while solving these tasks. It was recently proposed[126] that one of the major causes of behavioral variability might not be internal noise, but suboptimal inference. Ideally, neural circuits should retain the

relevant aspects of their complex and high-dimensional inputs (the 'signal') and filter out all irrelevant aspects (the 'noise'). However, the process of extracting the relevant information may allow some of the irrelevant input variability to leak into the circuit's output and to potentially alter behavior[126,156]. According to this proposal, the bottleneck would then lie in the quality of the algorithm performing the inference. Recordings from the anterior piriform cortex (PC) of rats performing the odor mixture categorization task support this view. By monitoring spikes of only 50-100 aPC neurons, a simple decoder based on firing rates could extract more than enough information in a single sniff to account for the behavioral accuracy in this task, suggesting that rats might not use optimally the information contained in the activity of aPC. Similar observations have been made in the primary visual cortex of monkeys and rats[7,157,158].

6.2.2 Post-decisional processes and learning

Statistical learning theory proposes that 'active learners' use not only reinforcement but also their current estimates of uncertainty to set the size of updates, i.e. learn more when uncertain and less when certain[159]. This implies that the animal's choice in a given trial is not only influenced by previous reinforcement, but also by their current estimates of certainty (or confidence). Decision confidence has been measured previously for the mixture categorization task[159–161] showing that it is correlated with choice accuracy. For correct trials, decision confidence increases as the

stimulus gets easier, whereas for error trials the opposite trend prevails, i.e., lower confidence for easier stimuli. Given that confidence is correlated with accuracy, one would expect to observe similar confidence curves for the identification and categorization tasks. If this was true and assuming that reinforcement and decision confidence are the main key players for learning, then the animal's choice function relative to previous stimuli and outcome should be equivalent for both tasks. However, that is not the case: whereas in categorization choice bias increased with difficulty of previous trial and outcome, in identification this bias was dependent only on choice side and outcome. One possibility would be that the decision confidence profiles are different for the identification and categorization tasks. Another alternative could be that there is an additional source of uncertainty that does not depend on previous stimuli but that introduces a choice bias, being more predominant in the identification task. Preliminary work from our laboratory has shown that incorporating an additive choice bias term to the starting point of the expanded integration-to-bound model described above helps explaining the learning curve of the identification task. This bias term is equivalent to a prior that is being dynamically updated on a trial-by-trial basis depending on the outcome of the previous trial. This type of architecture has been used before to explain the effect of prior probability on choice and RT[31] and similar response modulations have been observed in LIP activity in relation to prior expectation about the stimulus[162].

What is then the relationship between decision confidence profiles and history-dependent choice functions? Comparing these two types of curves for the identification and categorization tasks would provide important insights regarding this question. Another relevant analysis would be to look at history-dependent choice bias as a function of decision confidence instead of stimulus difficulty.

6.2.3 Decision response time and decision confidence

A recent study showed that decision confidence in the RDMD task depends both on stimulus evidence and response times, with certainty being directly correlated with motion strength and inversely correlated with response times[136]. In the light of these observations, we would expect decision confidence to be smaller for identification compared to categorization, for the same level of accuracy, given the RT differences between these two tasks. This prediction could be easily tested by introducing a confidence report measure in the identification and categorization tasks[159–161]. Since we want to test the influence of decision response time on decision confidence, the best approach would be to use a metric for confidence that could be directly compared to decision time, i.e., a metric that uses time as a report of confidence. This could be implemented by incorporating the 'leaving decision' task[159,161] in our behavioral protocol, which provides a graded measure of decision confidence given by the amount of time that animals are willing to wait for the reward. The suitable behavioral protocol

for this would be the “mixture identification task”, where the two tasks are combined, by interleaving the full set of stimuli from the categorization and identification tasks as well as intermediate mixtures. Like this, it would be possible to compare, on a trial-by-trial basis, decision response time and decision confidence in the two different tasks. According to our hypothesis, the sources of uncertainty that are limiting accuracy and RT in the identification and categorization tasks are different. In the identification task, errors are mainly due to the small amount of evidence for lower concentrations, which produces long RTs. On the other hand, in the categorization task, even for low contrast mixtures, there is actually a large rate of evidence, producing fast RTs, but the accuracy is low because the mean evidence is being updated on a trial-by-trial basis due to ongoing RL, leading to sub-optimal behavior; i.e., RTs reflect the amount of evidence available in both tasks, but accuracy is limited by different sources of uncertainty in identification and categorization. If decision confidence depends on the evidence and response times, as suggested by Kiani and colleagues[136], one should observe a correlation between response time and decision confidence across the different stimuli of the “mixture identification task”. On the other hand, if decision confidence also depends on the distance between the sampled evidence and the evidence that was computed throughout the last trials due to RL, as we would hypothesize for categorization, this correlation between response time and decision confidence across the stimulus space would not be observed.

6.3 Olfactory coding: insights from neural circuits

6.3.1 Coding of odor intensity in the olfactory system

Our results are consistent with the idea that identifying an odor at low concentrations and distinguishing closely related odors poses very different demands for the brain. More specifically, we hypothesized that, in the case of the identification task, the observed accuracy and RTs are due to the reduced amount of odor information at lower concentrations.

But how is odor intensity encoded in the olfactory system? What do we know already from physiology studies? First of all, it is important to mention that there is no data available, to our knowledge, from electrophysiological recordings in awake and behaving animals, from the ORNs, OB or PC for changing concentrations. Therefore, the available datasets are mainly from anesthetized animals, whose neural responses are very different from awake animals, namely in the OB, where the firing rates are much higher compared to anesthetized animals[163].

Overall, recordings from the ORNs and OB have shown that increasing odor concentration leads to an increase in the number of recruited ORNs and glomeruli and in response amplitude[164–167], and to a decrease in response latency[165,168–171]. Based on these observations, a variety of schemes have been proposed for spike encoding of odor intensity, namely a spike rate code and a spike latency code. However, there is still not a unified view of how odor intensity is encoded in the brain. For example, although

some M/TCs respond to odor stimuli with increased spike excitation at higher odorant concentration, others are inhibited, or respond with more complex temporal patterns of mixed excitation and inhibition that may change with concentration[138,172]. On the other hand, even though it has been shown that response latency decreases with increasing concentration, the range of magnitudes observed is remarkably distinct, e.g. from 50 ms latency for a 10-fold change in mouse isolated ORNs[169] to > 900 ms change for a ~150-fold difference in anesthetized rat ORNs[170]. Moreover, odor-evoked electro-olfactogram (EOG) recordings from the ORNs of anesthetized rats have shown that the EOG onset latency is almost unaltered across concentrations[170]. And there are also examples of MCs that show increased firing latencies with increasing concentration[172]. Furthermore, in awake rodents, spontaneous firing of M/TCs is generally high compared to anesthetized animals[163], preventing reliable detection of the onset of odor-evoked activity[138,173]. Recently, it was also suggested that tufted cells (TCs) could transmit a parallel rate code of concentration[173–175]. TCs receive direct monosynaptic excitation from ORNs and respond to odorants with short latencies that display much smaller dependency on concentration. By contrast, MCs receive polysynaptic excitation via external TCs and show longer latencies with decreasing concentration[173–175].

Regarding our results on the odor identification task, although we cannot rule out the existence of sensory delays, the examples that we cited indicate that there are heterogeneous response profiles across the odor-responsive cells and that increases in response

latency with decreasing concentration are not a universal property of olfactory processing. This implies that the existence of neurons with minimally concentration-dependent delays (e.g, TCs in the OB) would be sufficient for animals to begin to perform odour identification rapidly. Comparing with the visual system, it was shown that the latency of visually responsive neurons increases with decreasing stimulus contrast in different structures along the visual pathway[176–178]. This increment in response latency is considerably greater in higher visual areas, such as the anterior superior temporal sulcus than in the primary visual cortex[178,179]. This increasing dependency of neuronal response latency on stimulus contrast reveals that latency change is not retinal or V1 in origin, suggesting that each cortical processing step adds latency at lower contrasts. These observations are in agreement with the predictions of an optimal decoder applied to the neural population responses from V1 during a detection task[157], which outperformed the monkey's behavior in both speed and accuracy. Altogether, this implies that there might be sources of noise downstream to primary structures such as V1 or aPC[127], that limit behavioral performance, both in terms of RTs and accuracy.

6.3.2 Recordings from the olfactory system: future directions

Evidence from the last years has suggested that there is a profound transformation in the way odors are represented in the OB[138,140] and in the anterior PC[127]. First, spontaneous firing of

M/TCs in awake rodents is generally high (on average 10–25 spikes per second[163]), whereas aPC shows relatively low spontaneous activity (6.15 ± 9.01, mean ± SD[127]). Second, each M/TC fires maximally at a particular latency from inhalation onset, tiling the entire cycle of sniffing[138], and odor inhalation triggers rapid and reliable cell- and odor-specific temporal spike patterns[138,140]. On the other hand, the temporal responses of anterior PC neurons consist mainly of transient burst spiking that is tightly locked to sniff onset[127]. And third, in the OB most of the information is conveyed within the first 100 ms after inhalation onset at a resolution of tens of milliseconds[138,140], while in the anterior aPC reliable odor information is provided by total spike counts over the entire sniff cycle[127]. Given these differential responses to odors in the OB and aPC, namely in terms of the type of information relevant for each area, simultaneous recordings from these two areas, in rats performing the odor identification task, would provide important insights about how odor intensity is encoded in the brain and how this information is used in a decision-making process.

If the performance in the mixture categorization task is limited by trial-to-trial fluctuations introduced by RL signals, this influence of trial history on odor perception should be most likely reflected in the neural activity of a brain structure that receives coincident input from the olfactory and reward systems. A potential candidate is the olfactory tubercle (OT). The OT sits at the interface between olfactory and reward circuits. On one hand, it receives monosynaptic olfactory input from both the OB and the

PC[180] and displays odorant-evoked responses[180,181]. On the other hand, the OT is considered part of the ventral striatum and is heavily interconnected with the reward system[182], receiving projections from several areas including the ventral tegmental area, the nucleus accumbens and the substantia nigra[180].

The modulation of OT activity due to RL signals could be reflected in the variability of OT neuronal responses, as observed for single dorsal premotor neurons in an arm reach countermanding task[183], where the variability (and not the mean) of neural activity in a given trial increased with the number of previous trials containing a stop signal. An alternative could be a change in the mean firing rate of the odor-evoked responses or a change in the spontaneous activity. This modulation could be mediated by neuromodulatory inputs, namely noradreneline from the locus coeruleus or serotonin (5-HT) from the raphe nucleus, which have been shown to influence OT activity in rats[180]. Preliminary work from our laboratory has shown that 5-HT neurons from the dorsal raphe nucleus (DRN) respond to reward-predictive cues in a way similar to a prediction error[184] and that optogenetic activation of DRN 5-HT neurons, in anesthetized rats, produces a rapid and profound inhibition of spontaneous (but not odor-evoked) firing of olfactory cortex neurons[185], which was multiplicative and frequency-dependent. Slice experiments also revealed that DRN 5-HT activation inhibits cortical feedback compared to feedforward input[185]. We postulate that the same type of modulation that was observed in PC could also happen in the OT, which receives direct input from the raphe nucleus[180].

Interestingly, based on differential projections from the OB, it has been suggested that the PC and OT may allow parallel processing of odors. Whereas OB input to the PC mostly stems from MCs, OB input to the OT originates predominately from TCs[186]. Given that MC and TC differ in their odor response thresholds[175,187], width of odor receptive fields[187], and local connectivity to interneuron networks[188,189], this could imply that OT odor responses will differ from those of the PC, namely that the OT will be responsive to odors at much lower thresholds than the PC.

Overall, these hints given by the olfactory neural circuits clearly indicate that recordings from the PC and OT in rats performing both the identification and categorization tasks would provide valuable information about the strategies employed by the brain to solve these tasks.

6.3.3 Decision variables in the brain

The behavioral results from the odor identification task, in terms of mean RT and accuracy, were captured by two different model variants based on 'a integration-to-threshold' model, one that included temporal integration, and another one where the evidence was directly compared to the bound (no integration). Although our behavioral dataset did not allow us to disambiguate between these two computational mechanisms, both of them were consistent with the hypothesis that the main cause for the increase in RTs was the reduced amount of odor information at lower

concentrations.

One possibility to help constraining the model parameters would be to compare the predictions of the models with physiological data[131]. A neurophysiological expedition in search for neural activity resembling odor-driven DVs would be imperative to nail down this question. Previous studies have provided some clues of where to start looking. Neural representations of evidence accumulation have long been shown in monkeys[34], however in rodents the evidence is scarce. Very recently, electrophysiological recordings in the posterior parietal cortex (PPC) and frontal orienting fields (FOF) of rats performing an auditory task (Poisson clicks task[35]) revealed classic neural correlates of evidence accumulation[190]. While PPC encoded graded value of the accumulating evidence, the FOF had a more categorical encoding that indicated, throughout the trial, the decision provisionally favoured by the evidence accumulated so far. Recordings in humans using functional magnetic resonance imaging (fMRI) during an olfactory categorization task have implicated the OFC in the integration of sensory evidence[57]; however, the authors could not rule out the hypothesis that the observed OFC activity could had been related with a confidence signal[160]. Another interesting structure where to look at would be the PC, in particular the posterior PC. On one hand, the PC has strong reciprocal connections with the OB and it is the largest recipient of afferent fibers from the bulb. On the other hand, all parts of the PC have direct cortico-cortical connections with higher-order association areas. However, the extent and patterns

of these connections is strongly subdivision-dependent, with the posterior PC establishing more reciprocal connections with higher-order brain structures, namely insular and infralimbic regions of prefrontal cortex, amygdala, and perirhinal and entorhinal cortices[167].

Another relevant question to the field of olfaction regards the impact of sniffing on sensory processing. When performing a mixture categorization task, similar to the one used in our study, rats sample odors at ~8 Hz[52]. Additionally, sniff frequency was shown not to change as task difficulty is increased by lowering odorant concentration[141]. Sniffing has not been measured for the identification task, but given the increased RTs for lower concentrations, if we consider that rats are sniffing at ~8 Hz and that sniff frequency is not changing across concentrations, then rats should be taking an extra 1-2 sniffs for lower concentrations. Sniffing has been shown to provide a reference frame for neural responses in the OB and PC[127,138,140] and the timing of M/TCs firing in the OB is conserved across various respiration frequencies[138]. However, it is not known how this information is used to build a representation of the evidence, and what is the impact of extra sniffs. Does the sniff cycle reset or erase olfactory information? Recent evidence has shown that odor representation in the OB evolves after the first breath and persists as an odor afterimage[191]. Investigating how these representations contribute to the formation of the evidence will be critical to understand the mechanisms underlying the decision process across multiple sniffs.

Although standard accumulator models generally account for SAT with one parameter adjustment (threshold or baseline), interestingly a recent study showed that SAT is accomplished through multiple adjustments in the activity of visual, visuomovement and movement neurons in the monkey frontal eye fields, including baseline activity before stimulus onset, visual response gain and magnitude of movement activity[192]. These observations raise an important theoretical issue, suggesting that the mapping of SAT manipulations is not as straightforward as conceptualized before.

6.4 Temporal uncertainty and decision-making: the multiple shades of reaction times

RTs reflect the total amount of time consumed by all the subsystems that contribute to a choice or decision process. For instance, when a subject executes an action in response to a sensory scene, RT must comprise, at least, the time necessary for processing the sensory information plus the amount of time required to plan the motor action that is congruent with that information[193]. Discerning just these two components has been challenging because the underlying neural networks are themselves strongly interrelated: neurons that encode a subject's perceptual decision, that participate in motor planning, or that do both, are typically found within the same local

microcircuits[e.g.,42,194,195]. On top of this, RTs are modulated by variables such as reward[e.g.,150,151], prior probability[e.g.,31,196] and attention, especially temporal expectation[88,90].

In agreement with this, we showed that RTs, in both identification and categorization tasks, were modulated by non-sensory variables, namely by temporal expectation. This expectation-sensitive component of RTs was correlated with task difficulty, with lower accuracies displaying larger changes in RT.

This correlation between the magnitude of temporal modulation and task difficulty suggests that: 1) there is an interaction between temporal estimation processes and the mechanisms that account for choice accuracy in a decision-making process; or 2) it is not task difficulty that is mediating this modulation but a variable correlated with it, such as reward expectation. The first hypothesis is not likely given that it would predict a change in accuracy for the different temporal expectation conditions, which we did not observe. On the other hand, reward probability decreases with stimulus difficulty, and reward expectation has been shown before to influence RTs[56,150,151], making it a likely candidate.

In order to understand these putative interactions, it would be important to disambiguate the contributions of the different components. One important experiment would be to eliminate the stimulus difficulty variable and test if the effect still holds. For that, instead of having 4 odor mixture (or odor concentration) pairs, one would have 4 pairs of pure odors equally easy to discriminate. Each odor pair would be associated with a given

probability of reward, mimicking the different reward expectations for the different stimulus difficulties.

Another strategy would be to have a behavioural manipulation where one would eliminate the effect of temporal expectation or the effect of reward expectation in order to reveal the other component. In our experiments, temporal expectation was manipulated by using a uniform distribution for odor onset, which created a rising hazard rate, leading to an increase in stimulus onset expectation. Then, for distributions with different hazard rate functions, one would expect RTs to change differently across different odor delay conditions[89,107]. Therefore, if instead we used an exponential distribution, which creates an almost flat hazard rate, i.e., constant temporal expectation across time, we would expect to see no difference in RTs for the different odor delay conditions. A way to eliminate the effect of reward expectation would be to equalize the reward rates.

We also observed that the mean and SD of RTs, for both tasks, followed a linear relationship, as predicted by diffusion models[123] and by data from a wide range of RT tasks[149]. This scalar property has been widely observed in the field of interval timing regarding estimated times and is consistent with Weber's law[73] in the temporal domain. Interestingly, this scaling between the mean and SD of RT was conserved across the different temporal expectation conditions, as would be expected from the scalar timing property if time estimation is changing across these conditions.

Linear scaling has been studied extensively in human and animal

models and holds over several orders of magnitude, though to date there is no clear explanation for its physiological basis. Over the years many theories have been proposed to account for scalar timing. SET[72,76] is based on a counter and accumulator model, conceptually similar to counting the ticks of a mechanical clock, and variability arises from comparing errors with remembered reference values. Another class of models assumes an ensemble of neurons oscillating at different frequencies, and timing is produced by decision neurons which become active only when a precise set of the oscillating neurons are coactive[78]. DDMs have also been proposed to provide a mechanistic basis of interval timing[80], suggesting that integration-based models should play as prominent a role in interval timing theory as they do in theories of perceptual decision-making, and that a common neural mechanism may underlie both types of behavior.

Learned temporal relationships were shown to be represented in the frontal and parietal cortices[89,97,197,198], namely by the same type of neurons that furnish a representation of the state of the evidence during perceptual decision-making tasks. Interestingly, neurons within the primary visual cortex are also capable of providing information about the learned timing of reward in relation to sensory input[199]. Very recently, it was also shown that striatal neurons fire over tens of seconds during timing behavior and that the timing of these neurons rescales with the interval being timed, reflecting an interaction between time and action[200]. Similar results have been observed in the medial prefrontal cortex[201].

These studies suggest that timing is a ubiquitous feature of the nervous system and is critical for guiding behavior. Although we cannot tell from our data what is the source of the linear scaling between the mean and SD of RTs, our results suggest that temporal estimation mechanisms might play a role in the observed response times. In future experiments, it would be interesting to manipulate the time before odor onset in a way that would allow disambiguating between the contribution of absolute preparation time and the perceived probability of stimulus time[202]. Understanding which factors govern the relationship between the mean and SD of response times will also provide important insights about the underlying mechanisms[203].

References

1. Gold, J. I. & Shadlen, M. N. The Neural Basis of Decision Making. *Annu. Rev. Neurosci.* **30,** 535–574 (2007).
2. Hauser, C. K. & Salinas, E. in *Encyclopedia of Computational Neuroscience* (eds. Jaeger, D. & Jung, R.) 1–21 (Springer New York, 2014). at <http://link.springer.com/10.1007/978-1-4614-7320-6_317-1>
3. Carpenter, R. H. S. & Williams, M.L.L. Neural computation of log likelihood in control of saccadic eye movements. *Nature* **377,** 59–62 (1995).
4. Platt, M. L. & Glimcher, P. W. Neural correlates of decision variables in parietal cortex. *Nature* **400,** 233–238 (1999).
5. Sugrue, L. P. Matching Behavior and the Representation of Value in the Parietal Cortex. *Science* **304,** 1782–1787 (2004).
6. Basso, M. A. & Wurtz, R. H. Modulation of neuronal activity in superior colliculus by changes in target probability. *J. Neurosci.* **18,** 7519–7534 (1998).
7. Busse, L. *et al.* The Detection of Visual Contrast in the Behaving Mouse. *J. Neurosci.* **31,** 11351–11361 (2011).
8. Fechner, G. T. *Elemente der psychophysik*. (Breitkopf und Härtel, 1860).
9. Smith, P. L. Fechner's legacy and challenge. *J Math Psychol* **38,** 407–420 (1994).
10. Green, D. M. & Swets, J. A. *Signal detection theory and psychophysics*. (Wiley & Sons, Inc., 1966).
11. Stüttgen, M. C. Mapping spikes to sensations. *Front. Neurosci.* **5,** (2011).
12. Glimcher, P. W. & Fehr, E. *Neuroeconomics: Decision-making and the Brain*. (Elsevier Inc, 2008).
13. Luce, R. D. *Response Times: Their Role in Inferring Elementary Mental Organization*. (New York: Oxford University Press, 1986).
14. Townsend, J. T. & Ashby, F. G. *The Stochastic Modeling of Elementary Psychological Processes*. (Cambridge: Cambridge University Press, 1983).

15. Vickers, D. Evidence for an accumulator model of psychophysical discrimination. *Ergonomics* **13,** 37–58 (1970).
16. Vickers, D. *Decision Processes in Visual Perception (Academic Press series in cognition and perception)*. (Academic Press Inc, 1979).
17. Laming, D. R. J. *Information, theory of choice-reaction times*. (New York: Academic Press, 1968).
18. Usher, M. & McClelland, J. L. The time course of perceptual choice: the leaky, competing accumulator model. *Psychol. Rev.* **108,** 550–592 (2001).
19. Ratcliff, R. & Smith, P. L. A comparison of sequential sampling models for two-choice reaction time. *Psychol. Rev.* **111,** 333 (2004).
20. Wald, A. & Wolfowitz, J. Optimum character of the sequential probability ratio test. *Ann Math Stat.* **19,** 326–39 (1947).
21. Good, I. J. Studies in the history of probability and statistics. XXXVII A.M. Turing's statistical work in World War II. *Biometrika* **66,** 393–96 (1979).
22. Good, I. J. *Good Thinking: The Foundations of Probability and Its Applications*. (Minneapolis: Univ. Minn. Press).
23. Sternberg, S. Memory-scanning: mental processes revealed by reaction-time experiments. **57,** 421–57 (1969).
24. Ratcliff, R., Zandt, T. V. & McKoon, G. Connectionist and Diffusion Models of Reaction Time. *Psychol. Rev.* **106,** 261–300 (1999).
25. Palmer, J., Huk, A. C. & Shadlen, M. N. The effect of stimulus strength on the speed and accuracy of a perceptual decision. *J. Vis.* **5,** 1–1 (2005).
26. Krajbich, I., Armel, C. & Rangel, A. Visual fixations and the computation and comparison of value in simple choice. *Nature* **13,** 1292–1298 (2010).
27. Krajbich, I. & Rangel, A. Multialternative drift-diffusion model predicts the relationship between visual fixations and choice in value-based decisions. *Proc. Natl. Acad. Sci.* **108,** 13852–13857 (2011).
28. Krajbich, I., Lu, D., Camerer, C. & Rangel, A. The Attentional Drift-Diffusion Model Extends to Simple Purchasing Decisions. *Front. Psychol.* **3,** (2012).

29. Milosavljevic, M., Malmaud, J., Huth, A., Koch, C. & Rangel, A. The Drift Diffusion Model can account for the accuracy and reaction time of value-based choices under high and low time pressure. *Judgm. Decis. Mak.* **5,** 437–449 (2010).
30. Feng, S., Holmes, P., Rorie, A. & Newsome, W. T. Can Monkeys Choose Optimally When Faced with Noisy Stimuli and Unequal Rewards? *PLoS Comput. Biol.* **5,** e1000284 (2009).
31. Hanks, T. D., Mazurek, M. E., Kiani, R., Hopp, E. & Shadlen, M. N. Elapsed Decision Time Affects the Weighting of Prior Probability in a Perceptual Decision Task. *J. Neurosci.* **31,** 6339–6352 (2011).
32. Mulder, M. J., Wagenmakers, E.-J., Ratcliff, R., Boekel, W. & Forstmann, B. U. Bias in the Brain: A Diffusion Model Analysis of Prior Probability and Potential Payoff. *J. Neurosci.* **32,** 2335–2343 (2012).
33. Ratcliff, R., Philiastides, M. G. & Sajda, P. Quality of evidence for perceptual decision making is indexed by trial-to-trial variability of the EEG. *Proc. Natl. Acad. Sci.* **106,** 6539–6544 (2009).
34. Roitman, J. D. & Shadlen, M. N. Response of neurons in the lateral intraparietal area during a combined visual discrimination reaction time task. *J. Neurosci.* **22,** 9475–9489 (2002).
35. Brunton, B. W., Botvinick, M. M. & Brody, C. D. Rats and Humans Can Optimally Accumulate Evidence for Decision-Making. *Science* **340,** 95–98 (2013).
36. DasGupta, S., Ferreira, C. H. & Miesenböck, G. FoxP Influences the Speed and Accuracy of a Perceptual Decision in Drosophila. *Science* **344,** 901–904 (2014).
37. Ratcliff, R. & McKoon, G. The diffusion decision model: theory and data for two-choice decision tasks. *Neural Comput.* **20,** 873–922 (2008).
38. Uchida, N., Poo, C. & Haddad, R. Coding and Transformations in the Olfactory System. *Annu. Rev. Neurosci.* **37,** 363–385 (2014).
39. Burr, D. C. & Santoro, L. Temporal integration of optic flow, measured by contrast and coherence thresholds. *Vision Res.* **41,** 1891–1899 (2001).

40. Britten, K. H., Shadlen, M. N., Newsome, W. T. & Movshon, J. A. The analysis of visual motion: a comparison of neuronal and psychophysical performance. *J. Neurosci.* **12,** 4745–4765 (1992).
41. Shadlen, M. N. & Newsome, W. T. Motion perception: seeing and deciding. *Proc. Natl. Acad. Sci.* **93,** 628–633 (1996).
42. Shadlen, M. N. & Newsome, W. T. Neural basis of a perceptual decision in the parietal cortex (area LIP) of the rhesus monkey. *J. Neurophysiol.* **86,** 1916–1936 (2001).
43. Shadlen, M. N. & Gold, J. I. *The neurophysiology of decision-making as a window on cognition." In: The Cognitive Neurosciences*. (MIT Press, 2004).
44. Smith, P. L. & Ratcliff, R. Psychology and neurobiology of simple decisions. *Trends Neurosci.* **27,** 161–168 (2004).
45. Schall, J. D. Neural correlates of decision processes: neural and mental chronometry. *Curr. Opin. Neurobiol.* **13,** 182–186 (2003).
46. Hanes, D. P. & Schall, J. D. Neural Control of Voluntary movement initiation. *Science* **274,** 427–430 (1996).
47. Mazurek, M. E. A Role for Neural Integrators in Perceptual Decision Making. *Cereb. Cortex* **13,** 1257–1269 (2003).
48. Gold, J. I. & Shadlen, M. N. Representation of a perceptual decision in developing oculomotor commands. *Nature* **404,** 390–394 (2000).
49. Gold, J. I. & Shadlen, M. N. The influence of behavioral context on the representation of a perceptual decision in developing oculomotor commands. *J. Neurosci. Off. J. Soc. Neurosci.* **23,** 632–651 (2003).
50. Chittka, L., Dyer, A. G., Bock, F. & Dornhaus, A. Psychophysics: bees trade off foraging speed for accuracy. *Nature* **424,** 388 (2003).
51. Chittka, L., Skorupski, P. & Raine, N. E. Speed–accuracy tradeoffs in animal decision making. *Trends Ecol. Evol.* **24,** 400–407 (2009).
52. Uchida, N. & Mainen, Z. F. Speed and accuracy of olfactory discrimination in the rat. *Nat. Neurosci.* **6,** 1224–1229 (2003).

53. Abraham, N. M. *et al.* Maintaining accuracy at the expense of speed: stimulus similarity defines odor discrimination time in mice. *Neuron* **44,** 865–876 (2004).
54. Rinberg, D., Koulakov, A. & Gelperin, A. Speed-Accuracy Tradeoff in Olfaction. *Neuron* **51,** 351–358 (2006).
55. Histed, M. H., Carvalho, L. A. & Maunsell, J. H. R. Psychophysical measurement of contrast sensitivity in the behaving mouse. *J. Neurophysiol.* **107,** 758–765 (2012).
56. Zariwala, H. A., Kepecs, A., Uchida, N., Hirokawa, J. & Mainen, Z. F. The Limits of Deliberation in a Perceptual Decision Task. *Neuron* **78,** 339–351 (2013).
57. Bowman, N. E., Kording, K. P. & Gottfried, J. A. Temporal integration of olfactory perceptual evidence in human orbitofrontal cortex. *Neuron* **75,** 916–927 (2012).
58. Marques, T. G., Dias, R. F. & Petreanu, L. A cortex-dependent motion discrimination task in head-fixed mice. *Soc. Neurosci. Poster* (2014).
59. Khan, R. M. & Sobel, N. Neural processing at the speed of smell. *Neuron* **44,** 744–747 (2004).
60. Summerfield, C. & Tsetsos, K. Building Bridges between Perceptual and Economic Decision-Making: Neural and Computational Mechanisms. *Front. Neurosci.* **6,** (2012).
61. Shadlen, M. N., Britten, K. H., Newsome, W. T. & Movshon, J. A. A computational analysis of the relationship between neuronal and behavioral responses to visual motion. *J. Neurosci.* **16,** 1486–1510 (1996).
62. Bogacz, R., Brown, E., Moehlis, J., Holmes, P. & Cohen, J. D. The physics of optimal decision making: a formal analysis of models of performance in two-alternative forced-choice tasks. *Psychol. Rev.* **113,** 700–765 (2006).
63. Rorie, A. E., Gao, J., McClelland, J. L. & Newsome, W. T. Integration of sensory and reward information during perceptual decision-making in lateral intraparietal cortex (LIP) of the macaque monkey. *PloS One* **5,** e9308 (2010).
64. Serences, J. T. & Saproo, S. Population response profiles in early visual cortex are biased in favor of more valuable stimuli. *J. Neurophysiol.* **104,** 76–87 (2010).
65. Summerfield, C. & Koechlin, E. Economic value biases uncertain perceptual choices in the parietal and prefrontal cortices. *Front. Hum. Neurosci.* **4,** 208 (2010).

66. Gold, J. I., Law, C.-T., Connolly, P. & Bennur, S. The relative influences of priors and sensory evidence on an oculomotor decision variable during perceptual learning. *J. Neurophysiol.* **100,** 2653–2668 (2008).
67. Law, C.-T. & Gold, J. I. Reinforcement learning can account for associative and perceptual learning on a visual-decision task. *Nat. Neurosci.* **12,** 655–663 (2009).
68. Rescorla, R. A. & Wagner, A. R. *'A theory of Pavlovian con- ditioning: variations in the effective- ness of reinforcement and nonrein- forcement,' in Classical Condition- ing II: Current Research and The- ory, eds A. H. Black and W. F. Prokasy*. (New York: Appleton Cen- tury Crofts, 1972).
69. Sutton, R. & Barto, A. *Reinforcement Learning*. (Cambridge: MIT press, 1998).
70. Law, C.-T. & Gold, J. I. Neural correlates of perceptual learning in a sensory-motor, but not a sensory, cortical area. *Nat. Neurosci.* **11,** 505–513 (2008).
71. Gallistel, C. R. *The organization of learning*. (Cambridge, MA: Bradford Books/MIT Press).
72. Meck, W. H. *Functional and Neural Mechanisms of Interval Timing*. (CRC Press, 2003).
73. Weber, E. H. *Annotationes Annatomicae et Physiologicae*. (Leipsig: CF Koehler, 1851).
74. Gallistel, C. R. & Gibbon, J. Time, rate, and conditioning. *Psychol. Rev.* **107,** 289–344 (2000).
75. Gibbon, J., Malapani, C., Dale, C. L. & Gallistel, C. Toward a neurobiology of temporal cognition: advances and challenges. *Curr. Opin. Neurobiol.* **7,** 170–184 (1997).
76. Gibbon, J. Scalar expectancy theory and Weber's Law in animal timing. *Psychol Rev* **84,** 279–325 (1977).
77. Ivry, R. B. & Spencer, R. M. C. The neural representation of time. *Curr. Opin. Neurobiol.* **14,** 225–232 (2004).
78. Matell, M. S. & Meck, W. H. Neuropsychological mechanisms of interval timing behavior. *BioEssays News Rev. Mol. Cell. Dev. Biol.* **22,** 94–103 (2000).
79. Buhusi, C. V. & Meck, W. H. What makes us tick? Functional and neural mechanisms of interval timing. *Nat. Rev. Neurosci.* **6,** 755–765 (2005).

80. Simen, P., Balci, F., deSouza, L., Cohen, J. D. & Holmes, P. A Model of Interval Timing by Neural Integration. *J. Neurosci.* **31,** 9238–9253 (2011).
81. Mauk, M. D. & Buonomano, D. V. The neural basis of temporal processing. *Annu. Rev. Neurosci.* **27,** 307–340 (2004).
82. Killeen, P. R. & Fetterman, J. G. A behavioral theory of timing. *Psychol. Rev.* **95,** 274 (1988).
83. Machado, A. Learning the temporal dynamics of behavior. *Psychol. Rev.* **104,** 241–265 (1997).
84. Gibbon, J., Church, R. M. & Meck, W. H. Scalar timing in memory. *Ann. N. Y. Acad. Sci.* **423,** 52–77 (1984).
85. Killeen, P. R. & Fetterman, J. G. The behavioral theory of timing: transition analyses. *J. Exp. Anal. Behav.* **59,** 411–422 (1993).
86. Machado, A., Malheiro, M. T. & Erlhagen, W. Learning to Time: a perspective. *J. Exp. Anal. Behav.* **92,** 423–458 (2009).
87. Näätänen, R. Non-aging fore-periods and simple reaction time. *Acta Psychol. (Amst.)* **35,** 316–327 (1971).
88. Niemi, P. & Näätänen, R. Foreperiod and simple reaction time. *Psychol. Bull.* **89,** 133–162 (1981).
89. Janssen, P. & Shadlen, M. N. A representation of the hazard rate of elapsed time in macaque area LIP. *Nat. Neurosci.* **8,** 234–241 (2005).
90. Nobre, A., Correa, A. & Coull, J. The hazards of time. *Curr. Opin. Neurobiol.* **17,** 465–470 (2007).
91. Sanders, A. *Stage analysis of reaction processes. In G. E. Stelmach & J. Requin (Eds.), Tutorials of motor behavior (pp. 331–354)*. (New York, NY: North-Holland, 1980).
92. Jepma, M., Wagenmakers, E.-J. & Nieuwenhuis, S. Temporal expectation and information processing: A model-based analysis. *Cognition* **122,** 426–441 (2012).
93. Riehle, A., Grün, S., Diesmann, M. & Aertsen, A. Spike synchronization and rate modulation differentially involved in motor cortical function. *Science* **278,** 1950–1953 (1997).
94. Renoult, L., Roux, S. & Riehle, A. Time is a rubberband: neuronal activity in monkey motor cortex in relation to time estimation. *Eur. J. Neurosci.* **23,** 3098–3108 (2006).

95. Lucchetti, C. & Bon, L. Time-modulated neuronal activity in the premotor cortex of macaque monkeys. *Exp. Brain Res.* **141,** 254–260 (2001).
96. Heinen, S. J. & Liu, M. Single-neuron activity in the dorsomedial frontal cortex during smooth-pursuit eye movements to predictable target motion. *Vis. Neurosci.* **14,** 853–865 (1997).
97. Leon, M. I. & Shadlen, M. N. Representation of time by neurons in the posterior parietal cortex of the macaque. *Neuron* **38,** 317–327 (2003).
98. Loveless, N. E. The contingent negative variation related to preparatory set in a reaction time situation with variable foreperiod. *Electroencephalogr. Clin. Neurophysiol.* **35,** 369–374 (1973).
99. Hackley, S. A. & Valle-Inclán, F. Which stages of processing are speeded by a warning signal? *Biol. Psychol.* **64,** 27–45 (2003).
100. Coull, J. T., Frith, C. D., Büchel, C. & Nobre, A. C. Orienting attention in time: behavioural and neuroanatomical distinction between exogenous and endogenous shifts. *Neuropsychologia* **38,** 808–819 (2000).
101. Coull, J. & Nobre, A. Dissociating explicit timing from temporal expectation with fMRI. *Curr. Opin. Neurobiol.* **18,** 137–144 (2008).
102. Lasley, D. J. & Cohn, T. Detection of a luminance increment: effect of temporal uncertainty. *J. Opt. Soc. Am.* **71,** 845–850 (1981).
103. Westheimer, G. & Ley, E. Temporal uncertainty effects on orientation discrimination and stereoscopic thresholds. *J. Opt. Soc. Am. A Opt. Image Sci. Vis.* **13,** 884–886 (1996).
104. Correa, A., Lupiáñez, J. & Tudela, P. Attentional preparation based on temporal expectancy modulates processing at the perceptual level. *Psychon. Bull. Rev.* **12,** 328–334 (2005).
105. Rolke, B. & Hofmann, P. Temporal uncertainty degrades perceptual processing. *Psychon. Bull. Rev.* **14,** 522–526 (2007).
106. Rohenkohl, G., Cravo, A. M., Wyart, V. & Nobre, A. C. Temporal Expectation Improves the Quality of Sensory Information. *J. Neurosci.* **32,** 8424–8428 (2012).

107. Katzner, S., Treue, S. & Busse, L. Improving behavioral performance under full attention by adjusting response criteria to changes in stimulus predictability. *J. Vis.* **12,** 1–1 (2012).
108. Jones, M. R., Moynihan, H., MacKenzie, N. & Puente, J. Temporal aspects of stimulus-driven attending in dynamic arrays. *Psychol. Sci.* **13,** 313–319 (2002).
109. Doherty, J. R., Rao, A., Mesulam, M. M. & Nobre, A. C. Synergistic effect of combined temporal and spatial expectations on visual attention. *J. Neurosci. Off. J. Soc. Neurosci.* **25,** 8259–8266 (2005).
110. Guo, K. *et al.* Effects on orientation perception of manipulating the spatio-temporal prior probability of stimuli. *Vision Res.* **44,** 2349–2358 (2004).
111. Praamstra, P., Kourtis, D., Kwok, H. F. & Oostenveld, R. Neurophysiology of implicit timing in serial choice reaction-time performance. *J. Neurosci. Off. J. Soc. Neurosci.* **26,** 5448–5455 (2006).
112. Morillon, B., Schroeder, C. E. & Wyart, V. Motor contributions to the temporal precision of auditory attention. *Nat. Commun.* **5,** 5255 (2014).
113. Shuler, M. G. & Bear, M. F. Reward timing in the primary visual cortex. *Science* **311,** 1606–1609 (2006).
114. Lima, B., Singer, W. & Neuenschwander, S. Gamma responses correlate with temporal expectation in monkey primary visual cortex. *J. Neurosci. Off. J. Soc. Neurosci.* **31,** 15919–15931 (2011).
115. Ghose, G. M. & Maunsell, J. H. R. Attentional modulation in visual cortex depends on task timing. *Nature* **419,** 616–620 (2002).
116. Ghose, G. M. & Bearl, D. W. Attention directed by expectations enhances receptive fields in cortical area MT. *Vision Res.* **50,** 441–451 (2010).
117. Anderson, B. & Sheinberg, D. L. Effects of temporal context and temporal expectancy on neural activity in inferior temporal cortex. *Neuropsychologia* **46,** 947–957 (2008).
118. Jaramillo, S. & Zador, A. M. The auditory cortex mediates the perceptual effects of acoustic temporal expectation. *Nat. Neurosci.* **14,** 246–251 (2011).

119. Müller-Gethmann, H., Ulrich, R. & Rinkenauer, G. Locus of the effect of temporal preparation: evidence from the lateralized readiness potential. *Psychophysiology* **40,** 597–611 (2003).
120. Bueti, D., Bahrami, B., Walsh, V. & Rees, G. Encoding of temporal probabilities in the human brain. *J. Neurosci. Off. J. Soc. Neurosci.* **30,** 4343–4352 (2010).
121. MacDonald, C. J. & Meck, W. H. Systems-level integration of interval timing and reaction time. *Neurosci. Biobehav. Rev.* **28,** 747–769 (2004).
122. Shadlen, M. N. & Kiani, R. Decision Making as a Window on Cognition. *Neuron* **80,** 791–806 (2013).
123. Wagenmakers, E.-J., Grasman, R. P. P. P. & Molenaar, P. C. M. On the relation between the mean and the variance of a diffusion model response time distribution. *J. Math. Psychol.* **49,** 195–204 (2005).
124. Martelli, C., Carlson, J. R. & Emonet, T. Intensity Invariant Dynamics and Odor-Specific Latencies in Olfactory Receptor Neuron Response. *J. Neurosci.* **33,** 6285–6297 (2013).
125. Gupta, P., Albeanu, D. F. & Bhalla, U. S. Olfactory bulb coding of odors, mixtures and sniffs is a linear sum of odor time profiles. *Nat. Neurosci.* **18,** 272–281 (2015).
126. Beck, J. M., Ma, W. J., Pitkow, X., Latham, P. E. & Pouget, A. Not Noisy, Just Wrong: The Role of Suboptimal Inference in Behavioral Variability. *Neuron* **74,** 30–39 (2012).
127. Miura, K., Mainen, Z. F. & Uchida, N. Odor Representations in Olfactory Cortex: Distributed Rate Coding and Decorrelated Population Activity. *Neuron* **74,** 1087–1098 (2012).
128. Hanks, T., Kiani, R. & Shadlen, M. N. A neural mechanism of speed-accuracy tradeoff in macaque area LIP. *eLife* **3,** e02260 (2014).
129. Ratcliff, R. A theory of memory retrieval. *Psychol. Rev.* **85,** 59 (1978).
130. Link, S. W. *The wave theory of difference and similarity*. (L. Erlbaum Associates, 1992).

131. Ditterich, J. Stochastic models of decisions about motion direction: Behavior and physiology. *Neural Netw.* **19,** 981–1012 (2006).
132. Maloney, L. T. & Wandell, B. A. A model of a single visual channel's response to weak test lights. *Vision Res.* **24,** 633–640 (1984).
133. Wandell, B. A., Ahumada, P. & Welsh, D. Reaction times to weak test lights. *Vision Res.* **24,** 647–652 (1984).
134. Watson, A. B. Probability summation over time. *Vision Res.* **19,** 515–522 (1979).
135. Kepecs, A., Uchida, N. & Mainen, Z. F. Rapid and Precise Control of Sniffing During Olfactory Discrimination in Rats. *J. Neurophysiol.* **98,** 205–213 (2007).
136. Kiani, R., Corthell, L. & Shadlen, M. N. Choice Certainty Is Informed by Both Evidence and Decision Time. *Neuron* **84,** 1329–1342 (2014).
137. Sigman, M. & Dehaene, S. Parsing a Cognitive Task: A Characterization of the Mind's Bottleneck. *PLoS Biol.* **3,** e37 (2005).
138. Cury, K. M. & Uchida, N. Robust Odor Coding via Inhalation-Coupled Transient Activity in the Mammalian Olfactory Bulb. *Neuron* **68,** 570–585 (2010).
139. Kepecs, A. The Sniff as a Unit of Olfactory Processing. *Chem. Senses* **31,** 167–179 (2005).
140. Shusterman, R., Smear, M. C., Koulakov, A. A. & Rinberg, D. Precise olfactory responses tile the sniff cycle. *Nat. Neurosci.* **14,** 1039–1044 (2011).
141. Wesson, D. W., Verhagen, J. V. & Wachowiak, M. Why Sniff Fast? The Relationship Between Sniff Frequency, Odor Discrimination, and Receptor Neuron Activation in the Rat. *J. Neurophysiol.* **101,** 1089–1102 (2008).
142. Pirenne, M. H. Binocular and Uniocular Threshold of Vision. *Nature* **152,** 698–699 (1943).
143. Treisman, M. Combining information: Probability summation and probability averaging in detection and discrimination. *Psychol. Methods* **3,** 252 (1998).
144. Mendonca, A. G., Vicente, M. I., Pouget, A. & Mainen, Z. F. Odor Detection vs. Categorization: How two Different Noise Sources Can Limit Speed and Performance. *Poster Cosyne* (2012).

145. Mendonca, A. G., Vicente, M. I., DeWitt, E., Pouget, A. & Mainen, Z. F. Reinforcement learning limits performance in categorical decision making. *Prep.*
146. Mendonca, A. G., Vicente, M. I., Pouget, A. & Mainen, Z. F. Reinforcement learning limits performance in categorical decision-making. *Poster Cosyne* (2015).
147. Klemmer, E. T. Time uncertainty in simple reaction time. *J. Exp. Psychol.* **51,** 179–184 (1956).
148. Klemmer, E. T. Simple reaction time as a function of time uncertainty. *J. Exp. Psychol.* **54,** 195 (1957).
149. Wagenmakers, E.-J. & Brown, S. On the linear relation between the mean and the standard deviation of a response time distribution. *Psychol. Rev.* **114,** 830–841 (2007).
150. Lauwereyns, J., Watanabe, K., Coe, B. & Hikosaka, O. A neural correlate of response bias in monkey caudate nucleus. *Nature* **418,** 413–417 (2002).
151. Roesch, M. R. & Olson, C. R. Neuronal activity related to reward value and motivation in primate frontal cortex. *Science* **304,** 307–310 (2004).
152. Kiani, R. & Shadlen, M. N. Representation of confidence associated with a decision by neurons in the parietal cortex. *Science* **324,** 759–764 (2009).
153. Kepecs, A., Uchida, N. & Mainen, Z. F. Graded prediction error signal drives behavioral choice biases in rats. *Poster Cosyne* (2008).
154. Zohary, E., Shadlen, M. N. & Newsome, W. T. Correlated neuronal discharge rate and its implications for psychophysical performance. *Nature* **370,** 140–143 (1994).
155. Uchida, N., Kepecs, A. & Mainen, Z. F. Seeing at a glance, smelling in a whiff: rapid forms of perceptual decision making. *Nat. Rev. Neurosci.* **7,** 485–491 (2006).
156. Renart, A. & Machens, C. K. Variability in neural activity and behavior. *Curr. Opin. Neurobiol.* **25,** 211–220 (2014).
157. Chen, Y., Geisler, W. S. & Seidemann, E. Optimal Temporal Decoding of Neural Population Responses in a Reaction-Time Visual Detection Task. *J. Neurophysiol.* **99,** 1366–1379 (2008).
158. Chen, Y., Geisler, W. S. & Seidemann, E. Optimal decoding of correlated neural population responses in the primate visual cortex. *Nat. Neurosci.* **9,** 1412–1420 (2006).

159. Kepecs, A. & Mainen, Z. F. A computational framework for the study of confidence in humans and animals. *Philos. Trans. R. Soc. B Biol. Sci.* **367,** 1322–1337 (2012).
160. Kepecs, A., Uchida, N., Zariwala, H. A. & Mainen, Z. F. Neural correlates, computation and behavioural impact of decision confidence. *Nature* **455,** 227–231 (2008).
161. Lak, A. *et al.* Orbitofrontal Cortex Is Required for Optimal Waiting Based on Decision Confidence. *Neuron* **84,** 190–201 (2014).
162. Rao, V., DeAngelis, G. C. & Snyder, L. H. Neural Correlates of Prior Expectations of Motion in the Lateral Intraparietal and Middle Temporal Areas. *J. Neurosci.* **32,** 10063–10074 (2012).
163. Rinberg, D., Koulakov, A. & Gelperin, A. Sparse odor coding in awake behaving mice. *J. Neurosci. Off. J. Soc. Neurosci.* **26,** 8857–8865 (2006).
164. Johnson, B. A. & Leon, M. Modular representations of odorants in the glomerular layer of the rat olfactory bulb and the effects of stimulus concentration. *J. Comp. Neurol.* **422,** 496–509 (2000).
165. Spors, H. & Grinvald, A. Spatio-temporal dynamics of odor representations in the mammalian olfactory bulb. *Neuron* **34,** 301–315 (2002).
166. Carey, R. M., Verhagen, J. V., Wesson, D. W., Pirez, N. & Wachowiak, M. Temporal Structure of Receptor Neuron Input to the Olfactory Bulb Imaged in Behaving Rats. *J. Neurophysiol.* **101,** 1073–1088 (2008).
167. Haberly, L. B. Parallel-distributed processing in olfactory cortex: new insights from morphological and physiological analysis of neuronal circuitry. *Chem. Senses* **26,** 551–576 (2001).
168. Reisert, J. & Matthews, H. R. Adaptation-induced changes in sensitivity in frog olfactory receptor cells. *Chem. Senses* **25,** 483–486 (2000).
169. Reisert, J. & Matthews, H. R. Response properties of isolated mouse olfactory receptor cells. *J. Physiol.* **530,** 113–122 (2001).
170. Duchamp-Viret, P., Chaput, M. A. & Duchamp, A. Odor response properties of rat olfactory receptor neurons. *Science* **284,** 2171–2174 (1999).

171. Cang, J. & Isaacson, J. S. In vivo whole-cell recording of odor-evoked synaptic transmission in the rat olfactory bulb. *J. Neurosci. Off. J. Soc. Neurosci.* **23,** 4108–4116 (2003).
172. Bathellier, B., Buhl, D. L., Accolla, R. & Carleton, A. Dynamic ensemble odor coding in the mammalian olfactory bulb: sensory information at different timescales. *Neuron* **57,** 586–598 (2008).
173. Mainland, J. D., Lundström, J. N., Reisert, J. & Lowe, G. From molecule to mind: an integrative perspective on odor intensity. *Trends Neurosci.* **37,** 443–454 (2014).
174. Fukunaga, I., Berning, M., Kollo, M., Schmaltz, A. & Schaefer, A. T. Two Distinct Channels of Olfactory Bulb Output. *Neuron* **75,** 320–329 (2012).
175. Igarashi, K. M. *et al.* Parallel Mitral and Tufted Cell Pathways Route Distinct Odor Information to Different Targets in the Olfactory Cortex. *J. Neurosci.* **32,** 7970–7985 (2012).
176. Shapley, R. M. & Victor, J. D. The effect of contrast on the transfer properties of cat retinal ganglion cells. *J. Physiol.* **285,** 275–298 (1978).
177. Reich, D. S., Mechler, F. & Victor, J. D. Temporal coding of contrast in primary visual cortex: when, what, and why. *J. Neurophysiol.* **85,** 1039–1050 (2001).
178. Van Rossum, M. C., van der Meer, M. A., Xiao, D. & Oram, M. W. Adaptive integration in the visual cortex by depressing recurrent cortical circuits. *Neural Comput.* **20,** 1847–1872 (2008).
179. Oram, M. W. Contrast induced changes in response latency depend on stimulus specificity. *J. Physiol.-Paris* **104,** 167–175 (2010).
180. Wesson, D. W. & Wilson, D. A. Sniffing out the contributions of the olfactory tubercle to the sense of smell: Hedonics, sensory integration, and more? *Neurosci. Biobehav. Rev.* **35,** 655–668 (2011).
181. Murakami, M., Kashiwadani, H., Kirino, Y. & Mori, K. State-dependent sensory gating in olfactory cortex. *Neuron* **46,** 285–296 (2005).
182. Ikemoto, S. Dopamine reward circuitry: two projection systems from the ventral midbrain to the nucleus

accumbens-olfactory tubercle complex. *Brain Res. Rev.* **56,** 27–78 (2007).
183. Marcos, E. *et al.* Neural Variability in Premotor Cortex Is Modulated by Trial History and Predicts Behavioral Performance. *Neuron* **78,** 249–255 (2013).
184. Matias, S., Lottem, E., Dugue, G. P. & Mainen, Z. F. Encoding of reward prediction errors by serotonin neurons revealed by bulk fluorescence recordings. *Poster Cosyne* (2015).
185. Lottem, E., Lorincz, M., Piszár, I. & Mainen, Z. F. Divisive inhibition of spontaneous activity in olfactory cortex by serotonin. *Prep.*
186. Scott, J. W., McBride, R. L. & Schneider, S. P. The organization of projections from the olfactory bulb to the piriform cortex and olfactory tubercle in the rat. *J. Comp. Neurol.* **194,** 519–534 (1980).
187. Mori, K. & Shepherd, G. M. Emerging principles of molecular signal processing by mitral/tufted cells in the olfactory bulb. *Semin. Cell Biol.* **5,** 65–74 (1994).
188. *The synaptic organization of the brain*. (Oxford University Press, 2004).
189. Wachowiak, M. & Shipley, M. T. Coding and synaptic processing of sensory information in the glomerular layer of the olfactory bulb. *Semin. Cell Dev. Biol.* **17,** 411–423 (2006).
190. Hanks, T. D. *et al.* Distinct relationships of parietal and prefrontal cortices to evidence accumulation. *Nature* **520,** 220–223 (2015).
191. Patterson, M. A., Lagier, S. & Carleton, A. Odor representations in the olfactory bulb evolve after the first breath and persist as an odor afterimage. *Proc. Natl. Acad. Sci.* **110,** E3340–E3349 (2013).
192. Heitz, R. P. & Schall, J. D. Neural Mechanisms of Speed-Accuracy Tradeoff. *Neuron* **76,** 616–628 (2012).
193. Salinas, E., Scerra, V. E., Hauser, C. K., Costello, M. G. & Stanford, T. R. Decoupling speed and accuracy in an urgent decision-making task reveals multiple contributions to their trade-off. *Front. Neurosci.* **8,** (2014).
194. Hernández, A. *et al.* Decoding a perceptual decision process across cortex. *Neuron* **66,** 300–314 (2010).

195. Costello, M. G., Zhu, D., Salinas, E. & Stanford, T. R. Perceptual modulation of motor--but not visual--responses in the frontal eye field during an urgent-decision task. *J. Neurosci. Off. J. Soc. Neurosci.* **33,** 16394–16408 (2013).
196. Carpenter, R. H. S. Contrast, probability, and saccadic latency: evidence for independence of detection and decision. *Curr. Biol.* **14,** 1576–1580 (2004).
197. Genovesio, A., Tsujimoto, S. & Wise, S. P. Feature- and Order-Based Timing Representations in the Frontal Cortex. *Neuron* **63,** 254–266 (2009).
198. Mita, A., Mushiake, H., Shima, K., Matsuzaka, Y. & Tanji, J. Interval time coding by neurons in the presupplementary and supplementary motor areas. *Nat. Neurosci.* **12,** 502–507 (2009).
199. Shuler, M. G. & Bear, M. F. Reward Timing in the Primary Visual Cortex. *Science* **311,** 1606–1609 (2006).
200. Mello, G. B. M., Soares, S. & Paton, J. J. A Scalable Population Code for Time in the Striatum. *Curr. Biol.* **25,** 1113–1122 (2015).
201. Xu, M., Zhang, S. -y., Dan, Y. & Poo, M. -m. Representation of interval timing by temporally scalable firing patterns in rat prefrontal cortex. *Proc. Natl. Acad. Sci.* **111,** 480–485 (2014).
202. O'Neill, M. & Brown, V. J. Amphetamine and the adenosine A2A antagonist KW-6002 enhance the effects of conditional temporal probability of a stimulus in rats. *Behav. Neurosci.* **121,** 535–542 (2007).
203. Madelain, L., Champrenaut, L. & Chauvin, A. Control of Sensorimotor Variability by Consequences. *J. Neurophysiol.* **98,** 2255–2265 (2007).

ITQB-UNL | Av. da República, 2780-157 Oeiras, Portugal
Tel (+351) 214 469 100 | Fax (+351) 214 411 277

www.itqb.unl.pt